The Radio Science Bulletin

ISSN 1024-4530

INTERNATIONAL
UNION OF
RADIO SCIENCE

UNION
RADIO-SCIENTIFIQUE
INTERNATIONALE

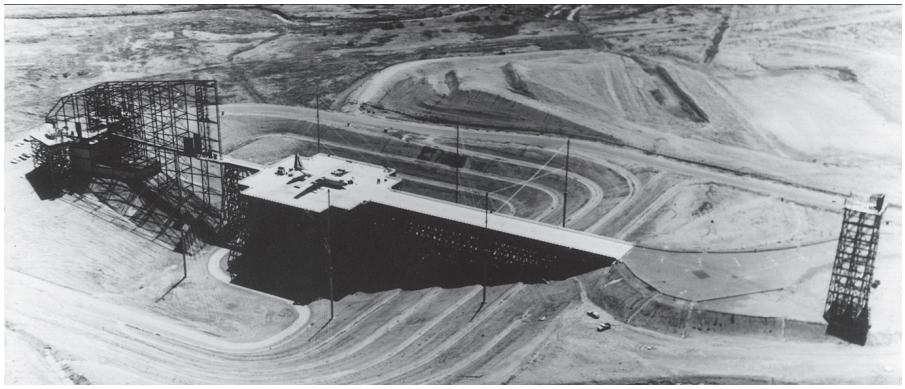

No 312
March 2005

Publié avec l'aide financière de l'ICSU
URSI, c/o Ghent University (INTEC)
St.-Pietersnieuwstraat 41, B-9000 Gent (Belgium)

Contents

Front cover: The ATLAS I (Trestle), which is the only simulator capable of testing large aircraft in an in-flight mode (more on pp. 6-16)

For information, please contact :
The URSI Secretariat
c/o Ghent University (INTEC)
Sint-Pietersnieuwstraat 41, B-9000 Gent, Belgium
Tel.: (32) 9-264 33 20, Fax: (32) 9-264 42 88
E-mail: info@ursi.org
http://www.urs.org

Editorial

Special Section Honoring Carl E. Baum

This issue and the June issue of the *Radio Science Bulletin* contain special sections honoring Carl E. Baum on his 65th birthday. We have two guest Editors for these special sections, Jürgen Nitsch and Frank Sabath, and they have provided an excellent introduction to the special section. I've had the honor and pleasure of knowing Carl for about 25 years. His impact on electromagnetics and the field of EMP has been tremendous, and his personal contributions to radio science – and to radio scientists – have been equally significant. I'm very pleased that we are able to publish these special sections in his honor.

Special thanks go to Jürgen Nitsch and Frank Sabath for the excellent job they have done in organizing and preparing these special sections. Their introduction to the special section provides a brief but insightful overview of Carl Baum's many contributions, both to radio science and in other areas.

Bill Prather, Dave Giri, and Bob Gardner have provided an excellent review of Carl Baum's work, which has included significant contributions in five decades, and continues today. Their largely historical paper also serves as a fascinating history of the development of the field of EMP, lightening, and high-power microwave generation and simulation. The photos of the major simulators included in this paper are a real treat!

Transmission-line theory is a common approach to analyzing and predicting coupling in electromagnetic systems. It is an important tool in the field of electromagnetic compatibility. When the wavelengths involved approach the dimensions of the wires or lines in the system, the approximations of classical transmission-line theory no longer hold. It therefore becomes necessary to generalize the transmission-line equations to include the effects of electromagnetic radiation. Jürgen Nitsch and Sergey Tkachenko describe how this can be done in their paper. They go on to establish the connection between the parameters involved in this analysis and their physical meaning, including an explicit formulation connecting the parameters to the radiation losses. They develop and demonstrate a rapidly convergent iterative approach for solving problems using this method.

The BLT (Baum-Liu-Tesche) equation is used to determine the voltage and current responses in a general multiconductor transmission-line network. A recent extension of the BLT equation includes the effect of electromagnetic propagation in space. The paper by Fred Tesche, J. M. Keen, and Chalmers Butler illustrates the use of this extended BLT equation with a numerical example. The example considered involves a two-wire transmission line near a conducting ground plane, excited by a point source. The ground plane affects both the incident excitation and the re-radiation of the line. Several tests of the reasonableness of the results obtained are presented, along with verification by an independent integral-equation analysis. The authors then go on to explore several related areas where future work could be done.

In their paper, J-P. Parmantier, S. Bertuol, and F. Issac present a practical approach to modeling the emission from and coupling to a multiconductor cable in a complex, three-dimensional geometry. This involves first using a three-dimensional EM solver (such as an FDTD code) to calculate the fields incident on the cable, followed by the use of a multiconductor cable network code to calculate the response of the cable to the fields. The authors develop a reciprocity method for implementing this approach. They then go on to provide numerical validation, and validation with experimental measurements using cables in a mockup of a satellite. Some of the results from the experiments underscore the importance of the effects of neighboring cables on the emitted fields.

Reviews of Radio Science

This issue also contains an invited contribution to the *Reviews of Radio Science*, from Commission B. Phil Wilkinson coordinates the *Reviews*, and Lot Shafai is the Associate Editor for Commission B: their efforts are greatly appreciated.

The field of metamaterials is one of the fastest-growing areas of radio science. These are artificial materials that have interesting electromagnetic properties. George Eleftheriades presents a fascinating review of one class of such materials: isotropic materials with a negative permeability and a negative permittivity, and thus a negative refractive index. The examples considered in this paper are produced as planar structures made of networks of transmission lines that are periodically loaded with lumped inductors and capacitors. A variety of devices implemented using such structures are described. These include lenses that resolve better than the classical diffraction limit;

broadband, compact phase-shifting lines; a compact, backward leaky-wave antenna; and a high-directivity microstrip coupler.

Tumors and Cell-Phone Use

If you have used a cell phone for a long time or know someone who has – or if you plan to use one for a long time – you need to read Jim Lin's Radio-Frequency Radiation Safety and Health column. He reports on and discusses results from a new study that found an increased risk of a particular type of tumor of the auditory nerve in people in Sweden with 10 or more years of cell-phone use. It's important to understand what the results of this study do and do not imply.

Make Your General Assembly Plans *Now*!

Now is the time to make your plans to attend the XXVIIIth General Assembly of URSI, which will be held October 23-29, 2005, in New Delhi, India. More than 1500 papers have been submitted, so there will be a memorable technical program. If you need to make hotel reservations or have other concerns related to travel, Thomas Cook India is the professional meeting planner for the General Assembly. Their e-mail address: ThomasCookConferences.NewDelhi@in.thomascook.com. Other information is available at the General Assembly Web site: http://www.ursiga2005.org. Do plan on going: this will be a historic General Assembly.

New Delhi General Assembly

CURRENT STATUS OF THE SCIENTIFIC PROGRAM

XXVIIIth General Assembly of URSI will be held in New Delhi in October 2005. More than 1000 delegates including many young scientists are expected to participate in the event. The preparations for the scientific programme are now in the busiest phase. The paper submission has now been closed, and the Commissions are busy reviewing all papers. In total about 1600 submissions have been processed by the system, including those, which are duplicates or triplicates of one submission. The final number of valid abstracts submitted will be known after the review process is complete for all the Commissions. This number compares favorably with those of previous two assemblies. Until now review process is complete for Commissions C and F and the status communicated to the authors. For other commissions it is expected to be completed in next two weeks.

The Local Organizing Committee and the Commission chairs and vice chairs are busy sorting out all details for successful organization. So far, the preparations are running according to schedule. From the management office we are trying to answer many questions that are inevitably received.

The next events to happen are:

- All authors who have submitted an abstract will receive notification of the decision on their proposed paper, this will include session (with location, date and time) to which contribution has been allocated and the form of presentation (oral or poster)
- By mid June the preliminary programme, based on review decision, will be on the web site of the Assembly.
- By then, the management office must receive full Proceedings versions of all papers.

We wish all authors success in the preparation of the Proceedings papers and hope to meet all at the most exciting event that the URSI community knows!

Commission F		Commission C	
FO1	10	CO1	7
FO2	10	CO2	10
FO3	7	CO3	10
FO4	7	CO4	7
FO5	7	CO5	7
FO6	7	CO6	7
FO7	7	CO7	6
FO8	10	CO8	4
FO9	7	CO9	10
F10	10	CB	6
FG	7	CBA	9
FP01	15	CP1	7
FP02	2	CP2	17
FP03	--	CP3	24
FP04	--	CP4	24
FP05	1	CP5	15
FP06	2		
FP07	1		
FP08	1		
FP09	--		
FP10	19		
FG-Poster	4		
FP-General	5		
FT	--		

As of now this list is tentative and it is anticipated that this will need some amendments later.

Dr. J. Behari
Associate Coordinator Scientific Program

The preparation for the scientific programme is taking final shape. The abstract submission has been closed. The site worked well for on-line submission of abstracts. In few cases there were some problems and the abstracts were sent to us by e-mail. All the abstracts received through e-mail have been uploaded on the web-site by the organizer. In total more than 1800 abstracts have been processed including those withdrawn and/or resubmitted.

The final number of valid abstracts is more than 1550 which is almost the same as in the Maastricht General Assembly. The tentative distribution of abstracts among Commissions is as follow:

COM A	68
COM B	227
COM C	158
COM D	103
COM E	111
COM F	148
COM G	240
COM H	207
COM J	160
COM K	135

In the initial abstract submission, no provision was made to give session codes where the author would like to present his/her abstract. So authors have been requested to give us the session code where they would like to place their abstract. This information was incorporated in our database and sent to the respective commission chair persons. The review process at present is on and we are communicating to the authors about the status of their abstracts as and when we are receiving the review report from the commission chairman. We are receiving quite a good number of queries which are being responded promptly to avoid any confusion.

Hopefully, very soon all authors will be communicated the notification on the status of abstracts. This communication includes the session where this abstract will be presented. The date and time of all sessions is already available on the web-site and the exact time of presentation in a particular session will be given in the technical programme which will be sent to all authors well in advance.

By 15 June, full proceedings versions of all papers must be received electronically in pdf format. Thus all colleagues who have enthusiastically submitted their abstracts must be busy with the preparation of the Proceedings abstracts and we look forward to meet all of you at the URSI meeting in New Delhi, India in October this year.

The on-line registration has also been started and we have kept a provision for on-line payment or pay later. Also we have given the pdf file of registration form on the web-site, so that one can fill it up and send us in case one does want to register on-line. We are receiving a good number of applications for hotel bookings also.

On behalf of the Local Organizing Committee,
P. Banerjee, Convener, URSIGA2005

ATTEND THE XXVIIITH URSI GENERAL ASSEMBLY

All the radio scientists are invited to attend the XXVIIIth General Assembly of URSI, to be held at New Delhi, India in October this year. All the attendees are urged to make the travel plans, hotel reservations and to register for the General Assembly as early as possible. Complete information, including on-line registration, registration form etc. is available on web-site: http://ursiga2005.org

The Scientific Program

The Scientific Program of the General Assembly includes individual sessions of the ten commissions, and joint sessions organized by two or more commissions on topics of common interest (a report on the status of the scientific program appears elsewhere in this bulletin: more than 1550 abstracts have been submitted). Each commission will also offer tutorials delivered by distinguished scientists.

Prior to opening ceremony one workshop will be held on rural communication on 23rd Oct. 2005. There are two public lectures on popular topics to be delivered on 25th and 27th Oct. during the assembly. These lectures are (1) Electronic connectivity to billion people by A.P.J. Abdul Kalam, Hon'ble President of India and (2) 100 years of Radio Science in India by V. Radhakrishnan. Apart from these there will be three general lectures on (1) Solar Power Satellites on 24th Oct. (2) UWB Systems And Spectrum Management on 26th Oct. and (3) Impacts of Extreme Solar Disturbances on the Earth's Near-Space Environment 28th Oct.

There will be an exhibition during the assembly period. The internet facility will be available for the conference participants.

Venue

The General Assembly will be held at Vigyan Bhawan which is located in the heart of New Delhi, the capital city of India. Vigyan Bhawan is large enough to provide ample

space to hold the 2005 General Assembly. All the sessions will be held in the same building or the adjoining building.

New Delhi (28° 38' N, 77° 10' E) - the host city for the URSI - GA 2005 - the capital city and the nerve center of India, is a sprawling metropolis with a fascinating blend of the past and the present. Delhi has grown steadily and today it possesses some of the finest examples of ancient, as well as modern architecture. Delhi features monuments, mausoleums, places of worship, forts and business centres, universities, gardens and stadia. Spread over an area of 1483 sq.km at 216 mtrs. above mean sea level, Delhi is "India in Miniature" where the essence of every culture and tradition is felt and is a feast for one with a keen sense of interest in history and architecture.

Delhi is on the map of major International Airlines. Indian Airlines, private airlines and Indian Railways link Delhi to all major places in India.

For VISA one may contact Indian Embassy in the respective country.

Thomas Cook (I) Limited will arrange reception counter at International airport at New Delhi. Chauffeur driven cars and metered taxies are freely available. Kindly send your arrival details to arrange them well in advance.

Social Activity

A comprehensive social program is planned in conjunction with the scientific sessions. The Opening Reception, on Sunday, the 23 October is included in the registration fees. Kindly note that the General Assembly will be inaugurated on Sunday, the 23 October by Hon'ble President of India. He will also give a public lecture on 25th October. A cultural function will be held on 25th October followed by High Tea. A Young Scientist Party will be held on 24th October. Banquet will be held on 26th October. (Dates of social activities may change.)

As in the previous General Assemblies, URSI has encouraged for the participation of Young Scientists. These awardees are given free boarding/lodging, free registration, a given amount of money and in certain cases their travel is also supported. President of India will meet the Young Scientist Awardees in his official residence, Rashtrapati Bhawan. This is a special honour for awardees.

For accompanying persons, some social program functions are being worked out separately. A full range of pre and post sight-seeing tours is available for participants and the details of these tours are available on the web-site http://www.ursiga2005.org

Registered participants and students may attend all scientific sessions and Opening Ceremony and reception. They will also receive copies of *Proceedings* on CD-ROM. Coffee and Tea during breaks for all participants are included in the fee.

A limited number of hotel rooms New Delhi have been kept for the participants. However they have to book these rooms by 30th June 2005. The on-line registration has also been started and we have kept a provision for on-line payment or pay later. Also we have given the pdf file of registration form on the web-site, so that one can fill it up and send us in case one does want to register on-line.

Registration

	Foreign	Indian
Participant		
Upto 30 June	450 USD	Rs. 5000
After 30 June	500 USD	Rs. 6000
Students*		
Upto 30 June	300 USD	Rs. 3000
After 30 June	350 USD	Rs. 4000
Accompanying Person	75 USD	Rs. 1000

*Ph. D. Students have to enclose a proof of full time student status or a letter of endorsement from the supervisor.

XXVIIIth URSI GENERAL ASSEMBLY
October 23-29, 2005, New Delhi, India

REGISTRATION FORM

Kindly fill the following details and mail this Registration Form to us.

Family Name _____ First Name _____

Occupation _____

Address

_____
_____
_____

Country _____ Nationality _____

Telephone (Work) _____ (Home) _____
Fax _____ Email _____

Passport details (Foreign nationals only):

Passport No.	Date of Birth	Place of Issue	Date of Issue	Date of Expiry

Payments:
Indian delegates and delegates from SAARC countries can pay the Registration Fee in Indian Rupees. All other delegates are required to pay in US Dollars.

Payment may be made in advance or at the venue at the time of Conference.

Payment Mode:

A delegate can pay through one of the following modes:

- By Demand Draft in favour of "URSI GA 2005", payable at New Delhi, India
- By Bank Transfer using
- Swift Code: SYNBINBBA019 Account No.: 91001010000142 Account Name: URSI-GA 2005

Fax copy of the Transfer Form to Thomas Cook

- By Credit Card [fax (a) and (b) below to Thomas Cook (I) Limited]:

(a) Clear photocopy of both sides of your credit card
(b) Fill up the following details and fax to Thomas Cook

I authorize Thomas Cook (India) Ltd. To Charge US$ _____ to my credit card No. _____ expiry date _____
(Visa/MasterCard/American Express **ONLY**)_____ Card Holder's Name _____ Signature _____

Fax Credit Card details (a) and (b) to: Mr. Sudip Sinha, Sr. Executive – Conferences, Thomas Cook (I) Limited, Rishyamook Building, 85-A, Panchkuin Road, New Delhi – 110 001, India. Tel: (+91 11) 23383111 or 23747404 Fax: 23367469

Mail this Registration form to: Dr. P. Banerjee, National Physical Laboratory, Dr. K. S. Krishnan Road, New Delhi – 110 012, India. Telefax: +91 11 25841506

Registration Fees

	Foreign Participants	Indian Participants
Participants		
On or Before 30 June, 2005	450 USD	Rs. 5000
After 30 June, 2005	500 USD	Rs. 6000
Ph. D. Students*		
On or Before 30 June, 2005	300 USD	Rs. 3000
After 30 June, 2005	350 USD	Rs. 4000
Accompanying person	75 USD	Rs. 1000

*Ph. D. Students have to enclose a proof of full time student status or a letter of endorsement from the supervisor.

Each foreign participant / accompanying person will have to pay total US$ 50.00 for lunches during the conference. Those who would like to attend Banquet will have to pay an additional amount US$ 35.00

.

Hotel Reservation

On-line hotel reservation has already been started. Participants are requested to visit web-site http://www.ursiga2005.org for hotel details and they may contact our PCO (Professional Conference Organizer) at the following address, if necessary.

Mr. Sudip Sinha
Thomas Cook (India) Ltd
Rishya Mook Building
85-A, Panchkuin Road
New Delhi 110 001, India
Email : thomascookconferences.newdelhi@in.thomascook.com

Guest Editor's Remarks

On February 6, 2005, Dr. Carl Edward Baum celebrated his 65th birthday. To commemorate this occasion, the March and June, 2005, issues of the URSI *Radio Science Bulletin* are dedicated with special sections in honor of this outstanding scientist and engineer, for his unique personality and his excellent scientific achievements in the field of electrical engineering. Some of his friends, former and present colleagues, and collaborators chose the publication of these two special issues to express their affection, high esteem, kudos, gratitude, and pleasure to their partner and friend. In particular, the two guest Editors have had a close, amicable, long-term, scientific collaboration with Dr. Baum. We hope that you, the reader, will derive as much pleasure and scientific benefit from reading the papers as the contributing authors had preparing their interesting and valuable contributions. Further, we want to inform the reader that although the figures in the printed version of the March and June issues will appear with figures in black and white, color versions are also available in the downloadable files on the URSI Web site (http://www.ursi.org).

Since the first of the dedicated papers deals with Dr. Baum's remarkable career, we restrict ourselves here to mentioning selected characteristic properties of his personality. On viewing his long list of outstanding technical achievements and musical compositions, one naturally expects an individual who possesses highly focused, goal-oriented, scientific, managerial, and organizational qualities. The numerous honors and awards recognizing Dr. Baum attest to the fact that he excels in these qualities. With an extraordinary dedication to his profession and through the sheer force of his personality, he has promulgated and expounded his science with an almost evangelic fervor in many countries. In addition to significant contributions to general electromagnetic problems, his name stands out within the Nuclear Electromagnetics (NEM) community. In particular, NEMP simulators, which are located all over the world, are calculated, designed, and constructed on the advice of Carl Baum. Even former adversaries – now friends – respectfully acknowledge his contributions to EMP simulators and related topics. In recent times, Dr. Baum's efforts have concentrated on the invention and improvement of ultra-wideband antennas and their deployment in the field.

While Dr. Baum dedicates much of his time to technical endeavors, he has an avocation that deserves mention. Not only is he an accomplished pianist, but he also is an outstanding composer of classical and religious music. Symphonic groups in the US and Europe have played his compositions, and a number of CDs of his music have been recorded. His mathematical insight, which is so useful for his EM research, is also apparent in the highly complex structure and rich content of his music.

The authors, Editors, colleagues, and friends dedicate the subsequent two issues of the URSI *RSB* to Carl Edward Baum on the occasion of his sixty-fifth birthday. We wish him health, enduring creative power, and success in the coming years, and hope that our modest tribute to this extraordinary, distinguished scientist conveys our deep gratitude, affection, and admiration.

Jürgen Nitsch
Frank Sabath

Jürgen Nitsch is with the Institute of Fundamental Electrical Engineering and EMC, Otto-von-Guericke-University, Universitätsplatz 1, D-39106 Magdeburg, Germany; Tel: +49 (391) 671-8387; Fax: +49 (391) 671-1236; E-mail: juergen.nitsch@et.uni-magdeburg.de

Frank Sabath is with the Electromagnetic Effects Branch of the Federal Armed Forces Research Institute for Protective Technologies, Humboldtstrasse 1, D-29633 Munster, Germany; Tel: +49 (5192) 136 606; Fax: +49 (5192) 136 355; E-mail: FrankSabath@bwb.org.

Dr. Carl Baum: One Remarkable Career

W.D. Prather
D.V. Giri
R.L. Gardner

Abstract

In a career that has spanned more than four decades, this remarkably creative engineer has introduced innumerable new concepts in mathematics, electromagnetic theory, and system design, many of which remain the standards of excellence today. From his earliest designs in electromagnetic pulse (EMP) sensors and simulators to the latest developments in high-power microwave and ultra-wideband antenna and system design, Dr. Carl Baum's research has remained ever on the forefront of technology. His advances in EM theory have left an indelible mark and a lasting legacy on the technical world, and have led to much of what we do today in EMP, high-power microwaves (HPM), and target identification (ID).

Dr. Baum continues to be a prolific writer and publisher, and has written many technical notes, articles, and books. He is the Editor of the *Note Series* that has published state-of-the-art research results for the past 40 years. The *Note Series* [1-3] is still one of the foremost references of current research in the world. He has published four authoritative books, 63 book chapters, and a very large number of technical notes on electromagnetics and mathematics. Among other things, he still heads the SUMMA Foundation that he established in 1984, a non-profit organization that sponsors grants to deserving young researchers the world over, as well as sponsoring short courses, symposia, and the publication of books.

1. Introduction

Dr. Carl E. Baum, whose likeness is shown in Figure 1, was born in Binghamton, New York, on February 6, 1940. He received his BS (with honors), MS, and PhD degrees in Electrical Engineering from the California Institute of Technology, Pasadena, CA, in 1962, 1963, and 1969, respectively. Following his BS, he received his commission in the Air Force and was stationed at the Air Force Weapons Laboratory at Kirtland AFB, Albuquerque, NM. He served from 1963 until 1971 as an officer, and then accepted the civilian position of Senior Research Engineer that he holds today, at what is now the Air Force Research Laboratory. During his military career, he was awarded the Air Force Research and Development Award and the Air Force Nomination to Ten Outstanding Young Men of America, and became the Editor of the well-known *Note Series* on the nuclear electromagnetic pulse (EMP) and related subjects. Since becoming a civilian employee, he has received the Richard R. Stoddart award of the IEEE EMC Society (1984), and the Harry Diamond Memorial Award (1987), the AFSC (Air Force Systems Command) Harold Brown Award (1990), and the Air Force Basic Research Award (Honorable Mention) (1999). In addition, he has received five Best Paper Awards from the AMEREM /EUROEM Awards Committee, and he and his research team have been honored as an AFOSR Star Team for 2000-2002, and received the first annual R. Earl Good Award from AFRL (Air Force Research Laboratory) (2004), for their work in target identification. He was named an IEEE Fellow in 1984, an EMP Fellow in 1986, and the first AFRL Fellow

Figure 1. Dr. Carl E. Baum

William D. Prather is with the High Power Microwave Division, Air Force Research Laboratory, 3550 Aberdeen, SE, Kirtland AFB NM 87117, USA; E-mail: pratherw@aol.com.
D. V. Giri is with Pro-Tech, 11-C Orchard Court, Alamo, CA 94507-154, USA; E-mail: Giri@DVGiri.com.

Robert L. Gardner is a consultant at 6152 Manchester Park Circle, Alexandria, VA 22310, USA; E-mail: Robert.L.Gardner@verizon.net.

This invited paper is part of the special section honoring Carl E. Baum on his 65th birthday

in 1996. However, the honor that means the most to him came in July of 2004, when he was bestowed an Honorary Doctorate of Engineering by Otto von Guericke University in Magdeburg, Germany, during EUROEM 2004, and received a special honor from his colleagues in Russia for his lifetime of achievements. He has published four books: *Transient Lens Synthesis: Differential Geometry in Electromagnetic Theory*; *Electromagnetic Symmetry*; *Ultra-Wideband, Short-Pulse Electromagnetics-3*; and *Detection and Identification of Visually Obscured Targets*. He is a member of Commissions A, B, and E of the US National Committee of the International Union of Radio Science (URSI). He is founder and President of the SUMMA Foundation, which sponsors various electromagnetics-related activities, including scientific conferences, publications, short courses, fellowships, and awards. He has led EMP short courses and HPE (high-power electromagnetics) workshops around the globe.

Dr. Baum has always been an active organizer of scientific conferences and workshops that bring together researchers from all over the United States and the world to share the latest in electromagnetic research. The technical meetings began in 1974, with the first Forum for Understanding the Latest Methods in the EMP Notes (FULMEN), held at the (then) Air Force Weapons Laboratory (AFWL). These were subsequently replaced by the Nuclear Electromagnetics Meetings (NEMs) in 1978, which continued on until the beginning of the AMEREM/EUROEM meetings, with which we are all now familiar. The first EUROEM meeting was held in Bordeaux in 1994. With the changes that were then occurring in world politics and defense, the new meetings expanded to include ultra-wideband/short-pulse and unexploded ordnance (UXO) detection and identification technologies, but continued to include EMP research under the title of high-power electromagnetics (HPE). The first two UWB/SP meetings were hosted by Leo Felsen at Brooklyn Polytechnic University in 1992 and 1994 [4, 5]. However, in 1994, these meeting were absorbed into the AMEREM/EUROEM meetings, a practice that has continued on a biennial basis ever since. The subsequent meetings have been AMEREM 1996 in Albuquerque, EUROEM 1998 in Tel Aviv, EUROEM 2000 in Edinburgh, AMEREM 2002 in Annapolis, and, most recently, EUROEM 2004 in Magdeburg, Germany. Selected proceedings from the UWB/SP part of the meeting have been published each time in an attractive hardback book [6-10]. The next two meetings, which are in the planning stages, are AMEREM 2006, to be held in Albuquerque (in conjunction with the IEEE/AP-S/USNC/URSI), and EUROEM 2008, to be held in Lausanne, Switzerland.

In addition to the scientific conferences and workshops, Dr. Baum has also organized and served as lead instructor for numerous short courses in EMP and HPM. The EMP course, entitled EMP Interaction and Hardening (EMP 201), was first held at New Mexico Tech in Socorro, NM, in 1983. Since then, there have been eight additional short courses offered in Nottingham, England (1984); Interlaken, Switzerland (1985); Socorro NM (1985); Yxnerum, Sweden (1986); Karmiel, Israel (1987); Ann Arbor MI (1988); and Bangalore, India (1989). The latest short course, in high-power microwaves, was called High-Power EM: Environments, Interaction, Effects, and Hardening (HPE 201), and was presented at NM Tech in Socorro in July, 2003.

Dr. Baum has also organized and presented over two dozen workshops on EMP, EM theory, antennas, UWB technology, target identification, and high-power electromagnetics at universities, laboratories, and research institutes in numerous countries across the globe.

When not putting his new ideas in mathematics and electromagnetics (EM) into new technical notes or organizing meetings, Dr. Baum enjoys playing the piano and creating his own musical compositions, many of which have been heard at the biennial AMEREM and EUROEM conferences. His compositions can also be heard at one of the many churches in Albuquerque that host the annual concerts of the Albuquerque Symphony Orchestra and Chorus, and even at his own church, where he used to be the choir director. Twenty-three of these compositions have been recorded and are available on CDs, just for the asking.

Dr. Baum has mentored many graduate students, post docs, visiting scientists from Europe, and all young engineers who were eager to learn and to have the opportunity to co-author a paper with him. Singaraju, Giri, Wilton, Tesche, Nitsch, Farr, Parmantier, and many others have worked with Dr. Baum on a wide range of topics.

This special issue of the *Radio Science Bulletin* is being prepared to honor the occasion of Dr. Baum's 65th birthday on February 6, 2005. It has been assembled by friends and colleagues who have known Dr. Baum for many, many years, and consider it an honor to be asked to compile this very special article.

Some of his career accomplishments were described in an earlier article, published in 1989 [11]. In this paper, we will seek to bring that list up to date. We have had the pleasure of working with Dr. Baum for most of our professional careers, and it is an honor to be able to show our appreciation for his friendship and professional leadership during that time by presenting this review of the major highlights of his career.

2. Electromagnetic Theory

Much of Dr. Baum's early work centered on the development of sensors and simulators for evaluating the effects of nuclear electromagnetic pulse (NEMP). This was a new phenomenon at the time, and required new research and new understanding of transient fields that were at once of very high energy and extremely wide instantaneous bandwidth. Up to that time, little attention had been paid to ultra-wideband transient phenomenon, but with the advent

of the nuclear age, it became important not only for EMP, but for radiation and other effects. This required the development of antennas, pulsed power, and sensors that would radiate and receive transient fields and currents over several decades of frequency with little or no dispersion. It was also required to deliver uniform fields at high levels to very large test objects. Thus was first born the research into wideband electromagnetics that persists today.

2.1 Transmission lines

Parallel-Plate Transmission Lines: Much of the early research in EMP was devoted to transmission lines, especially parallel-plate transmission lines, which became the basis for some of the EMP simulators, such as ALECS, ARES, and ATLAS-I (Trestle) [12-14].

Multi-Conductor Transmission Lines: Advances in transmission-line theory [15-17] also found widespread use in the design of EMP sensors and instrumentation, and new analytical tools to help understand the interaction of this wideband phenomenon with test objects. Understanding of multi-conductor transmission lines was also important because it was an important part of the development and application of EM topology, as seen below. Such research remains important today, as we move from the relatively low-frequency EMP fields to the higher frequencies found in ultra-wideband (UWB) transient radars.

2.2 EM Interaction and Coupling

SEM and EEM: Dr. Baum conceived of the Singularity Expansion Method (SEM) and its companion, the Eigenmode Expansion Method (EEM), in order to better understand the coupling of EMP to aircraft and missiles [18-22]. It was, of course, later applied quite extensively to the new theory of resonant scattering for target identification for aircraft, unexploded ordnance (UXO), and concealed objects of various kinds. Today, it still forms the basis for much of our target ID work.

2.3 EM Scattering

Target Identification: Dr. Baum combined the best features of SEM, EEM, and symmetry to form the theoretical basis for his work in target identification. The first applications were to the detection and identification of unexploded ordnance (UXO). In recent years, this has been expanded to include a wide variety of concealed objects [23-28].

2.4 Electromagnetic Topology

EM Topology and Topological Decomposition: The concept of electromagnetic topology and topological decomposition was developed as a way of breaking down a shielded system into smaller pieces, in order to make the analysis more tractable [29]. Of course, it leads one to the proper way to think about EM shielding: how to design it and how to analyze it.

2.5 Coupling Phenomena

Norms and Bounds: In an electromagnetically complex structure, there are typically many coupling paths for the EM energy to reach a terminal or port of interest. In addition, there are many ports of interest, which makes the data set of coupling measurements quite voluminous. Dr. Baum devised ways of understanding the complex coupling phenomena via a set of scalar norms and upper bounds [30-35]. Each of these norms is associated with an effect in the electronic subsystem or component. The bounds permit one to predict that somewhere in the deep layers of the system, the coupled signals can not exceed certain levels. The hardness design and maintenance of complicated systems are significantly aided by such an approach.

2.6 Symmetry

Symmetry: Anyone who has worked with Dr. Baum gets used to hearing about symmetry [36-38]. Although fewer papers have actually been written on symmetry itself, it permeates much of his work. It is found in his designs of sensors, antennas, simulators, target ID theory, shielding, and analysis methods. The most complete description of the fundamentals of symmetry is found in [38].

3. Electromagnetic Pulse Sensors and Simulators

3.1 Sensors

One of the first applications of electromagnetic pulse (EMP) sensor technology was the development of the Weapon Effects Buoy System (WEBS, shown in Figure 2) that (then) LT. Baum and his colleagues developed and tested in the Bahamas [39]. It was literally a floating EMP sensor on a barge, as can be seen in Figure 2.

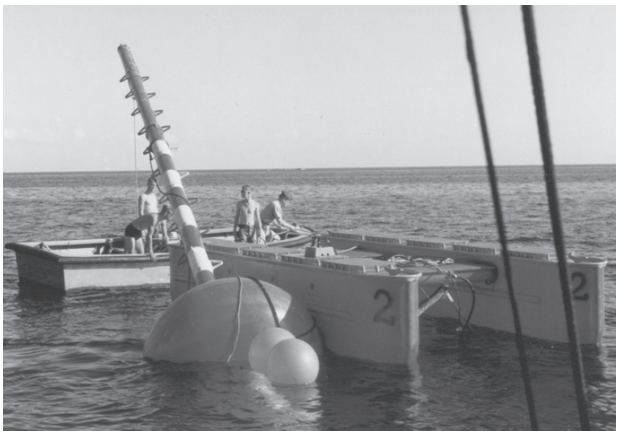

Figure 2. WEBS: LT. Baum gets his sea legs during field trials near Nassau in 1965.

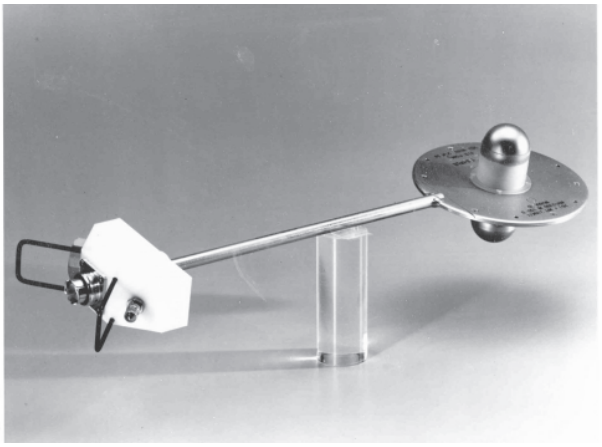

Figure 3. D-dot sensor: This electric field sensor is but one example of the wide variety of sensors designed by Dr. Baum.

Later, with assistance and manufacturing capability from EG&G, Dr. Baum created a whole catalog full of electromagnetic-field [40-42] and current sensor designs, which are still the standard today. From the large, low-frequency sensors to very tiny, high-frequency models, we have used these on virtually all our work in EMP, HPM, and UWB measurements. In Figure 3 there is an example of an electric-field (D-dot) sensor, commonly used for both EMP and HPM measurements today.

3.2 Simulators

One of the first EMP simulators to be fielded was the Radiating Electromagnetic Simulator (RES) I. The RES I, or Flying Dipole (seen in Figure 4) as it came to be known, consisted of a 2.3 MV Marx generator feeding a 120 W bi-cone in the center [43]. The late-time antenna was a 100-foot-long inflated fiberglass dipole, with periodic resistive loading to shape the late-time radiated field. The system was manufactured in both horizontal and vertical versions, and was carried over the site to be tested by a Chinook helicopter. The horizontal model is shown in Figure 4.

The early nuclear electromagnetic pulse (NEMP) simulators were of the parallel-plate transmission-line type,

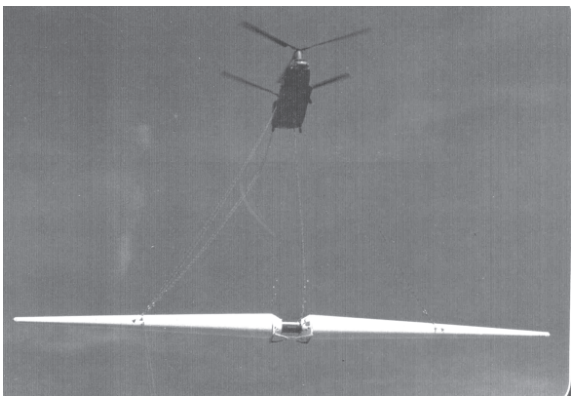

Figure 4. RES I : The Flying Dipole is shown here carried by a Chinook helicopter, ready to deliver a pulse to targets below.

Figure 5. ATHAMAS-I: The ATHAMAS I simulator was commonly called the horizontally polarized dipole or HPD. Two 4 MV Marx generators supplied the pulsed power for this simulator.

such as ALECS, ARES, and SIEGE [44]. DISCUS was a concept that was demonstrated to simulate the high-frequency propagation along the air-Earth interface and the low-frequency penetration into the ground, which was simulated by a parallel-plate transmission line under the ground.

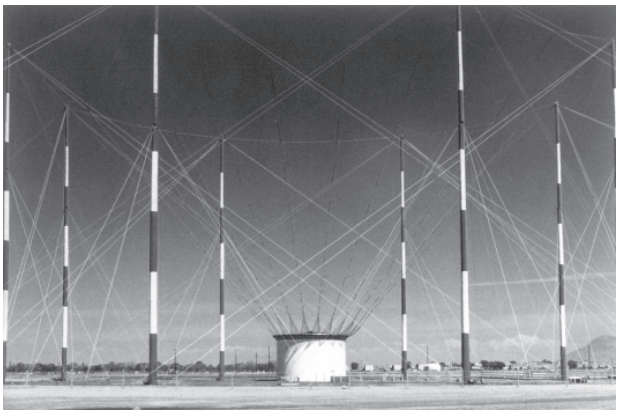

Figure 6. ATHAMAS-II: The ATHAMAS II simulator was commonly called the vertically polarized dipole II or VPD II. A 5 MV Marx generator is located beneath the simulator.

ATHAMAS I, seen in Figure 5, was an elliptical loop type of simulator, with a largely horizontal electric field simulation [45]. ATHAMAS II, seen in Figure 6, was a resistively loaded mono-cone radiator, producing a vertically polarized NEMP simulation. ATHAMAS II has also been used in EMP tests in an aircraft flyby mode. NAVES/EMPRESS, seen in Figure 7, was similar to ATHAMAS-II, except it was built on a barge out on the sea, designed for EMP testing of ships. Then came the world's largest parallel-plate transmission-line type of simulator, ATLAS-I (Figure 8). This simulated a horizontally polarized, horizontally propagating EMP environment for EMP tests of large aircraft. ATLAS-I [46] was designed by Dr. Baum to avoid the ground bounce, and was thus suitable for simulated tests of aircraft in flight.

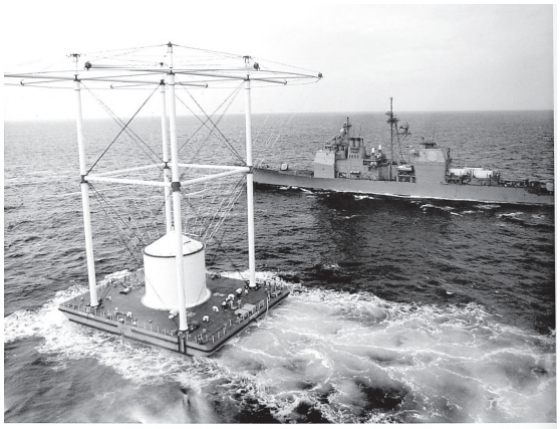

Figure 7. EMPRESS II: The Navy commissioned this version of the VPD to test their ships at sea.

With many EMP-hardened aircraft coming into the inventory, it was desirable to develop technology that could be used for surveillance and maintenance. A number of designs for low-voltage, swept-frequency systems were tried, but the most satisfying was undoubtedly the Ellipticus. Built of a single strand of coaxial cable, it employed a novel method of achieving the resistive loading needed for proper pulse shaping, and a unique wideband balun design. It was the same overall shape as the ATHAMAS I, but only two-thirds as large. As a result, it produced much the same spatial distribution and impedance of fields as did its big brother. In order to demonstrate its usefulness, a test-bed aircraft was placed in each simulator, in turn, and the results were compared with the help of the Fourier transform. The results were almost identical. Details can be found in [47-49]. As Dr. Baum's sensor and simulator concepts and designs found increasing use in the US, other countries began to build their own systems. At last count, EMP simulators were being built and used in at least 12 other countries worldwide.

3.3. EMP Interaction

Several researchers followed Dr. Baum's lead in the important area of EMP interaction [50, 51], which ultimately resulted in the publication of a widely used book [52]. Many of his contributions in EM interaction were described in the EM theory section, because his advances have also been applied to lightning and HPM interaction, as well.

4. Lightning

Beginning in the late 1970s, Dr. Baum applied his many skills developed in EMP to the problem of understanding lightning. This work began with the application of the new sensors developed in EMP research to a lightning facility called the Kiva, on South Baldy Peak, in south-central New Mexico. He applied his expertise in atmospheric physics and electromagnetic theory to better understand the complex nonlinear behavior of lightning and its interaction with systems. In the process, he became a much-sought-after advisor for several large lightning measurement programs in the United States and Europe. Finally, he applied the theory and data to quantify the differences between lightning and EMP on the surface of an aircraft.

4.1 Lightning Measurements

Lightning measurements – before Dr. Baum's application of EMP measurement techniques – were limited to sub-megahertz measurements, and were usually made with traditional bandlimited antenna designs. The EMP sensors and recording devices introduced by Dr. Baum allowed the recording of lightning waveforms to 10 ns resolution, and with windows out to 20 ms [53]. By the time the measurements were complete, in the 1980s, the Kiva facilities were able to simultaneously measure lightning currents, fields, and brightness, thereby opening the door to new understanding and fundamental comparisons with the newly developed lightning models [54-58].

4.2 Analysis

The analysis program was an important adjunct to the experimental program, since it allowed Dr. Baum to correlate various parts of the data sets and to set proper limits [54]. The fundamental limits came from a new, nonlinear transmission-line model that he developed, and the resulting characterization of the electromagnetic shock. Dr. Baum's picture of the initiation of the lightning channel was new to the community: it showed a leader propagating upward from the ground and meeting the downward-

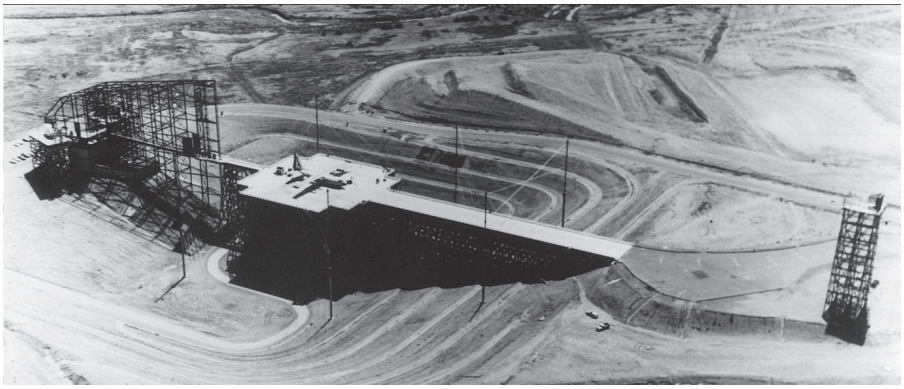

Figure 8. Trestle: The crown jewel of EMP simulators is undoubtedly the ATLAS I (Trestle), which is the only simulator capable of testing large aircraft in an in-flight mode.

propagating stepped leader. The model predicted an initial return-stroke propagation speed of near c, slowing to $c/3$ later in the stroke [56]. That prediction has since been confirmed by experiment.

4.3 System Tests and Analysis

Lightning interacts with aircraft and other complex systems through currents, charges, and fields. It is much more energetic than EMP, sufficiently so that it can cause mechanical damage. Dr. Baum's first fundamental contribution was to show that the charge transfer is as important as the surface currents for the prediction of lightning's effects on an aircraft [59, 60]. That understanding, the experimental work on lightning, and his pioneering analysis led many to seek his advice and guidance on large experimental programs. This work included the NASA F-106 program [61, Chapter 22], the CV-580 program at Wright-Patterson AFB [61, Chapter 23], and a number of French experimental and analytical efforts. This work was used to compare the coupling of lightning and high-altitude electromagnetic pulse (HEMP) to an aircraft in flight [61, Chapter 25].

5. High Power Microwaves

5.1 Hypo or Narrowband HPEM Systems

Dr. Baum has introduced a number of novel concepts into the hypo-band (or narrowband) high-power electromagnetic (HPEM) world [62]. Among these are the Phaser (pulsed high-amplitude sinusoidal electromagnetic radiation), the COBRA, and, most recently, the Traveling Wave Array Antenna.

The Phaser concept, developed in collaboration with Dr. D. V. Giri, was described in detail in [63-67]. A progression of potential Phaser designs was conceptualized as the "Mark N Phaser" in [66]. A Mark N Phaser is nominally defined by an output power of 10^N GW at a frequency of ~1 GHz: thus, a Mark 0 Phaser has an output power of 1 GW, nominally at 1 GHz. It consists primarily of a high-power microwave source and a paraboloidal reflector antenna illuminated by a pyramidal horn. Examples are to be found in [67].

The Coaxial Beam-Rotating Antenna (COBRA), developed in collaboration with Dr. C. Courtney [68], is a combination of a mode converter and a radiating structure, as shown in Figure 9. Using a segmented parabolic reflector, it effectively converts a TM_{01} field from a circular HPM source into a TE_{10} wave, and radiates it in a focused beam. It can produce either linearly or circularly polarized fields, and is surprisingly broad-band. This unique antenna system

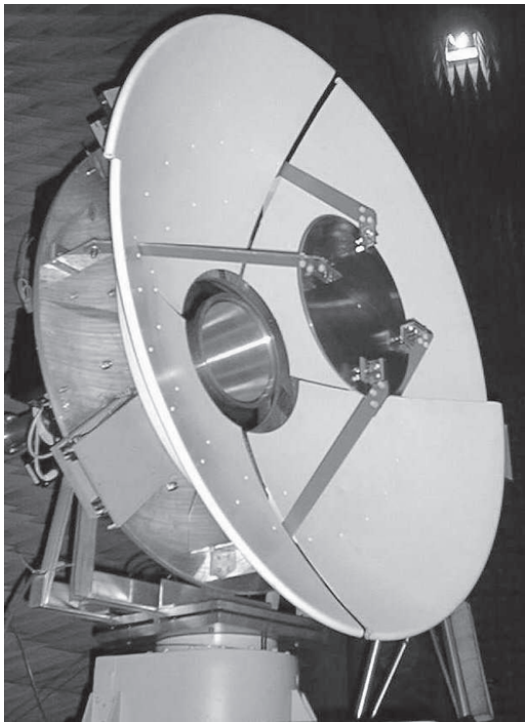

Figure 9. COBRA: The Coaxial Beam-Rotating Antenna (COBRA) is a combination of a mode converter and focusing antenna designed to operate from a circular waveguide.

was described in a feature article in the *IEEE Antennas and Propagation Magazine* [69], and earned the authors the Best Applied Paper Award at the 1998 EUROEM Symposium in Tel Aviv.

For HPM tubes that deliver their energy via a rectangular waveguide, the Traveling Wave Array Antenna concept was developed, in order to be able to deliver large bursts of power without causing air breakdown. The concept, as shown in Figure 10, is to segment the waveguide, thereby dividing up the energy, and to then spread the field out before depositing it into the atmosphere. Details of this design can be found in [70].

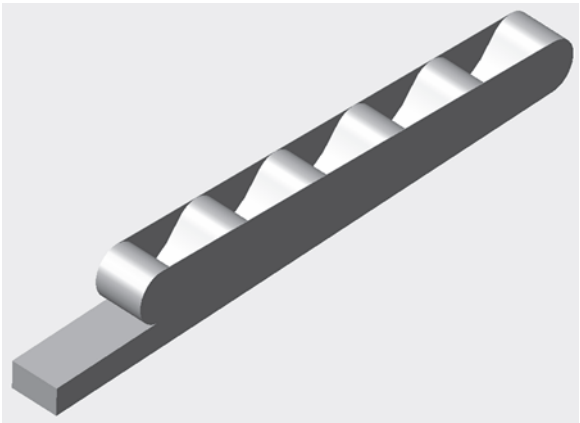

Figure 10. Traveling Wave Array Antenna: This unique antenna makes it possible to radiate high levels of microwave power from a rectangular waveguide.

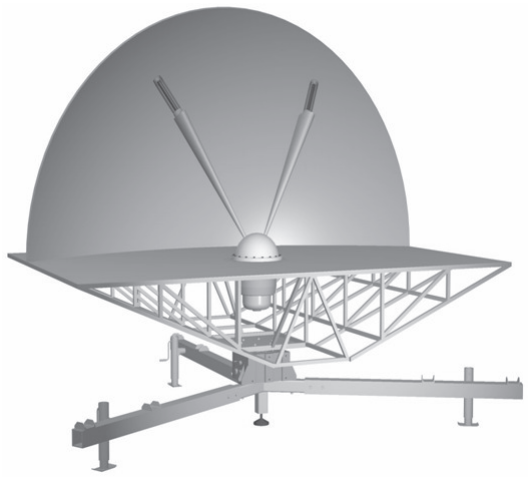

Figure 11. MATRIX: This system will deliver a tightly focused beam of meso-band energy.

5.2 Meso- or Moderate-Band HPEM Systems

Meso-band sources have been successfully designed and built to generate high-power electromagnetic (HPEM) energy between 100 and 700 MHz, a frequency range not easily reached by current narrowband (electron-beam) technology. These sources are typically designed in one of two ways. One may feed a damped-sinusoidal waveform into a wideband antenna, or one may switch a wideband transient (from a Marx generator, for example) into an oscillating antenna, with perhaps elements of differing lengths, in order to radiate a broad range of frequencies. Following the first method, Baum described certain concepts that switch a high-voltage transmission-line oscillator into a wideband antenna [71, 72]. The oscillator consisted of a quarter-wave section of transmission line, charged by a high-voltage source. It employed a self-breaking switch at the lower end of the transmission line. When the switch closed, the system generated a damped-sinusoidal signal that was fed into a UWB antenna, such as half of an impulse-radiating antenna (IRA). The frequency and damping constant could be adjustable. An initial working model of this type of source, called the MATRIX (see Figure 11) began full-scale testing at AFRL during 2003. It consisted of quarter-wave transmission line charged to 150 kV, connected to a 3.667 m (12 ft) diameter half-IRA. The frequency of oscillation was adjustable between 180 and 600 MHz. It radiated a damped-sinusoidal waveform, as shown in Figure 12, with a peak electric field of 6 kV/m at 15 m, with about a 10% bandwidth (band ratio of 1.10). With the 300 kV charging supply that is planned, this source will radiate energy in the GW range.

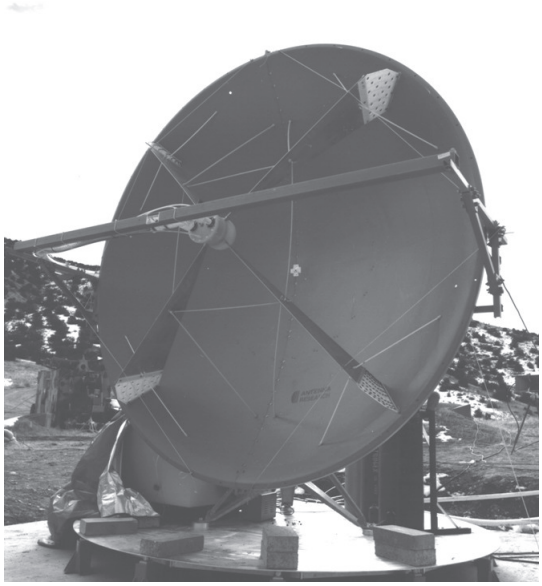

Figure 12. The IRA: The 4 m impulse-radiating antenna (IRA), built in 1994, opened up a new era in ultra-wideband, short-pulse technology.

5.3 Hyper-Band HPEM Systems

Dr. Baum suggested design concepts for two kinds of impulse-radiating antennas (IRAs): a balanced design [73-76] and an unbalanced design [77, 78]. The original IRA, developed and fielded in 1994, is shown in Figure 12. It was a balanced design that used a high-pressure hydrogen switch, a focusing lens, and a four-arm TEM horn to produce an extremely powerful hyper-band pulse from a 3.67 m reflector. With a charge of only ±60 kV, this system generated a transient signal with a peak electric field (E_p) of 4.6 kV/m at a distance of 305 m and a maximum pulse-repetition frequency (PRF) of 200 Hz. The radiated spectrum of the IRA has been measured to be flat from ~40 MHz to around 4 GHz, with a band ratio of ~100, or two decades.

The design of balanced hyper-band sources, such as the IRAs, presents some difficulties, particularly at very high voltages, where trigger jitter or balun design become issues. Therefore, in some cases it is preferable to design a half-IRA over a symmetry plane, so that the high voltage signal can be fed directly to the antenna from below the

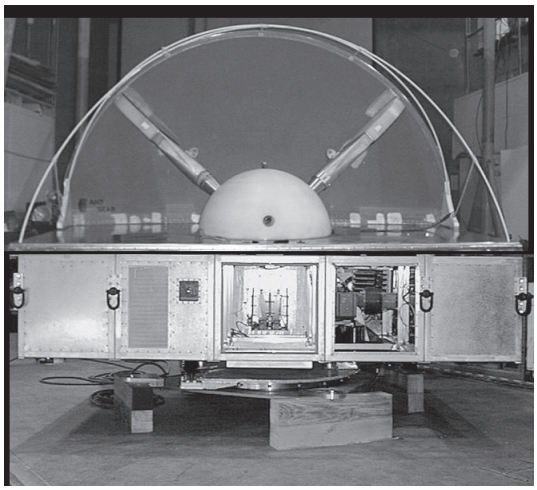

Figure 13. Jolt: Designed around a 1 MV resonant transformer and some unique new switches, this record-setting system will deliver very powerful UWB transients.

ground plane with a coaxial transmission line. Such designs make the high-voltage problem much more tractable, but they lack the uniformly symmetric field pattern of a full parabolic antenna, due to the presence of the finite ground plane [77, 78].

Under Dr. Baum's leadership, one such unit was built by the Air Force Research Laboratory in 1997-99, and named "Jolt" [77, 78]. This large, transient system was powered by a very compact 1 MV resonant transformer that was connected, via an integrated transfer capacitor and an oil-peaking switch, into an 85 Ω half-IRA. This unique system delivered a tightly focused radiated field with a FWHM on the order of 100 ps, and a field-range product of approximately 5.3 MV at 200 Hz. A photograph of the system is shown in Figure 13, and the performance features may be found in [77, 78]. The *Sensor and Simulation Note* describing this design [77] won the Best Applied Paper Award at the EUROEM 2004 meeting in Magdeburg, Germany.

6. Summary

In this paper, we have tried to summarize the valuable work in the theory and applications of electromagnetics contributed by Dr. Carl Baum. His career has spanned over four decades, and he has made significant and original contributions in the areas of EM sensors, NEMP simulators, generalized transmission lines, EM topology, antennas and scattering, SEM, EEM, EM interaction and coupling, lightning, and HPEM systems, such as Phasers, MATRIX, and the IRA. In addition to being a remarkable scientist and engineer, Dr. Baum has varied interests in music, philanthropy, and the arts. He heads the SUMMA Foundation, which sponsors research by young scientists and organizes short courses and technical workshops the world over. We were honored to be asked to write this paper, documenting major highlights of his career.

7. Acknowledgements

The authors would like to thank Prof. Jürgen Nitsch and Dr. Frank Sabath for serving as the Guest Editors of the special issue, honoring Dr. Carl Baum, and for giving us the opportunity to prepare this paper.

8. References

Copies of the *Notes* and *Memos* cited in the references and bibliography can be obtained from the authors, or from the series Editor, Dr. Carl Baum, Air Force Research Laboratory/DEHP, 3550 Aberdeen Avenue SE, Kirtland AFB, NM 87117, USA. Copies of the *Notes* may also be found at http://www-e.uni-magdeburg.de/notes/.

1. C. E. Baum (ed.), *Sensor and Simulation Notes (EMP 1), Notes 1-422*, 1964-1998, September 1999.
2. C. E. Baum (ed.), *Interaction Notes (EMP 3), Notes 1-568*, 1965-2001 (two CDs), June 2001.
3. C. E. Baum (ed.), *Miscellaneous Notes*.
4. H. L. Bertoni, L. Carin, and L. B. Felsen (eds.), *Ultra-Wideband, Short-Pulse Electromagnetics 1,* New York, Plenum Press, 1993.
5. L. Carin and L. B. Felsen (eds.), *Ultra-Wideband, Short-Pulse Electromagnetics 2,* New York, Plenum Press, 1995.
6. C. E. Baum, L. Carin, and A. P. Stone (eds.), *Ultra-Wideband, Short-Pulse Electromagnetics 3*, New York, Plenum Press, 1997.
7. E. Heyman, B. Mandelbaum, and J. Shiloh (eds.), *Ultra-Wideband, Short-Pulse Electromagnetics 4,* New York, Plenum Press, 1999.
8. P. D. Smith and S. R. Cloude (eds.), *Ultra-Wideband, Short-Pulse Electromagnetics 5*, New York, Plenum Press, 2001.
9. E. L. Mokole, M. Kragalott, and K. R. Gerlach **(**eds.), *Ultra-Wideband, Short-Pulse Electromagnetics 6,* New York, Plenum Press, 2003.
10. Frank Sabath et al. (eds.), *Ultra-Wideband, Short-Pulse Electromagnetics 7*, New York, Plenum Press, 2005, in press.
11. C. E. Baum, "A Career (To Date) in Electromagnetics," *IEEE Antennas and Propagation Newsletter*, **AP-31**, 6, December 1989, pp. 12-17.
12. C. E. Baum, "Impedance and Field Distributions for Symmetrical Two-Wire and Four-Wire Transmission Line Simulators," *Sensor and Simulation Note 27*, October 10, 1966.
13. C. E. Baum, "The Conical Transmission Line as a Wave Launcher and Terminator for a Cylindrical Transmission Line," *Sensor and Simulation Note 31*, 16 January 1967.
14. C. E. Baum, "A Circular Conical Antenna Simulator," *Sensor and Simulation Note 36*, 3 March 1967.
15. C. E. Baum, "High-Frequency Propagation on Non-uniform Multi-conductor Transmission Lines in Uniform Media," *Interaction Note 463*, January 1988.
16. C. E. Baum, "Approximation of Non-uniform Multi-conductor Transmission Lines by Analytically Solvable Sections," *Interaction Note 490*, 2 October 1992.
17. C. E. Baum, "Non-uniform Multiconductor Transmission Lines, *Interaction Note 516*, 2 February 1996.
18. C. E. Baum, "On the Singularity Expansion Method for the Solution of Electromagnetic Interaction Problems, *Interaction Note 88*, 11 December 1971.
19. C. E. Baum, "Singularity Expansion of Electromagnetic Fields and Potentials Radiated from Antennas or Scattered from Objects in Free Space," *Sensor and Simulation Note 179*, 25 May 1973.
20. C. E. Baum, "On the Eigenmode Expansion Method for Electromagnetic Scattering and Antenna Problems," *Interaction Note 229*, 13 January 1975.
21. C. E. Baum, "Scattering, Reciprocity, Symmetry, EEM, and SEM," *Interaction Note 475*, 31 May 1989.
22. C. E. Baum, "Properties of Eigenterms of the Impedance Integral Equation," *Interaction Note 487*, 1 April 1992.
23. C. E. Baum, "SEM Backscattering," *Interaction Note 476*, 19 July 1989.
24. C. E. Baum, E. J. Rothwell, K. M. Chen, and D. P. Nyquist, "The Singularity Expansion Method and Its Application to Target Identification," *Proceedings of the IEEE*, **79**, 10, October 1991, pp. 1481-92.
25. C. E. Baum (ed.), *Detection and Identification of Visually Obscured Targets*, New York, Taylor & Francis, 1998.
26. C. E. Baum, "Signature-Based Target Identification and Pattern Recognition," *IEEE Antennas and Propagation Magazine*, **36**, 3, June 1994, pp. 44-51.
27. C. E. Baum, "Discrimination of Buried Targets via the Singularity Expansion," *Interaction Note 521*, 4 August 1996.
28. C. E. Baum, "The SEM Representation of Acoustic and Elastodynamic Scattering," *Interaction Note 512*, 12 June 1995.
29. C. E. Baum, "On the Use of Electromagnetic Topology for the Decomposition of Scattering Matrices for Complex Physical Structures," *Interaction Note 454*, 1 July 85.

30. C. E. Baum, "Black Box Bounds," *Interaction Note 429*, 19 May 1983.
31. C. E. Baum, "Maximization of Electromagnetic Response at a Distance," *IEEE Transactions on EMC*, **EMC-34**, 3, August 1992, pp. 148-153.
32. C. E. Baum, "Transfer of Norms Through Black Boxes," *Interaction Note 462*, 30 October 1987.
33. C. E. Baum, "Norms of Vectors of Time-Domain Signals Passing Through Filters and Norm Limiters at Subshields," *Interaction Note 469*, 2 January 1988.
34. C. E. Baum, "Norms of Time-Domain Functions and Convolution Operators," in H. N. Kritikos and D. L. Jaggard (eds.), *Recent Advances in Electromagnetic Theory*, Heidelberg, Springer-Verlag, 1990, Chapter 2.
35. C. E. Baum, "Bounds on Norms of Scattering Matrices," *Interaction Note 432*, June 1983.
36. C. E. Baum, "Target Symmetry and the Scattering Dyadic," *Interaction Note 507*, 11 September 1994.
37. C. E. Baum, "Symmetry in Electromagnetic Scattering as a Target Discriminant," *Interaction Note 523*, 15 October 1996.
38. C. E. Baum and H. N. Kritikos (eds.), *Electromagnetic Symmetry*, New York, Taylor & Francis, 1995.
39. C. E. Baum, "Some Electromagnetic Considerations for a Sea-Water-Based Platform for Electromagnetic Sensors," *Sensor and Simulation Note 39*, 27 March 1967.
40. C. E. Baum, "Electrically Small Cylindrical Loops for Measuring the Magnetic Field Perpendicular to the Cylinder Axis," *Sensor and Simulation Note 78*, 17 March 1969.
41. C. E. Baum, E. L. Breen, J. C. Giles, J. P. O'Neill, and G. D. Sower, "Sensors for Electromagnetic Pulse Measurements Both Inside and Away from Nuclear Source Regions," *Sensor and Simulation Note 239*, January 1978; *IEEE Transactions on Antennas and Propagation*, **AP-26**, 1, January 1978, pp. 22-35; and *IEEE Transactions on EMC*, February 1978, .
42. C. E. Baum, "Electromagnetic Sensors and Measurement Techniques," in J. E. Thompson and L. H. Luessen, (eds.), *Fast Electrical and Optical Measurements*, Dordrecht, Martinus Nijhoff, 1986.
43. C. E. Baum, "Design of a Pulse-Radiating Dipole Antenna as Related to High-Frequency and Low-Frequency Limits," *Sensor and Simulation Note 69*, 13 January 1969.
44. C. E. Baum, "EMP Simulators for Various Types of Nuclear EMP Environments: An Interim Categorization," *Sensor and Simulation Note 240*, 1 January 1978; *IEEE Transactions on Antennas and Propagation*, **AP-26**, 1, January 1978, pp. 35-53; and *IEEE Transactions on EMC*, February 1978.
45. C. E. Baum, "Some Characteristics of Electric and Magnetic Dipole Antennas for Radiating Transient Pulses," *Sensor and Simulation Note 125*, 23 January 1971.
46. C. E. Baum, "General Principles for the Design of ATLAS I and II. Part I. ATLAS: Electromagnetic Design Considerations for Horizontal Version," *Sensor and Simulation Note 143*, 1 January 1972.
47. C. E. Baum, W. D. Prather and D. P McLemore, "Topology for Transmitting Low-Level Signals from Ground Level to Antenna Excitation Position in Hybrid EMP Simulators," *Sensor and Simulation Note 333*, 30 September 1991.
48. Y. G. Chen, R. Crumley, S. Lloyd, C. E. Baum, and D. V. Giri, "Field-Containing Inductors" with Y. G. Chen, R. Crumley, S. Lloyd, and D. V. Giri, *IEEE Transactions on EMC*, **EMC-30**, 3, August 1988, pp. 345-350.
49. C. E. Baum, "Winding Topology for Transformers," *IEEE Transactions on EMC*, **EMC-30**, 3, August 1988, pp. 358-363.
50. C. E. Baum, "Single Port Equivalent Circuits for Antennas and Scatterers," *Interaction Note 295*, 29 March 1976.
51. C. E. Baum, "EMP Simulation and its Impact on EMP Testing," *Sensor and Simulation Note 246*, 26 December 1978.
52. K. S. H. Lee (ed.), *EMP Interaction: Principles, Techniques, and Reference Data*, New York, Hemisphere Publishing Corp., 1986.
53. C. E. Baum, L. Baker, R. L. Gardner, A. H. Paxton, and W. Rison, "Simultaneous Measurement of Current, Electromagnetic Fields, and Optical Emission from a Lightning Stroke," *Electromagnetics*, 1987.
54. C. E. Baum, "Simulation of Electromagnetic Aspects of Lighting," in H. Kikuchi (ed.), *Environmental and Space Electromagnetics*, Heidelberg, Springer Verlag, 1991, Chapter 11.
55. C. E. Baum and R. L. Gardner, "An Introduction to Leader-Tip Modeling," *Electromagnetics*, 1986.
56. C. E. Baum, "Analytic Return-Stroke Transmission-Line Model," with L. Baker, *Electromagnetics*, 1987.
57. C. E. Baum, "Motion of Ion Clouds in Air," *Electromagnetics*, 1987.
58. C. E. Baum, "Electromagnetic Measurement of and Location of Lightning," with J. P. O'Neill, E. L. Breen, D. L. Hall, and C. B. Moore, *Electromagnetics*, 1987.
59. C. E. Baum, "Simulation of Electromagnetic Aspects of Lightning," *Lightning Simulation Note 1*, 10 February 1980.
60. C. E. Baum, E. L. Breen, F. L. Pitts, G. D. Sower, and M. E. Thomas, "The Measurement of Lightning Environmental Parameters Related to Interaction with Electronic Systems," *Sensor and Simulation Note 274*, May 1982.
61. R. L. Gardner (ed.), *Lightning Electromagnetics*, New York, Hemisphere Publishing, 1990.
62. C. E. Baum, "From the Electromagnetic Pulse to High-Power Electromagnetics," *Proceedings of the IEEE*, **80**, 6, June 1992, pp. 789-817.
63. C. E. Baum, "A Rational Approach to the Development of a HPM Weapon," *Microwave Memo 1*, October 1988.
64. C. E. Baum, "The Phaser," *Microwave Memo 2*, November 1988.
65. C. E. Baum, "Preliminary Near-Term Criterion for Single-Pulse HPM," *Microwave Memo 4, July 1991*.
66. C. E. Baum and D. V. Giri, "Mark N Phaser," *Microwave Memo 5*, February 1992.
67. C. D. Taylor and D. V. Giri, *High-Power Microwave Systems and Effects*, New York, Taylor and Francis, 1994.
68. C. C. Courtney and C. E. Baum, "Coaxial Beam-Rotating Antenna (COBRA) Concepts," *Sensor and Simulation Note 395*, April 1996.
69. C. C. Courtney, D. E. Voss, C. E. Baum, W. D. Prather, and R. J. Torres, "A Description and Measured Performance of Three Coaxial Beam-Rotating Antenna Prototypes," *IEEE Antennas and Propagation Magazine*, **AP-44**, 3, June 2002, pp. 30-47.
70. C. E. Baum, "High-Power Scanning Waveguide Array, Sensor and Simulation Note 459, December 2001.
71. C. E. Baum, "Switched Oscillators," *Circuit and EM System Design Note 45*, September 2000.
72. J. Demarest, D. V. Giri, et al., "Modular Low Frequency Oscillator Source," AFRL-DE-TR-2002-10038, Air Force Research Laboratory, Kirtland AFB NM, May 2002.
73. C. E. Baum, "Emerging Technology for Transient and Broadband Analysis and Synthesis of Antennas and Scatterers," *Interaction Note 300*, November 1976; AFRL-TR-78-502, Air Force Research Laboratory, Kirtland AFB NM; *Proceedings of the IEEE*, November 1976.
74. C. E. Baum, *Transient Lens Synthesis: Differential Geometry in Electromagnetic Theory*, with A. P. Stone, New York, Hemisphere Publishing Corp., Taylor & Francis, 1991.
75. C. E. Baum, "Focused Aperture Antennas," *Sensor and Simulation Note 306*, May 1987.
76. D. V. Giri, H. Lackner, I. D. Smith, D. W. Morton, C. E. Baum, J. R. Marek, W. D. Prather, and D. W. Scholfield, "Design, Fabrication, and Testing of a Paraboloidal Reflector Antenna and Pulser System for Impulse-Like Waveforms," *IEEE Transactions on Plasma Science*, **25**, 2, April 1997, pp. 318-326.
77. C. E. Baum, "Jolt: A Highly Directive, Very Intensive, Impulse-Like Radiator," with D. V. Giri, et al, *Sensor and Simulation Note 480*, November 2003.

78.C. E. Baum, et al., "Jolt: A Highly Directive, Very Intensive, Impulse-Like Radiator," *Proc. IEEE*, **92**, 7, July 2004, pp. 1096-1109.

9. Bibliography

In addition to the references cited above, we have also included this bibliography containing further references to Dr. Baum's published work arranged by topic.

General Electromagnetics

79.C. E. Baum, "Quantum Electrodynamics: Potentials, Gauge Invariance, and Analogy to Classical Electrodynamics," in M. Evans (ed.), *Modern Nonlinear Optics, Part II*, New York, Wiley, 2001.
80.C. E. Baum, "Generalized TEM, E, and H Modes," with A. P. Stone, *Electromagnetics*, 2003.

Transmission Lines

81. J. Nitsch, C. E. Baum, and R. Sturm, "Analytical Treatment of Uniform Multi-conductor Transmission Lines," *IEEE Transactions on EMC*, **EMC-35**, 2, May 1993, pp. 285-294.
82.C. E. Baum, "Neue analytische Lösungen für ungleichförmige Vielfachleiter," with J .B. Nitsch, *Elektromagnetische Verträglichkeit*, VDE-Verlag, Berlin, 1994.
83.C. E. Baum, "Analytical Solution for Uniform and Nonuniform Multiconductor Transmission Lines with Sources," with J. B. Nitsch and R. J. Sturm, in W. R. Stone (ed.), *Review of Radio Science 1993-1996*, Oxford, Oxford University Press, 1996.
84.C. E. Baum, "High Frequency Propagation on Non-uniform Multi-conductor Transmission Lines in Uniform Media," *International Journal of Numerical Modeling: Electronic Networks, Devices, and Fields*, December 1988.
85.C. E. Baum, "Analytische Lösung des nicht-gleichförmigen Merfachleiterproblems mit beliebigen Quellen," with J. Nitsch and R. Sturm, *Kleinheubacher Berichte, Deutsche Telekom*, **39**, Darmstadt, Germany, 1996.

SEM and EEM

86.C. E. Baum, "The Singularity Expansion Method," in L. B. Felsen (ed.), *Transient Electromagnetic Fields*, Heidelberg, Springer-Verlag, 1976, Chapter 3.
87.C. E. Baum, "The Role of Scattering Theory in Electromagnetic Interference Problems," in P. L. E. Uslenghi, (ed.), *Electromagnetic Scattering*, New York, Academic Press, 1978, Chapter 13.
88.C. E. Baum, "Toward an Engineering Theory of Electromagnetic Scattering: The Singularity and Eigenmode Expansion Methods," in P. L. E. Uslenghi (ed.), *Electromagnetic Scattering*, New York, Academic Press, 1978, Chapter 15.
89.C. E. Baum, "The Singularity and Eigenmode Expansion Methods with Applications to Equivalent Circuits and Related Topics," with B. K. Singaraju, in V. K. Varadan and V. V. Varadan (eds.), *Acoustic, Electromagnetic and Elastic Wave Scattering*, New York, Pergamon Press, 1980, Part 6, Chapter 3.
90.C. E. Baum, "SEM and EEM Scattering Matrices, and Time-Domain Scatterer Polarization in the Scattering Residue Matrix," in W.-M. Boerner, et al, (eds.), *Direct and Inverse Methods in Radar Polarimetry*, Dordrecht, Kluwer Academic Publishers, 1992, Chapters 1-9.
91.C. E. Baum,. "Properties of Eigenterms of the Impedance Integral Equation," in A. Guran, R. Mittra, and P. J. Moser, (eds.), *Electromagnetic Wave Interactions*, New York, World Scientific, 1996, Chapter 3.
92.C. E. Baum, "Representation of Surface Current Density and Far Scattering in EEM and SEM with Entire Functions," in P. P. Delsanto and A. W. Saenz (eds.), *New Perspectives on Problems in Classical and Quantum Physics, Part II: Acoustic Propagation and Scattering, Electromagnetic Scattering*, New York, Gordon and Breach. 1998, Chapter 13.
93.C. E. Baum, E. G. Farr, and D. V. Giri, in W. R. Stone (ed.), "Review of Impulse-Radiating Antennas" *Review of Radio Science 1996-1999*, Oxford, Oxford University Press, 1999, Chapter 16.
94.C. E. Baum, "Target Symmetry and the Scattering Dyadic," in D. H. Werner and R. Mittra (eds.), *Frontiers in Electromagnetics*, New York, IEEE Press, 1999, Chapter 4.
95.C. E. Baum, "Symmetry in Single-Polarization Reflector Impulse Radiating Antennas," *Radio Physics and Radio Astronomy*, **7**, 2002.
96.L. Carin, R. Kapoor, and C. E. Baum, "Polarimetric SAR Imaging of Buried Landmines," *IEEE Transactions on Geoscience and Remote Sensing*, **GRS-36**, 6, November 1998, pp. 1985-1988.
97.N. Geng, C. E. Baum, and L. Carin, "On the Low-Frequency Natural Response of Conducting and Permeable Targets," *IEEE Transactions on Geoscience and Remote Sensing*, **GRS-37**, 1, January 1999, pp. 347-359.
98.L. Carin, H. Yu, Y. Dalichaouch, A. R. Perry, P. V. Czipott, and C. E. Baum, "On the Wideband EMI Response of a Rotationally Symmetric Permeable and Conducting Target," *IEEE Transactions on Geoscience and Remote Sensing*, **GRS-39**, 6, 2001, pp. 1206-1213.
99.C. E. Baum, "Singularity Expansion Method, Symmetry and Target Identification," with L. Carin, in R. Pike and P. Sabatier (eds.), *Scattering*, New York, Academic Press, 2002.
100. C. E. Baum, "Perturbation of the SEM-Pole Parameters of an Object by a Mirror Object," with T. H. Shumpert and L. S. Riggs, *Electromagnetics,* 1989.
101.C. E. Baum, "Perturbation Formula for the Natural Frequencies of an Object in the Presence of a Layered Medium," with G. W. Hanson, *Electromagnetics,* 1998.
102.C. E. Baum, "General Scaling Method for Electromagnetic Fields with Application to a Matching Problem," with T. C. Mo, C. H. Papas, *Journal of Mathematical Physics*, April 1973.
103.C. E. Baum, "A Priori Application of Results of Electromagnetic Theory to the Analysis of Electromagnetic Interaction Data," *Radio Science Reviews*, 1987.
104.C. E. Baum, "Discrimination of Buried Targets via the Singularity Expansion," *Inverse Problems*, **13**, Bristol, UK, Institute of Physics Publishing, 1997.
105. C. E. Baum, "On the Convergence and Numerical Sensitivity of the SEM Pole-Series in Early-Time Scattering Response," with L. W. Pearson, *Electromagnetics*, 1981.
106.C. E. Baum, "The Singularity Expansion Method: Background and Developments," *Electromagnetics*, 1981.

EM Topology

107.C. E. Baum, "Electromagnetic Topology for the Analysis and Design of Complex Electromagnetic Systems," in J. E. Thompson and L. H. Luessen (eds.), *Fast Electrical and Optical Measurements*, Ddordrecht, Martinus, 1986.
108.C. E. Baum, "Electromagnetic Topology and Soil Effects Applied to EMC Problems" with P. Degauque and M. Ianoz, in W. R. Stone (ed.), *Review of Radio Science 1990-199*2, Oxford, Oxford University Press, 1993, Chapter 12.
109.C. E. Baum, "Topological Considerations for Low Frequency Shielding and Grounding," *Electromagnetics*, 1983.
110.C. E. Baum, "The Theory of Electromagnetic Interference Control," in J. B. Andersen (ed.), *Modern Radio Science 1990*," Oxford, Oxford University Press, 1990. Chapter 5.

Novel Antennas and Lenses

111.A. P. Stone and C. E. Baum, "An Anisotropic lens for Transitioning Plane Waves between Media of Different Permittivities," *IEEE Transactions on Antennas and Propagation*, **AP-36**, 11, November 1988, pp. 1571-1579.

112. C. E. Baum, "General Properties of Antennas," *IEEE Transactions on EMC*, **EMC-44**, 1, February 2002, pp. 18-24.

113.C. C. Courtney and C. E. Baum, "The Coaxial Beam-Rotating Antenna (COBRA): Theory of Operation and Measured Performance," *IEEE Transactions on Antennas and Propagation*, **AP-48**, 2, February 2000, pp. 299-309.

114.C. E. Baum, "Design of Two-Dimensional EM Lenses via Differential Geometric Scaling," with A. P. Stone, *Electromagnetics*, 1988.

115.F. J. Agee, C. E. Baum, W. D. Prather, J. M. Lehr, J. P. O'Loughlin, J. W. Burger, J. S. H. Schoenburg, D. W. Scholfield, R. J. Torres, J. P Hull, and J. A. Gaudet, "Ultra-Wideband Transmitter Research," *IEEE Transactions on Plasma Science*, **26**, 3, June 1998, pp. 860-873.

116.F. J. Agee, C. E. Baum, W. D. Prather, J. M. Lehr, J. P. O'Loughlin, J. W. Burger, J. S. H. Schoenberg, D. W. Scholfield, R. J. Torres, J. P. Hull, J. A. C. Gaudet, "Ultra-Wideband Transmitter Research," *IEEE Transactions on Plasma Science*, **26**, 3, June 1998, pp. 860-873.

117.D. V. Giri, J. M. Lehr, W. D. Prather, C. E. Baum, and R. J. Torres, "Intermediate and Far Fields of a Reflector Antenna Energized by a Hydrogen Spark-Gap Switched Pulser," *IEEE Transactions on Plasma Science*, **28**, 5, October, 2000, pp. 1631-1636.

118.W. D. Prather, C. E. Baum, R. J. Torres, Frank Sabath, and Daniel Nitsch, "Survey of Worldwide Wideband High Power Capabilities," *IEEE Transactions on EMC*, **EMC-46**, 3, August 2004, pp. 335-344.

119.Musical Compositions:

Opus 1, "Four Eucharistic Memorial Acclamations and Amen," SATB Choir, 1981
Opus 2, "My Peace," SATB Choir and Organ or Piano, 1981
Opus 3a, "Mass No. 1 in E flat," SATB Choir and Organ, 1982
Opus 4, "The Two Commandments," SATB Choir and Organ or Piano, 1981
Opus 5, "Mass No. 2 in B minor," SATB Choir and Organ, 1982
Opus 6, "Mary's Song" (Magnificat), SSA Choir, 1982
Opus 7, "The Beatitudes," Three Soloists, SATB Choir and Orchestra or Piano, 1983, 1995 (orchestration)
Opus 8, "In the Beginning," SATB Choir and Orchestra or Organ or Piano, 1983, 1996 (orchestration)
Opus 9, "Come to Me," SATB Choir, 1984
Opus 10, "God is Love," SATB Choir, 1986
Opus 11, "Give Thanks To The Lord," SATB Choir and Organ or Piano, 1989
Opus 12, "A Time To Be Born," SATB Choir, 1989
Opus 13, "Mass No. 3 in D," SATB Choir and Organ, 1991
Opus 14, "Sonata for Piano No. 1 in C minor, for Spencer," 1992
Opus 15, "Sonata for Piano No. 2 in C, Pastoral Sunday," 1994
Opus 16, "Brass Quintet No. 1 in B flat, AMEREM," 1996
Opus 17, "March No. 1 in E flat," Marching band, 1998
Opus 18, "Fanfare for Brass No. 1 in B flat," Septet, 1998
Opus 19, "String Quartet No. 1 in G minor," 2001
Opus 20, "Woodwind Quintet No. 1 in B flat," 2001
Opus 21, "The Lord is My Shepherd," Soprano solo and Orchestra, 2004
Opus 22, "String Quartet No. 2 in C," 2004
Opus 23, "Fanfare for Brass No. 2 in B flat," 2004

Global and Modal Parameters in the Generalized Transmission-Line Theory and Their Physical Meaning

J.B. Nitsch
V. Tkachenko

Abstract

For a thin-wire model, we establish the connection between the global and modal representation of the parameters for a generalized (full-wave) transmission-line theory (the parameters of the "Maxwellian circuits"). The modal parameters are contained in the coupling equations for each Fourier mode of the current. Both representations of the parameters, global and modal, are complex-valued, frequency- and gauge-dependent, and they depend on the local coordinate or on the modal number, respectively. The connection of the parameters with the radiation of the system is presented in an explicit form.

1. Introduction

The investigation of electromagnetic field coupling with linear structures – which constitute an essential part in electronic and electric circuits – is one of the main issues in electromagnetic compatibility. Nowadays, the characteristic frequencies for the signals used, as well as for the interferences, increase up to several GHz. Thus, some characteristic wavelength of the system may become comparable to the cross section of the line (or even less), and the classical transmission-line (TL) approximation is no longer applicable. There then arises the problem of generalizing the transmission-line equations to include radiation corrections for the system. The possibility of such a generalization was demonstrated in [1-3] by applying the product integral, and in [4] by the analysis of the data with the aid of numerical calculations.

In the present paper, we show a way to generalize the usual transmission-line equations for the case of a linear system that is excited by two independent lumped sources, in particular, for the finite system near the ground with terminal loads and (or) terminal excitation. Instead of the classical nonuniform transmission-line equations, all terms of the parameter matrix of the transmission-line-like system obtained (the so-called global parameters in the generalized transmission-line theory) are complex, frequency dependent, and their diagonal elements are nonzero. The connection between the global parameter matrix and the radiation losses is achieved in an explicit form. A perturbation theory for the parameter matrix is described that delivers good results, even after the first iteration. We also establish a connection between global parameters and modal parameters, which are introduced as Fourier coefficients in the expansions of the kernels of integro-differential equations for the current and potential. The gauge-dependency of the parameter matrix is briefly discussed.

2. Global Parameters of the Generalized Transmission-Line Theory for the Homogeneous Problem

We consider a thin wire of arbitrary geometric form, $\vec{r}(l)$ (where l is the coordinate along the wire's axis), near the perfectly conducting ground. It may be excited by two independent local sources, $U_1 f_1(l)$ and $U_2 f_2(l)$. The functions $f_1(l)$ and $f_2(l)$ are only defined at the location of the sources1. Thus, in other parts of the wire, we have to solve the homogeneous problem. (For example, for a finite system these sources could be lumped voltage sources in the terminals, see Section 3; and for the infinite wire, these sources could be located at infinity). If the currents $I_1(l)$ and $I_2(l)$ are two fundamental solutions of an ordinary integro-differential equation with sources $U_1 f_1(l)$ and $U_2 f_2(l)$, then, because of the linearity of electrodynamics, the total solution, $I(l)$, can be represented as

$$I(l) = U_1 I_1(l) + U_2 I_2(l) \tag{1}$$

Jürgen B. Nitsch is with the Otto-von-Guericke-University Magdeburg, Universitätsplatz 2, D-39106 Magdeburg, Germany; E-mail: Juergen.Nitsch@E-Technik.Uni-Magdeburg.de.
Sergey V. Tkachenko is with the Otto-von-Guericke-University Magdeburg, Universitätsplatz 2, D-39106 Magdeburg, Germany; E-mail: Sergey.Tkachenko@E-Technik.Uni-Magdeburg.de

This invited paper is part of the special section honoring Carl E. Baum on his 65th birthday

The quantities U_1 and U_2 are the independent amplitudes of the sources.

Now, it is easy to show that the current $I(l)$ in Equation (1) satisfies a homogeneous second-order differential equation [4]:

$$I''(l)+\mathsf{U}(l)I'(l)+\mathsf{T}(l)I(l)=0 \qquad (2)$$

The parameters $\mathsf{U}(l)$ and $\mathsf{T}(l)$ can be found if one substitutes Equation (1) into Equation (2) and equates the expressions in front of the independent constants U_1 and U_2 to zero. This operation gives the following result:

$$\mathsf{U}(l)=-d\ln\left[W(l)\right]/dl \qquad (3a)$$

and

$$\mathsf{T}(l)=\left[I_1''(l)I_2'(l)-I_1'(l)I_2''(l)\right]W^{-1}(l), \qquad (3b)$$

where the function $W(l)$ is a Wronskian-like determinant of the functions $I_1(l)$ and $I_2(l)$:

$$W(l)=\begin{vmatrix} I_1'(l) & I_2'(l) \\ I_1(l) & I_2(l) \end{vmatrix}=I_1'(l)I_2(l)-I_1(l)I_2'(l) \quad (3\text{ c})$$

The parameters $\mathsf{T}(l)$ and $\mathsf{U}(l)$ are the square of the "propagation function" and the "damping function" of the current waves, respectively. Both of these are complex valued.

In this way, the exact integro-differential equation is transformed into a second-order differential equation, with the length-dependent parameters $\mathsf{T}(l)$ and $\mathsf{U}(l)$. The sources (as well as loads in the same points) can be taken into account via the boundary conditions (see Section 3). Of course, in order to define these parameters, it is necessary to know the solutions $I_1(l)$ and $I_2(l)$, or any other pair of linear independent solutions. This is possible to carry out in analogy to the data processing of a numerical solution [4] (for example, by the Method of Moments), or by some iteration procedure, which allows us to define the parameters for the following iteration with the aid of the solution for the current from the previous iteration. However, to organize this iteration procedure, it is more convenient to split up the differential equation of second order, Equation (2), into two differential equations of first order. This method should preferably be used because of the better numerical stability of the first-order differential equations with coefficients that are only approximately known.

The most general method of such a splitting procedure is to introduce an unknown auxiliary function, $\psi(l)$, which is linearly connected with the derivative of the current, $dI(l)/dl$, and the current, $I(l)$, itself:

$$\frac{dI(l)}{dl}+j\omega\left[P_{21}^{\psi}(l)\psi(l)+P_{22}^{\psi}(l)I(l)\right]=0, \qquad (4a)$$

or

$$\psi(l)=-\frac{1}{j\omega P_{21}^{\psi}}\frac{dI(l)}{dl}-\frac{P_{22}^{\psi}}{P_{21}^{\psi}}I(l) \qquad (4b)$$

(we have chosen this form of the coefficients for our computational convenience).

The system of the first-order differential equations then becomes

$$\frac{d\psi(l)}{dl}+j\omega P_{21}^{\psi}(l)I(l)+j\omega P_{11}^{\psi}(l)\psi(l)=0, \qquad (5a)$$

$$\frac{dI(l)}{dl}+j\omega P_{21}^{\psi}(l)\psi(l)+j\omega P_{22}^{\psi}(l)I(l)=0,$$

or

$$\frac{d}{dl}\begin{bmatrix}\psi(l)\\ I(l)\end{bmatrix}=-j\omega\begin{bmatrix}P_{11}^{\psi} & P_{12}^{\psi}\\ P_{21}^{\psi} & P_{22}^{\psi}\end{bmatrix}\begin{bmatrix}\psi(l)\\ I(l)\end{bmatrix}$$

$$=-j\omega\left[P^{\psi}(l)\right]\begin{bmatrix}\psi(l)\\ I(l)\end{bmatrix} \qquad (5b)$$

This is equivalent to Equation (2) if the parameter matrix, $\left[P^{\psi}(l)\right]$, of this system is connected with the parameters $\mathsf{T}(l)$ and $\mathsf{U}(l)$ in the following way:

$$\mathsf{U}(l)=-d\ln\left[P_{21}^{\psi}(l)\right]\Big/dl+j\omega\left[P_{11}^{\psi}(l)+P_{22}^{\psi}(l)\right], \qquad (6a)$$

$$\mathsf{T}(l)=j\omega P_{21}^{\psi}(l)\frac{d}{dl}\left[\frac{P_{22}^{\psi}(l)}{P_{21}^{\psi}(l)}\right]-\omega^2\det\left[P^{\psi}(l)\right]. \qquad (6b)$$

The simplest way to introduce a physically meaningful auxiliary function is to assume that $\psi(l)=q(l)$, where $q(l)$ is the distributed charge density. Using the continuity equation

$$j\omega q(l)+\frac{dI(l)}{dl}=0, \qquad (7)$$

and the general relations of Equations (6a) and (6b), we can find another representation of the parameter matrix $\left[P^{q}\right]$ for the pair "charge and current:"

$$\left[P^q\right]=\begin{bmatrix} \mathsf{U}(l)/j\omega & \mathsf{T}(l)/\omega^2 \\ 1 & 0 \end{bmatrix}. \quad (8)$$

The introduction of this special auxiliary function also corresponds to the usual way of reducing the order of differential equations. However, the difficulties in this case appear when we consider boundary conditions for the system of Equation (5). Usually, the boundary conditions are given in the terminal points as a linear relationship between currents and voltages. The latter ones can be considered for geometrically small loads or sources as a jump in the scalar potential. The connection between the potential and charge is not a local relation, and requires an additional integration. For this reason, it is convenient to assume that the auxiliary function is a scalar potential, $\varphi(l)$, along the wire:

$$\psi(l)=\varphi(l). \quad (9)$$

Then, the parameter $P_{21}(l)$ in Equation (4) has the dimension and meaning of some per-unit-length "capacitance," and, of course, for low frequencies it coincides with the capacitance per unit length of the classical transmission-line theory. We now obtain the parameters $P_{12}(l)$ and $P_{11}(l)$ from Equations (6), using Equations (4). However, from the point of view of determining the parameters in the explicit form, the following way is more reasonable.

We assume the functions $\varphi_1(l)$ and $\varphi_2(l)$ to be scalar potentials along the wire, which can be obtained by solving the exact integro-differential equations with lumped sources $U_1 f_1(l)$ and $U_1 f_1(l)$, respectively. Because of linearity of electrodynamics, the potential $\varphi(l)$ for any combination of these sources can be represented as

$$\varphi(l)=U_1\varphi_1(l)+U_2\varphi_2(l). \quad (10)$$

Now, the elements of the parameter matrix $\left[P^{\varphi}(l)\right]$ for the pair "potential and current" can be obtained after substitution of Equation (1) and Equation (10) into Equation (5), and setting the factors in front of the independent constants U_1 and U_2 to zero:

$$P_{11}^{\varphi}(l)=(j\omega)^{-1}\left[\varphi_1'(l)I_2(l)-I_1(l)\varphi_2'(l)\right]/\Delta_{I,\varphi}, \quad (11)$$

$$P_{12}^{\varphi}(l)=-(j\omega)^{-1}\left[\varphi_1'(l)\varphi_2(l)-\varphi_1(l)\varphi_2'(l)\right]/\Delta_{I,\varphi}, \quad (12)$$

$$P_{21}^{\varphi}(l)=(j\omega)^{-1}\left[I_1'(l)I_2(l)-I_1(l)I_2'(l)\right]/\Delta_{I,\varphi}, \quad (13)$$

$$P_{22}^{\varphi}(l)=-(j\omega)^{-1}\left[I_1'(l)\varphi_2(l)-\varphi_1(l)I_2'(l)\right]/\Delta_{I,\varphi}, \quad (14)$$

where

$$\Delta_{I,\varphi}=I_1(l)\varphi_2(l)-I_2(l)\varphi_1(l).$$

After substitution of Equations (11)-(14) into Equation (6) and some calculations, we get Equations (3) for the second-order parameters $\mathsf{U}(l)$ and $\mathsf{T}(l)$.

The first-order system of Equation (5) looks like a usual system of nonuniform transmission-line equations (however, with diagonal terms), and can be named a generalized transmission-line system [1-3]:

$$\frac{d}{dl}\begin{bmatrix}\varphi(l)\\ I(l)\end{bmatrix}+j\omega\begin{bmatrix}P_{11}^{\varphi}(l) & P_{12}^{\varphi}(l)\\ P_{21}^{\varphi}(l) & P_{22}^{\varphi}(l)\end{bmatrix}\begin{bmatrix}\varphi(l)\\ I(l)\end{bmatrix}=0. \quad (15)$$

Thus, we have shown that the system of linear integro-differential equations, the solution of which is defined by two independent constants, can be reduced to the differential Equations (15) with parameters in Equations (11)-(14). These parameters (global parameters in a generalized transmission-line theory, or the parameters of "Maxwellian circuits") are complex-valued, and also describe the radiation of the system (see also Section 4). They depend on the geometry of the system, and therefore on the local parameter l along the line. This fact was established earlier in [1-3] with the method of product integrals, and (up to a notation) in [4] by processing the numerical solutions for current and potential with the Method of Moments. We note that in the early 1970s, it describing the insulated dipole antenna in a relatively dense medium as a section of a transmission line with distributed radiation losses appearing as a part of the series impedance per unit length was suggested [5].

The parameter matrix $\left[P^{\varphi}(l)\right]$ in Equation (15) depends on the gauge of the potential, φ. For example, for the Coulomb gauge, it has a different form than in the Lorenz gauge.

3. Global Parameters for a Finite Line with Terminal Sources (Loads): Perturbation Approach

We consider a thin wire of arbitrary geometric form, $\vec{r}(l)$, near a perfectly conducting ground (see, for example, a semi-circular loop in Figure 1a), which may be loaded and excited by an external field, $\vec{E}^i(\vec{r})$, as well as by a point source, U_1^0. It is assumed that the line is connected with the ground plane at both ends.

Using the zero boundary condition for the total (scattered plus exciting) tangential electric field on the surface of the wire[2], the continuity equation for the induced current, $I(l)$, and the charge density, $q(l)$, we obtain the system of integro-differential equations for the "current and potential" pair:

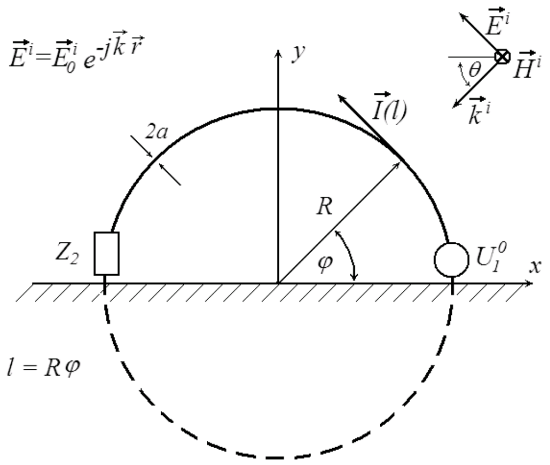

Figure 1a. The excitation of a semi-circular loop.

$$\begin{cases} \dfrac{d\varphi(l)}{dl} + j\omega\dfrac{\mu_0}{4\pi}\displaystyle\int_0^{L/2} g_I^L(l,l')I(l')dl' = E_l^e(l) \\ \displaystyle\int_0^{L/2} g_I^C(l,l')\frac{dI(l')}{dl'}dl' + j\omega 4\pi\varepsilon_0\varphi(l) = 0 \end{cases} \tag{16a,b}$$

Here, $E_l^e(l)$ is an exciting total tangential electric field (incident plus reflected), $\varphi(l)$ is the scalar potential along the wire (in the Lorenz gauge), a is the radius of the wire, and $L = \oint dl'$ is the length of the complete closed loop. The functions $g_I^L(l,l')$ and $g_I^C(l,l')$ are the Green's functions along the curved line for the vector potential and scalar potential, respectively, which take into account the reflection of the ground plane:

$$g_I^C(l,l') = \frac{e^{-jk\sqrt{[\vec{r}(l)-\vec{r}(l')]^2+a^2}}}{\sqrt{[\vec{r}(l)-\vec{r}(l')]^2+a^2}} - \frac{e^{-jk\sqrt{[\vec{r}(l)-\vec{\tilde{r}}(l')]^2+a^2}}}{\sqrt{[\vec{r}(l)-\vec{\tilde{r}}(l')]^2+a^2}} \tag{17}$$

$$g_I^L(l,l') = \vec{e}_l(l)\bullet\vec{e}_l(l')\frac{e^{-jk\sqrt{[\vec{r}(l)-\vec{r}(l')]^2+a^2}}}{\sqrt{[\vec{r}(l)-\vec{r}(l')]^2+a^2}}$$

$$-\vec{e}_l(l)\bullet\vec{\tilde{e}}_l(l')\frac{e^{-jk\sqrt{[\vec{r}(l)-\vec{\tilde{r}}(l')]^2+a^2}}}{\sqrt{[\vec{r}(l)-\vec{\tilde{r}}(l')]^2+a^2}} \tag{18}$$

The unit tangential vector $\vec{e}_l(l) = d\vec{r}(l)/dl$ of the curve is taken along the wire axis, $\vec{\tilde{r}}(l)$ is the radius vector reflected by the ground plane, and $\vec{\tilde{e}}_l(l) = d\vec{\tilde{r}}(l)/dl$ is the corresponding unit tangential vector.

Now, in order to define the global generalized transmission-line parameters, we consider an excitation of the transmission line by a point source, U_1^0, located at the beginning of the line. The line is assumed to be loaded by a lumped impedance, Z_2, at the far end. There are two possibilities to account for the source and the load: to treat both of them as boundary conditions, or to treat both of them as sources (with unknown amplitude for the "load source"). For the second possibility, the exciting field, $E_l^e(l)$, can be written as [6]

$$E^e{}_l(l) = U_1^0\delta(l-\Delta) + U_2^0\delta(l-L/2+\Delta), \tag{19}$$

$$U_2^0 = -Z_2 I(L/2-\Delta) \text{ with } \Delta\to 0\cdot \tag{20}$$

Now, let the response functions $Y(l,l')$ and $K(l,l')$ (the admittance function, $Y(l,l')$, has the dimension of conductance; the transfer function for the potential, $K(l,l')$, is dimensionless; see also Equations (55a) and (55b)) be solutions of the system of Equations (16a) and (16b) for the current and the potential with a $\delta(l-l')$ source of amplitude ½V located in the point l' (we have chosen this normalization for convenience; see Equations (55a) and (55b) below). Due to the linearity of the problem considered, we can write the solution for the total induced current as

$$I(l) = 2U_1^0 Y(l,0) - 2Z_2 I(L/2)Y(l,L/2)\cdot \tag{21}$$

Having this, it is easy to find the unknown current at the point $L/2$:

$$I(L/2) = 2U_1^0 Y(L/2,0)\Big/\left[1+2Z_2 Y(L/2,L/2)\right]\cdot \tag{22}$$

With that, we write the following for the total current:

$$I(l) = \tilde{U}_1^0 Y(l,0) + \tilde{U}_2^0 Y(l,L/2), \tag{23}$$

with

$$\tilde{U}_1^0 = 2U_1^0, \tag{24}$$

$$\tilde{U}_2^0 = -2Z_2 I(L/2)\cdot$$

It is obvious that any other solution with voltage-like lumped nonuniformities in the termination points (with excitation in point 2 and lumped load in point 1, or with voltage sources located in both points) can be presented in the form of Equation (23). For the potential $\varphi(l)$ along the wire, we find a similar equation:

$$\varphi(l) = \tilde{U}_1^0 K(l,0) + \tilde{U}_2^0 K(l,L/2)\cdot \tag{25}$$

Thus, we have found a general solution for the system of integro-differential equations, Equation (16), in the form of Equations (1) and (10), where the linearly independent solutions for the current and scalar potential can be written as

$$I_1(l) = Y(l,0), \tag{26a}$$

$$I_2(l) = Y(l,L/2), \tag{26b}$$

$$\varphi_1(l) = K(l,0), \tag{26c}$$

$$\varphi_2(l) = K(l,L/2). \tag{26d}$$

Equation (26) together with Equations (11)-(14) then yield the parameter matrix $\left[P^{\varphi}(l)\right]$. This procedure is convenient when exact values of the functions $Y(l,l')$ and $K(l,l')$ are known. We shall apply it in Section 5.

In the case that exact solutions are unknown, it is necessary to apply a different procedure to find the parameter matrix $\left[P^{\varphi}(l)\right]$. This will be outlined below. Using the strong weighting property of the Green's function [7] (the real part of Green's function has a sharp maximum when $|l-l'| \sim a$) for a thin wire $a \to 0$, we can calculate the logarithmical leading terms of the integrals in Equation (16) as

$$\int_0^{L/2} g_I^L(l,l')I(l')dl' \approx 2\ln\left(\tilde{L}/a\right)I(l), \tag{27a}$$

$$\int_0^{L/2} g_I^C(l,l')\frac{dI(l')}{dl'}dl' \approx 2\ln\left(\tilde{L}/a\right)\frac{dI(l)}{dl}. \tag{27b}$$

Here, $\tilde{L}$ is some characteristic length of the wire system (for smooth wiring, where horizontal and vertical dimensions are of the same order of magnitude, $\tilde{L} \sim L$, or for the long horizontal wire above ground, $\tilde{L} \approx 2h$).

Then we easily get for the currents and potentials for the zeroth iteration the regular result

$$\begin{cases} \dfrac{d\varphi(l)}{dl} + j\omega L'^{(0)} I(l) = E_l^e(l) \\ \dfrac{dI(l')}{dl'} + j\omega C'^{(0)}\varphi(l) = 0 \end{cases}$$

with parameter matrix

$$\left[P^{(0),\varphi}(l)\right] = \begin{bmatrix} 0 & L'^{(0)} \\ C'^{(0)} & 0 \end{bmatrix}. \tag{28}$$

The per-unit-length inductance and per-unit-length capacitance of the zeroth iteration are

$$L'^{(0)} = \frac{\mu_0}{2\pi}\ln\left(\tilde{L}/a\right), \tag{29}$$

$$C'^{(0)} = \frac{2\pi\varepsilon_0}{\ln\left(\tilde{L}/a\right)}.$$

With these parameters, we obtain the solution for the current (and its derivative) of the first iteration from Equations (28)-(29) in the form of forward- and backward-propagating current waves. However, for the scalar potential in the first iteration and its derivative, the exact equations, Equation (16), are used:

$$I_{1,2}^{(1)}(l) = e^{\mp jkl}, \tag{30a}$$

$$\frac{dI_{1,2}^{(1)}(l)}{dl} = \mp jke^{\mp jkl}, \tag{30b}$$

$$\varphi_{1,2}^{(1)}(l) = -\frac{1}{j\omega 4\pi\varepsilon_0}\int_0^{L/2} g_I^C(l,l')\frac{dI_{1,2}^{(1)}(l')}{dl'}dl', \tag{31a}$$

$$\frac{d\varphi_{1,2}^{(1)}(l)}{dl} = -j\omega\frac{\mu_0}{4\pi}\int_0^{L/2} g_I^L(l,l')I_{1,2}^{(1)}(l')\ dl' \tag{31b}$$

After some straightforward calculations, we obtain the parameter matrix in the first-order approximation:

$$P_{11}^{\varphi,(1)}(l) = c\left[L_+'^{(1)}(l) - L_-'^{(1)}(l)\right]$$

$$\left\{\left[C_+'^{(1)}(l)\right]^{-1} + \left[C_-'^{(1)}(l)\right]^{-1}\right\}^{-1}, \tag{32}$$

$$P_{12}^{\varphi,(1)}(l) = \left\{L_+'^{(1)}(l)\left[C_-'^{(1)}(l)\right]^{-1} + L_-'^{(1)}(l)\left[C_+'^{(1)}(l)\right]^{-1}\right\}$$

$$\left\{\left[C_+'^{(1)}(l)\right]^{-1} + \left[C_-'^{(1)}(l)\right]^{-1}\right\}^{-1}, \tag{33}$$

$$P_{21}^{\varphi,(1)}(l) = 2\left\{\left[C_+'^{(1)}(l)\right]^{-1} + \left[C_-'^{(1)}(l)\right]^{-1}\right\}^{-1}, \tag{34}$$

$$P_{22}^{\varphi,(1)}(l) = -c^{-1}\left\{\left[C_+'^{(1)}(l)\right]^{-1} - \left[C_-'^{(1)}(l)\right]^{-1}\right\}$$

$$\left\{\left[C_+'^{(1)}(l)\right]^{-1} + \left[C_-'^{(1)}(l)\right]^{-1}\right\}^{-1} \qquad (35)$$

In Equations (32)-(35), we have used the following expressions for the approximate inductance and capacitance, respectively:

$$L_\pm'^{(1)}(l) = \frac{\mu_0}{4\pi}\int_0^{L/2} g_I^L(l,l')e^{\mp jk(l'-l)}\,dl', \qquad (36a)$$

$$C_\pm'^{(1)}(l) = 4\pi\varepsilon_0\left[\int_0^{L/2} g_I^C(l,l')e^{\mp jk(l'-l)}\,dl'\right]^{-1} \qquad (36b)$$

For the low-frequency case ($k \to 0$), we find

$$L_+'^{(1)}(l) = L_-'^{(1)}(l) = L_0'(l),$$

$$C_+'^{(1)}(l) = C_-'^{(1)}(l) = C_0'(l).$$

The quantities $L_0'(l)$ and $C_0'(l)$ constitute the real, low-frequency length-dependent inductance and capacitance per unit length in the matrix of a nonuniform transmission line [3]. We obtain the parameter matrix in the classical anti-diagonal form:

$$\left[P^{(1),\varphi}(l)\right] \underset{k\to 0}{=} \begin{bmatrix} 0 & L_0'(l) \\ C_0'(l) & 0 \end{bmatrix}. \qquad (37)$$

For high frequencies, all elements of the parameter matrix in the first iteration have an imaginary part, which accounts for the radiation losses (see Section 4).

For the simple example of a vertical semicircular loop, where the exact solutions for the functions $Y(l,l')$ and $K(l,l')$ are known, the exact values of the parameters are in good agreement with the approximation of the first iteration (Equations (32)-(36), see Figure 2 in Section 5).

It is now obvious how to proceed for the higher-order iterations in this perturbation theory.

Equation (15) has to be solved with the parameters of the previous iteration and with arbitrary boundary conditions. For the calculation of the parameters in the next iteration (with the aid of Equations (11)-(14)), we use the current from this solution. However, the potential and its derivative have to be obtained via integrations similar to those in Equation (31). Notice that just the first iteration provides good agreement with the exact solution (compare the representation in Figure 2).

4. Global Parameters and Radiation Losses

In this section, we establish the connection between the global parameters for the generalized transmission-line theory and the losses in the wiring system. We again consider a system without distributed external excitation along the line, i.e., the wire may be excited at some points near the terminals:

$$E^e{}_l(l) = U_1^0\delta(l-\Delta) + U_2^0\delta(l-L/2+\Delta) \qquad (38)$$

with

$$\Delta \to 0 \cdot$$

Here, U_1^0, U_2^0 may be voltage sources as well as representations for the loads (as in Equation (19)).

The energy can be "pumped" into the system by a source (if we consider a voltage source as in point 1 of Figure 1a), or it can be absorbed by the system (if we consider a load, as in point 2 of Figure 1a). Taking into account the absorbed energy as a "pumped" energy, but with negative sign, we can write the following equation for the time-averaged power (which is "pumped" by the sources into the system):

$$W = \frac{1}{2}\ \mathrm{Re}\left[\int_0^{L/2} E_l^e(l)I^*(l)dl\right]$$

$$= \frac{1}{2}\ \mathrm{Re}\left[U_1^0 I^*(\Delta) + U_2^0 I^*\left(L/2-\Delta\right)\right]. \qquad (39)$$

Using the connection between the voltages and the potentials in the terminal points (which can be established, for example, by integration of Equation (16a) in the intervals $[0,\Delta]$ and $[L/2-\Delta, L/2]$, and by Equation (16b) in the points $l=0$, $l=L/2$),

$$\varphi(0) = \varphi\left(L/2\right) = 0,$$

$$\varphi\left(\Delta\right) = U_1^0, \qquad (40)$$

$$\varphi\left(L/2-\Delta\right) = -U_2^0,$$

we can write

$$W = \frac{1}{2}\ \mathrm{Re}\left\{\varphi(\Delta)I^*(\Delta) - \varphi\left(L/2-\Delta\right)I^*\left(L/2-\Delta\right)\right\}$$

$$= -\frac{\mathrm{Re}}{2}\left\{\int_{\Delta}^{L/2-\Delta}\frac{d}{dl}\left[\varphi(l)I^{*}(l)\right]\,dl\right\}. \qquad (41)$$

Now, after differentiation and use of Equation (15) in the region $[\Delta, L/2-\Delta]$, we find

$$W \underset{\Delta\to 0}{=} \int_{\Delta}^{L/2-\Delta} w'(l)\,dl\,, \qquad (42)$$

with

$$w'(l) = -\frac{1}{4}\frac{d}{dl}\left[\varphi(l)I^{*}(l)+\varphi^{*}(l)I(l)\right]$$

$$= -\frac{\omega}{2}\Big[\mathrm{Im}\left[P_{12}(l)\right]|I(l)|^{2} + \mathrm{Im}\left[P_{21}(l)\right]|\varphi(l)|^{2}$$

$$+\mathrm{Im}\left\{\left[P_{11}(l)-P_{22}^{*}(l)\right]\varphi(l)I^{*}(l)\right\}\Big]. \qquad (43)$$

This equation is the desired connection between the global parameters and the losses in the line (note that we consider a line without distributed ohmic losses). Here, the function $w'(l)$ describes the change of the "power" that propagates along the line. Of course, this value depends on the gauge in which the scalar potential is defined. The gauge-independent value is, however, the integral of Equation (42).

In the low-frequency case, when the parameter matrix of the system has the form of Equation (37), with real anti-diagonal terms and zero diagonal terms, the value of $w'(l) = 0$. This means that no power is pumped into the system. For example, when we have a source U_1^0 at point 1 and a load Z_2 at point 2, we arrive at

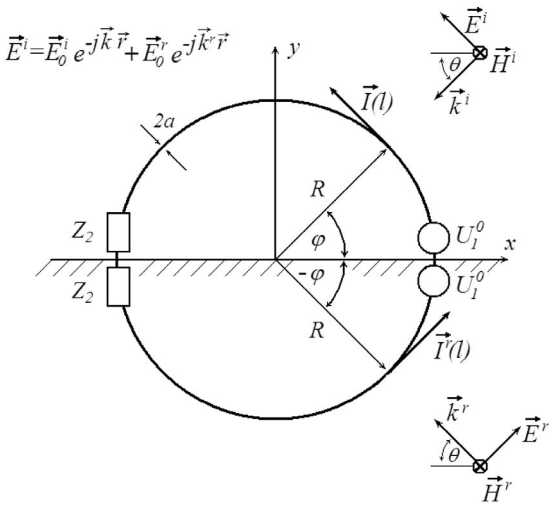

Figure 1b. The equivalent symmetrical excitation of a complete circular loop.

$$W = 0\,, \qquad (44a)$$

or

$$\frac{1}{2}\mathrm{Re}\left[U_1^0 I^{*}(0)\right] = \frac{1}{2}\mathrm{Re}(Z_2)\left|I(L/2)\right|^{2}, \qquad (44b)$$

i.e., all power that enters the system at point 1 is transported to the load at point 2, where it is absorbed. However, for high frequencies, when the anti-diagonal elements of the parameter matrix have imaginary parts and the diagonal elements are not zero, Equation (44) is not fulfilled. Then, the difference between the left- and right-hand sides of Equation (44b) yields the power for the radiation losses.

5. Modal Parameters in the Thin-Wire Model

In this section, we facilitate our calculation and consider the symmetrical problem (see Figure 1b). Using the mirror principle in electrodynamics, we can show that the problem of "half-loop" excitation is equivalent to the problem of excitation of the complete "closed loop" in space, but with sources and loads symmetrical with respect to the ground plane (see Figure 1b). This corresponds to a change

$$\vec{E}^{\,i}(\vec{r}) \to \vec{E}^{\,e,s}(\vec{r}) = \vec{E}^{\,i,s}(\vec{r}) + \vec{E}^{\,r,s}(\vec{r})\,,$$

where $\vec{E}^{\,i,s}(\vec{r})$ and $\vec{E}^{\,r,s}(\vec{r})$ are the incident and reflected electric fields, respectively. $\vec{E}^{\,e,s}(\vec{r})$ is the exciting electric field. All fields are extended into the entire space. For the symmetrical problem, the integro-differential Equation (16) looks like

$$\begin{cases} d\varphi(l)/dl + j\omega\dfrac{\mu_0}{4\pi}\oint \vec{e}(l)\bullet\vec{e}(l')g(l,l')I(l')\,dl' = E_l^{e,s}(l) \\ \oint g(l,l')\left(dI(l')/dl'\right)dl' + j\omega 4\pi\varepsilon_0\varphi(l) = 0 \end{cases} \qquad (45a,b)$$

with

$$g(l,l') = e^{-jk\sqrt{\left[\vec{r}(l)-\vec{r}(l')\right]^2+a^2}}\Big/\sqrt{\left[\vec{r}(l)-\vec{r}(l')\right]^2+a^2} \qquad (46)$$

Here, $g(l,l')$ is the scalar Green's function along the line, and integration is carried out along the complete closed loop.

By virtue of the fact that all functions in these equations are periodic (with period L) with respect to the distances l and l', we can solve this system by a Fourier-series expansion using the complete function system $\left\{e^{-jk_m l}\right\}$, where $k_m = m\,2\pi/L$, $m = \ldots -1,\ 0,\ 1, \ldots$. In the following, we use the matrix notation $\left[e^{-jk_m l}\right]_{m_1} = \exp(-jk_{m_1} l)$, and

introduce modal amplitudes for the exciting field and the induced potential and current:

$$E_l^{e,s}(l) = \sum_{m=-\infty}^{\infty} E_{l,m}^{e,s} e^{-jk_m l} = \left[e^{-jk_m l}\right]^T \left[E_{l,m}^{e,s}\right], \quad (47a)$$

$$\varphi(l) = \sum_{m=-\infty}^{\infty} \varphi_m e^{-jk_m l} = \left[e^{-jk_m l}\right]^T [\varphi_m], \quad (47b)$$

$$I(l) = \sum_{m=-\infty}^{\infty} I_m e^{-jk_m l} = \left[e^{-jk_m l}\right]^T [I_m]. \quad (47c)$$

Applying the orthogonality property of the functions $e^{-jk_m l}$, instead of the integro-differential Equations (45a) and (45b), we derive a linear system for the modal column vectors of the potential and the current, respectively:

$$\begin{cases} -j[k_m]\bullet[\varphi_m] + j\omega[L']\bullet[I_m] = \left[E_{l,m}^{e,s}(l)\right] \\ -j[k_m]\bullet[I_m] + j\omega[C']\bullet[\varphi_m] = 0 \end{cases}, \quad (48a,b)$$

$$[k_m]_{m_1,m_2} = k_{m_1}\delta_{m_1,m_2}.$$

In Equations (48a) and (48b), we have introduced per-unit-length matrices (of infinite dimension) for the modal inductance and capacitance $[L']$, $[C']$, which appear after the calculation of the Fourier representation of the kernels in the integro-differential equations:

$$[L'] = \frac{\mu_0}{4\pi}\left[G^L\right], \quad (49a)$$

$$\left[G^L\right]_{m,m_1} = \frac{1}{L}\oint dl e^{-j(k_{m_1}-k_m)l}$$

$$\oint \vec{e}_l(l)\bullet\vec{e}_l(l+\xi) g(l,l+\xi) e^{-jk_{m_1}\xi} d\xi, \quad (49b)$$

$$[C'] = 4\pi\varepsilon_0\left[G^C\right]^{-1}, \quad (50a)$$

$$\left[G^C\right]_{m,m_1} = \frac{1}{L}\oint dl e^{-j(k_{m_1}-k_m)l} \oint g(l,l+\xi) e^{-jk_{m_1}\xi} d\xi. \quad (50b)$$

In contrast to the classical line parameters, these parameters depend on the mode indices, and they are complex-valued and frequency and gauge dependent [6-8] (here, the Lorenz gauge is used).

The solution of Equation (48) for the current and potential amplitudes looks like

$$[I_m] = [Z']^{-1}\bullet\left[E_{l,m}^e\right], \quad (51a)$$

$$[\varphi_m] = \omega^{-1}[C']^{-1}\bullet[k_m]\bullet[Z']^{-1}\bullet\left[E_{l,m}^e\right]. \quad (51b)$$

Here, $[Z']$ is the per-unit-length impedance matrix for the modal amplitudes, which relates the current column vector to the column vector of the scattered field:

$$\left[E_{l,m}^{sc}\right] = -[Z'(j\omega)]\bullet[I_m], \quad (52a)$$

$$[Z'] = j\omega\,[L'] + \frac{[k_m]\bullet\left[C'\right]^{-1}\bullet[k_m]}{j\omega}. \quad (52b)$$

After a lengthy calculation, one can show that the matrix $[Z']$ is connected with the radiation of the scattered current in the system considered [6]. This means that the total radiated energy of the system per unit time (time averaged) can be obtained as

$$\overline{W} = \frac{L}{4}\mathrm{Re}\left\{[I_m]^{T^*}\bullet[Z'(j\omega)]\bullet[I_m]\right\}. \quad (53)$$

Now, we derive the connection between the modal and global parameters investigated in the previous sections. To do that, we consider a lumped δ source with amplitude one-half, located at the point with coordinate l_1. For such a source, the exciting symmetrical tangential field, $E_l^{e,\delta,s}(l)$, and its Fourier transform can be represented as

$$E_l^{e,\delta,s}(l) = \frac{V_0}{2}\delta(l-l_1) + \frac{V_0}{2}\delta(l+l_1), \quad (54a)$$

$$\left[E_{l,m}^{e,\delta}\right] = \frac{V_0}{2L}\left[e^{jk_m l_1}\right] + \frac{V_0}{2L}\left[e^{-jk_m l_1}\right], \quad (54b)$$

$$V_0 = 1V.$$

Using Equations (54b), (51a), (51b), (47b), and (47c), the corresponding response functions for the current and the potential along the wire then become

$$Y(l,l_1)=\frac{1}{2L}\left[e^{-jk_m l}\right]^T[Z']^{-1}\left\{\left[e^{jk_m l_1}\right]+\left[e^{-jk_m l_1}\right]\right\}, \quad (55a)$$

$$K(l,l_1)=\frac{1}{2L\ \omega}\ \left[e^{-jk_m l}\right]^T[C']^{-1}[k_m][Z']^{-1}$$

$$\left\{\left[e^{jk_m l_1}\right]+\left[e^{-jk_m l_1}\right]\right\}. \quad (55b)$$

The substitution of these functions into Equations (26) and (11)-(14) yields the desired matrix for the global parameters, $\left[P^{\varphi}(l)\right]$, and establishes the connection between the modal and global parameters.

Note that a detailed investigation of the functions $Y(l,l')$ and $K(l,l')$ requires the solution of the full electromagnetic wave problem for a thick wire, including the current and the field distributions in the source (load) region. In order to simplify the problem, we used a delta-function source (a slice generator) here (see also [9], [14]). However, such an idealization causes some difficulties, e.g., an infinite capacitance. Mathematically this means that the solution in the thin-wire approximation obtained by a Fourier transform contains logarithmically divergent series (or logarithmically divergent integrals for the infinite wire). One of the methods to prevent those divergences is to consider a finite extension of the source gap Δ, where the electric field is distributed according to some known physical law [14]. Since we do not know the internal structure of the source (load), we considered the lumped source with a finite extension $\Delta \gg a$, and truncated all the Fourier series (and, correspondingly, all matrices of the modal parameters) for $\lambda_m \sim< \Delta$ (or $m >\sim L/\Delta$).

For the case of a vertical semi-loop near a perfectly conducting ground (see Figure 1) – a finite closed wire of high symmetry – the matrices of the modal parameters become diagonal [6]:

$$[L']_{m,m_1}=L'_m\delta_{m,m_1}, \quad (56a)$$

$$[C']_{m,m_1}=C'_m\delta_{m,m_1}, \quad (56b)$$

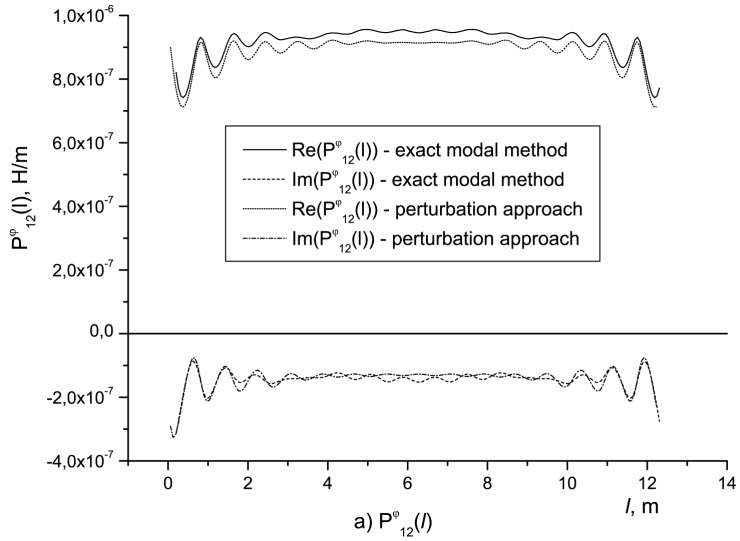

Figure 2a. The distributed global parameters $\left[P^{\varphi}(l)\right]$ for the semi-circular vertical loop terminated at both ends, calculated from the exact modal solution and in the first order of the developed iteration theory ($R=4\ m$, $a=1\ cm$, $\Delta_{Source}=0.1\ m$, $N_{modes}=400$). The parameter $P^{\varphi}_{12}(l)$ is shown.

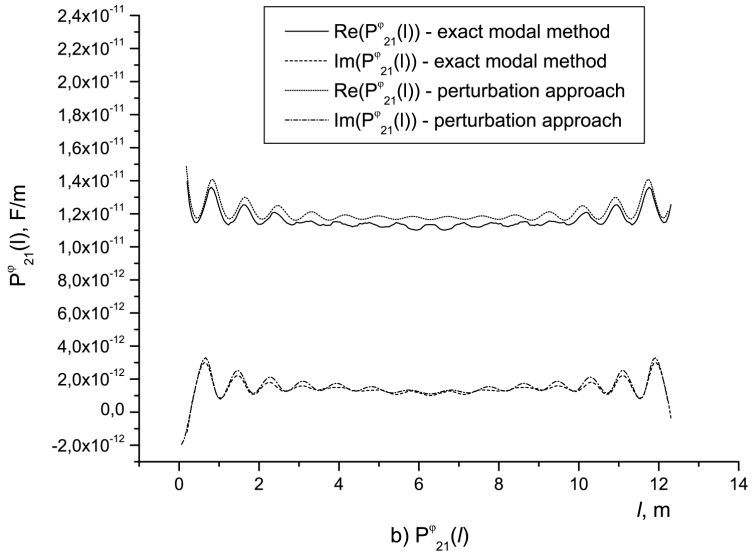

Figure 2b. The distributed global parameter $P^{\varphi}_{21}(l)$ for the case of Figure 2a.

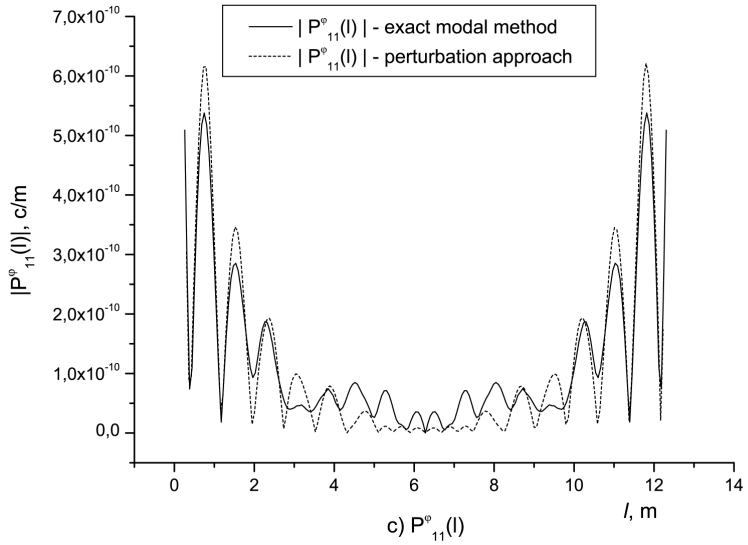

Figure 2c. The distributed global parameter $P_{11}^{\varphi}(l)$ for the case of Figure 2a.

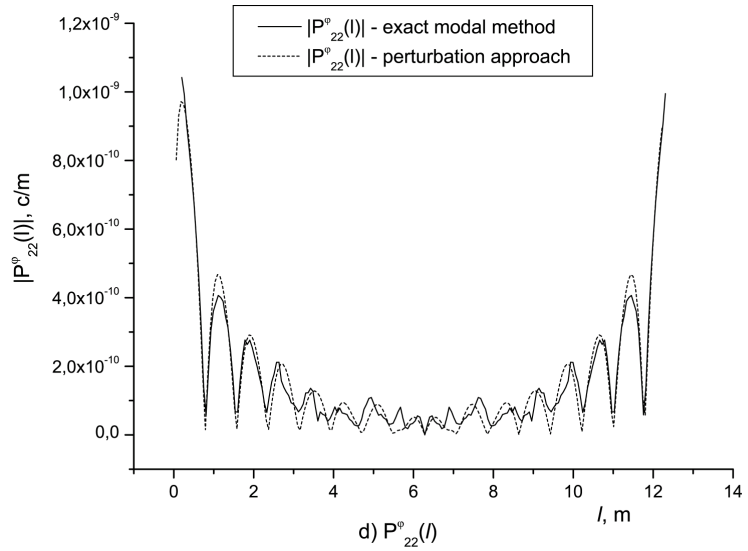

Figure 2d. The distributed global parameter $P_{22}^{\varphi}(l)$ for the case of Figure 2a.

with

$$L'_m = \mu_0 R\left[g_{m+1}(k,R,a)+g_{m-1}(k,R,a)\right]/8\pi\,, \quad (57a)$$

$$C'_m = 4\pi\varepsilon_0/\left[Rg_m(k,R,a)\right], \quad (57b)$$

and

$$g_m(k,R,a) = \int_0^{2\pi} \frac{e^{-jm\varphi - jk\sqrt{4R^2\sin^2(\varphi/2)+a^2}}}{\sqrt{4R^2\sin^2(\varphi/2)+a^2}} d\varphi\,, \quad (58)$$

$$g_m(k,R,a) \cong 2/R\left[\ln(2R/a) - \gamma - \psi\left(1/2-|m|\right)\right]$$

$$+\pi/R\int_0^{2kR}\left[E_{2|m|}(x) - jJ_{2|m|}(x)\right]dx \quad (59)$$

Here, R is the radius of the loop, a is the radius of the wire, and the quantity $E_{2|m|}(x)$ denotes the Weber function [12].

Using Equations (56)-(59) together with Equations (47), (51), and (52), we obtain the well-known modal solution for the current distribution in a vertical semi-loop [10, 11, 13]. The function g_m in Equations (57)-(59) corresponds to the known function in the analytical solution of the diffraction problem for the circular loop in free space [9-11].

In Figures 2a-2d we display the spatial dependence of the global parameters for this configuration, which have been calculated by the exact modal method as well as by the perturbation theory. A good agreement is observed.

6. Conclusion

In this paper, we have investigated the global parameters (the parameters of "Maxwellian circuits" that

describe the exact solution for the induced current of Maxwell's equations for a thin wire of arbitrary geometric form) in the generalized transmission-line theory. These parameters are complex-valued, frequency and gauge-dependent, and depend on the local coordinate along the line. The connection of these parameters with radiation losses was established in an explicit form. An iteration approach for the global parameters was also formulated.

We obtained these global parameters from the response functions of the current and scalar potential along the wire, which was excited by lumped voltage sources. These functions, in turn, are connected to the so-called modal transmission-line parameters. They were introduced as matrices in the Fourier representation of the electric-field integral equations for the current and the scalar potential. They are also complex-valued, depend on the gauge used, and are connected with radiation. The solution for an arbitrary wire can formally be derived from these modal parameters. For high-symmetry cases, which are characterized by constant "Differential Geometry Parameters" of the thin wire, e.g., curvature and/or torsion, the corresponding matrices of the modal parameters become diagonal.

Comparison of the exact values of the parameters for the vertical half-loop near the perfectly conducting ground with the result of the perturbation approach yielded good agreement, even after the first iteration.

7. Dedication

This paper is dedicated to honoring Dr. Dr.-Ing. E.h. C. E. Baum on the occasion of his 65th birthday. The authors know Dr. Baum and have been working with him for almost two decades. In particular, one of the authors (J. N.) spent a research year at Dr. Baum's lab on the Kirtland Air Force Base, New Mexico. At that time, they started their pioneering investigation of nonuniform transmission lines. It is fair to say that we, the authors, have learned a lot from him, and we enjoyed all the meetings and discussions with him, which were of great benefit for us. In recent years our research group has developed a new transmission-line theory as a full-wave theory, which has its roots in the late 1980s when J. N. cooperated with Carl Baum at the Kirtland Air Force Base. The present paper contains an important piece of our current research concerning nonuniform transmission lines. We hope and wish to continue the fruitful and amicable cooperation with Dr. Baum in the future.

8. Acknowledgement

This work was sponsored by the Deutsche Forschungsgemeinschaft DFG under contract number FOR 417. We would like to thank H. Haase for helpful discussions, and F. M. Tesche and F. Rachidi for useful comments.

9. References

1. H. Haase and J. Nitsch, "Full-Wave Transmission Line Theory (FWTLT) for the Analysis of Three-Dimensional Wire-Like Structures," *Proceedings of the 14th International Zurich Symposium and Technical Exhibition on Electromagnetic Compatibility*, February 2001, pp. 235-240.

2. H. Haase, T. Steinmetz, and J. Nitsch, "New Propagation Models for Electromagnetic Waves Along Uniform and Nonuniform Cables," *IEEE Transactions on Electromagnetic Compatibility*, **EMC-47**, 3, 2004, pp. 345-352.

3. H. Haase, J. Nitsch, and T. Steinmetz, "Transmission-Line Super Theory: A New Approach to an Effective Calculation of Electromagnetic Interactions," *Radio Science Bulletin*, 307, 2003, pp. 33-60.

4. K. K. Mei, "Theory of Maxwellian Circuits", *Radio Science Bulletin*, 305, 2003, pp. 6-13.

5. T. T. Wu, R. W. P. King, and D. V. Giri "The Insulated Dipole Antenna in a Relatively Dense Medium," *Radio Science*, **8**, 7, 1973, pp. 699-709.

6. J. Nitsch and S. Tkachenko, "Newest Developments in Transmission-Line Theory and Applications," *Interaction Notes*, Note 592, to be published.

7. J. Nitsch and S. Tkachenko, "Complex-Valued Transmission-Line Parameters and their Relation to the Radiation Resistance," *IEEE Transactions on Electromagnetic Compatibility*, **EMC-47**, 3, 2004, pp. 477-48;

8. J. Nitsch and S. Tkachenko," Telegrapher Equations for Arbitrary Frequencies and Modes: Radiation of an Infinite, Lossless Transmission Line," *Radio Science*, **39**, 2, 2004.

9. T. T. Wu, "Theory of the Thin Circular Loop Antenna," *Journal of Mathematical Physics*, 3, 6, 1962, pp. 1301-1304.

10. C. E. Baum and H. Chang, "Fields at the Center of a Full Circular TORUS and a Vertically Oriented TORUS on a Perfectly Conducting Earth," *Sensor and Simulation Notes*, Note 160, 1972.

11. C. E. Baum, H. Chang, and J. P. Martinez, "Analytical Approximations and Numerical Techniques for the Integral of the Anger-Weber Function," *Mathematical Notes*, Note 25, 1972.

12. M. Abramowitz and I. Stegun, *Handbook of Mathematical Functions*, New York, Dover, 1970.

13. J. Nitsch, S. Tkachenko, "Eine Transmission-Line Beschreibung für eine vertikale Halbschleife auf leitender Ebene," *11 Internationale Fachmesse und Kongress für Elektromagnetische Verträglichkeit*, Düsseldorf, 2004, pp. 291-300.

14. Z. L. Pine, F. M. Tesche, "Pulse Radiation by an Infinite Cylindrical Antenna with a Source Gap with a Uniform Field," *Sensor and Simulation Notes*, Note 159, October 1972.

1 The same approach, of course, can be realized for the case of distributed sources, when the functions $f_1(l)$ and $f_2(l)$ overlap, and we have an inhomogeneous problem, but this case is not considered in the present paper.

2 As usual in the thin-wire approximation, we assume that the current and charge are distributed along the wire's axis, and consider only the tangential component of the current.

Example of the Use of the BLT Equation for EM Field Propagation and Coupling Calculations[1]

F.M. Tesche
J.M. Keen
C.M. Butler

Abstract

This paper provides a numerical verification of the extended BLT (Baum-Liu-Tesche) equation for a transmission-line structure located in the vicinity of a perfect ground plane. The line is excited by a nearby infinitesimal current element, and as a consequence, it is illuminated by a spherical wave having a $1/r$ falloff of the field intensity. Using suitable Green's functions for the ground-plane effects, an extended BLT equation for the transmission-line voltages and the E field at observation locations is formulated. Solutions are obtained both numerically and symbolically. One key issue in this analysis is including both the common-mode (antenna) and differential-mode (transmission-line) contributions to the scattered field from the line. At the conclusion of this paper, there are several suggestions of future work that could be performed in this area.

1. Introduction

The original BLT (Baum-Liu-Tesche) equation was developed for determining the voltage and current responses at the nodes of a general multiconductor transmission-line network [1] . This equation is based on a topological decomposition of an electromagnetically complex geometry into smaller elements, which can be characterized separately and then combined together to provide a solution for the overall problem. As noted in [1] and [2], the solutions for these responses using the BLT equation are *approximate*, in that they involve the assumptions of transmission-line theory to describe the behavior of the electromagnetic waves being propagated along the branches (or "tubes") of the network. Recently, an extension of the BLT equation concept was proposed to include the effects of EM field propagation in space (along trajectories that can be thought of as being an imaginary field-propagation "tube") [3]. In this development, the possibility of non-plane-wave propagation was suggested, and the coupling of these fields to the lines was taken into account. Moreover, the re-radiation of EM fields from the transmission-line currents is provided. With these effects included, an extended BLT equation was formulated, with observables being a combination of both transmission-line voltage and E-field responses.

In this paper, the use of the extended BLT equation developed in reference [3] is illustrated with a numerical example. A simple geometry is postulated involving a two-wire transmission line, which is a structure that is appropriate for a conventional BLT analysis. However, this line is excited by a transient current element located near the line, and consequently, the excitation of the line is by a spherical wave. Moreover, the line is located next to a conducting ground plane, and this affects both the incident field exciting the line and the re-radiation of the line. A distant observation point is also defined in this problem, and the solution for the E field at this location is also included in the BLT formulation. For simplicity, the problem geometry is chosen so that the incident and reflected E fields at the line are in the broadside direction.

All of these features are included in the extended BLT equation, which permits an analysis in the frequency domain. Included in this analysis is not only the transmission-line response, but the common-mode (or antenna-mode) response of the transmission-line structure, which has an effect on the scattered field. As will be noted in what follows, however, these scattered fields from the antenna are small compared with the primary fields emitted from the source.

It is important to point out at the onset of this analysis that while spherical waves are used to represent the EM fields propagating to and from source and field observation points, these fields are assumed to be locally plane waves at the transmission-line structure.

F. M. Tesche, J. M. Keen, and C. M. Butler are with the Holcombe Department of Electrical and Computer Engineering, College of Engineering & Science, 337 Fluor Daniel Building, Box 340915, Clemson, SC 29634-0915 USA; E-mail: ftesche@clemson.edu.

This invited paper is part of the special section honoring Carl E. Baum on his 65th birthday

2. Problem Description and Geometry

The problem under discussion here involves a simple two-wire transmission line illuminated by an electric and/or a magnetic source, as shown in Figure 1. This line/source configuration is similar to that examined in reference [3], with the exception that now an infinite, perfectly conducting ground plane is added to the structure.

As in the problem discussed in [3] , the goal of the present analysis is to develop an *extended* BLT equation for computing the two load voltages on the transmission line, as well as the E fields at a distant observation point and at the transmission line.

In performing this analysis, the following assumptions are made:

1. The distances between the source, transmission line, ground plane, and any observation points are assumed to be large compared with the wavelength, so that far-field expressions for radiated or scattered fields can be used.

2. The transmission-line cross section is assumed to be electrically small, so that the induced differential-mode response can be represented by transmission-line theory. The transmission line length can be comparable to or larger than the wavelength.

3. The currents on the two-wire line are portioned into differential-mode (transmission-line) and common-mode (antenna) components. The common-mode response has no effect on the transmission line load responses, as it is zero at the ends of the line. However, it does affect the response of the EM field at distant observation points. The differential-mode current response is calculated using conventional transmission-line theory, and the common-mode response is calculated using an approximate transmission-line-like solution.

4. The transmission-line equations for the propagating voltage and current waves on the line in the presence of the ground plane are assumed to be identical to those of an isolated line. The excitation field for this line, however, is modified by the ground plane. This is equivalent to saying that the transmission is loosely coupled to its ground-plane image.

The $\vec{P}$ and $\vec{M}$ sources shown in Figure 1 radiate an EM field towards the transmission line (in a direction defined by the angle ψ_1) and towards the observation point (in a direction defined by the angle ψ_2). Due to the anisotropic nature of the radiation from general sources, the amplitudes of the EM fields in these directions will be different. Also shown in Figure 1 is the angle of incidence, ψ_s, of a field *incident* on the transmission line, and a scattering angle, ψ_0, which corresponds to an angle at which the *radiated* E field from the transmission line is observed.

The specific example of the two-wire line considered here is shown in Figure 2. The transmission line consists of two parallel conductors, each of radius *a* and length *L*, and separated by a distance *d*. This line is terminated by two impedance elements, ZL_1 and ZL_2 , and the induced voltages across these loads are the observation quantities. This line is located parallel to an infinite ground plane, at a distance *h* from the center of the line.

The excitation source for this problem is taken to be an infinitesimal source with current moment Idl. This source is parallel to both the transmission line and the ground plane (in the *z* direction), and is located on the *y* axis at a distance r_1 from the transmission-line center. The field observation point is also located along the *y* axis at a distance r_2 from the source, as shown in the figure. For this geometry, the various angles discussed above are all equal: $\psi_1 = \psi_2 = \psi_0 = \psi_s = \pi/2$.

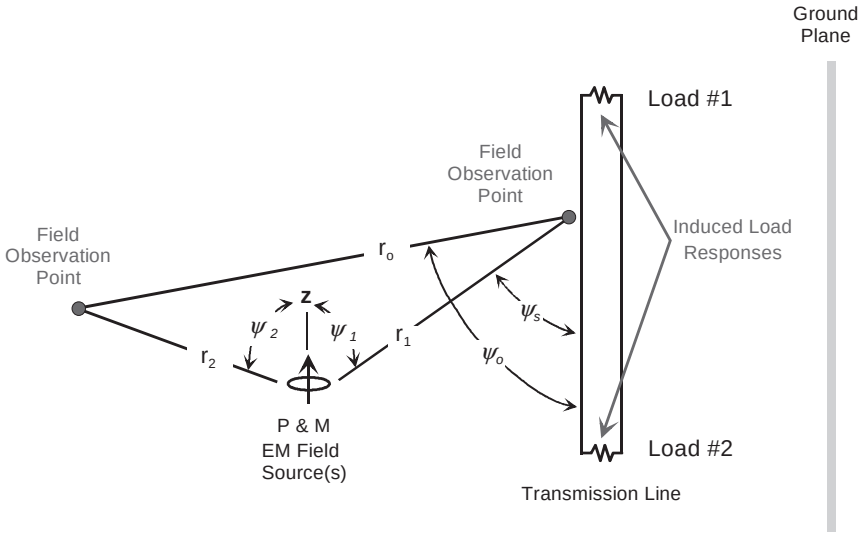

Figure 1. Geometry of a simple elementary source exciting a transmission line

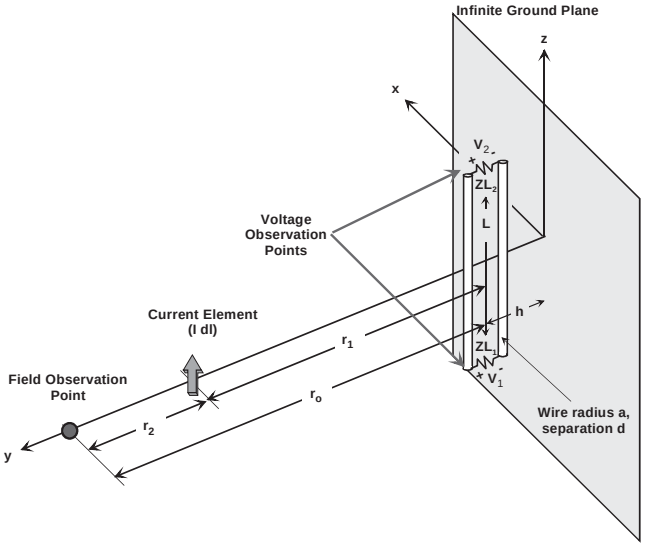

Figure 2. Specific example of the line geometry of a simple elementary source exciting a transmission line

As discussed in reference [3], the signal flow graph for the problem *without* the ground plane is the simple two-tube, four-node graph shown in Figure 3. With the ground plane present, the signal flow graph for the excited transmission line is the same, but the EM field coupling and propagation relationships on the tubes are formulated using modified Green's functions that take into account the presence of the conducting plate. Details of these Green's functions are provided in the next section.

3. The Extended BLT Equation

The derivation of the extended BLT equation for this problem begins by defining traveling-wave components of positive and negative traveling voltage waves on the transmission line (tube 1), and similar positive and negative propagating E-field waves on the field-propagation tube (tube 2). These traveling waves are determined at each of the nodes in the network, and are re-expressed as *incident* and *reflected* waves at the nodes. Figure 4 illustrates the incident and reflected voltages and E fields on the signal flow graph.

The development of the extended BLT equation for this network involves combining both the tube propagation relationships and the node reflection relationships, as described in reference [3]. However, in the present analysis with the ground plane, the effect of the ground plane on the field coupling and radiation of the transmission line must be taken into account.

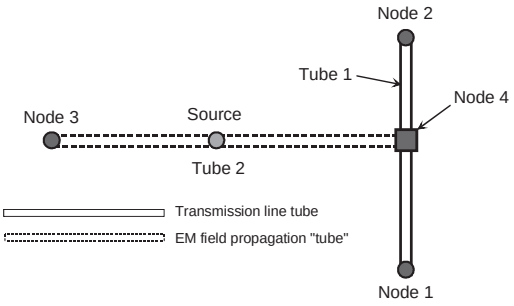

Figure 3. The signal flow graph for the EM interaction geometry of Figure 2

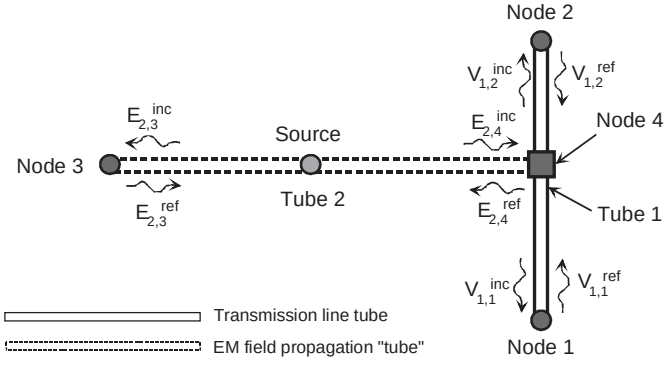

Figure 4. Definition of the incident and reflected voltages and E-fields on the signal flow graph

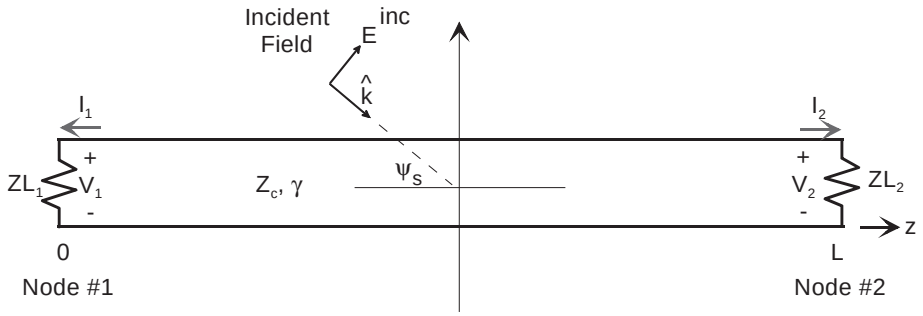

Figure 5. Field Excitation of a two-wire transmission line

3.1 Tube Propagation Relationships

3.1.1 Propagation on Tube 1 (the Transmission Line)

To begin with the development of the extended BLT equation, we first review the propagation relationships for the positive and negative traveling voltage waves on the transmission line. For the transmission line tube 1 *located in free space and excited by an incident plane wave*, reference [3] has developed the following matrix equation relating the reflected and incident voltage waves at nodes 1 and 2:

$$\begin{bmatrix} V_{1,1}^{ref} \\ V_{1,2}^{ref} \end{bmatrix} = \begin{bmatrix} 0 & e^{\gamma L} \\ e^{\gamma L} & 0 \end{bmatrix} \bullet \begin{bmatrix} V_{1,1}^{inc} \\ V_{1,2}^{inc} \end{bmatrix} - \begin{bmatrix} F_1(\psi_s) E_{2,4}^{inc} \\ F_2(\psi_s) E_{2,4}^{inc} \end{bmatrix} \quad (1)$$

As shown in Figure 5, the excitation of this line is provided by an incident EM field with the E field in the plane of the transmission line and an angle of incidence ψ_s. This incident field induces charge and current everywhere on the line, and the specific observation quantities of interest are the load currents and voltages, as noted in the figure.

For this lossless transmission line with wire radius *a* and separation *d*, the characteristic impedance of the line is

$$Z_c = 120 \ln\left(\frac{d}{a}\right) \Omega, \quad (2)$$

and simple TEM transmission-line theory provides the wave propagation constant, γ, as

$$\gamma = j\frac{\omega}{c}, \quad (3)$$

where ω is the angular frequency ($2\pi f$), and c is the speed of light $= 3.0 \times 10^8$ m/s.

Note that Equation (1) contains two terms. The first is a matrix relationship relating the propagation of the incident and reflected voltage waves on the line. The second is a vector term that describes the excitation of voltage waves by the incident E field, $E_{2,4}^{inc}$, at the "field coupling node" (node 4), as introduced in reference [3]. This excitation is represented by the integral functions $F_1(\psi_s)$ and $F_2(\psi_s)$, developed in Appendix A of [3], multiplied by the incident field $E_{2,4}^{inc}$. These *F* functions depend on the local angle of incidence on the line, ψ_s, and in the more general case, on the azimuthal incidence and polarization angles (see Equation (7.40) of reference [2]). For the special geometry of Figure 2, the incident field on the transmission line is broadside to the line, so that $\psi_s = \pi/2$.

From Appendix A of [3], the general expressions for the terms coupling the field to the transmission line, $F_1(\psi_s)$ and $F_2(\psi_s)$, are given as

$$F_1(\psi_s) = \frac{d}{2}\left[e^{jkL(1-\cos\psi_s)} - 1\right], \quad (4)$$

$$F_2(\psi_s) = \frac{d}{2} e^{jkL}\left[e^{-jkL(1+\cos\psi_s)} - 1\right],$$

and for $\psi_s = \pi/2$, these terms simplify to

$$F_1 = \frac{d}{2}\left(e^{jkL} - 1\right), \quad (5)$$

$$F_2 = \frac{d}{2}\left(1 - e^{jkL}\right) = -F_1 .$$

It is important to note that in Equation (4), the excitation of the transmission-line conductors *and* the orthogonal "ends" of the line are taken into account. Also, note that the excitation of the line, and hence the line response, are *even* functions of the angle of incidence, ψ_s, on the transmission line. Thus, for the excitations shown in Figure 6, the line responses I_1, I_2, V_1, and V_2 will be identical for the two different incident fields shown in this figure.

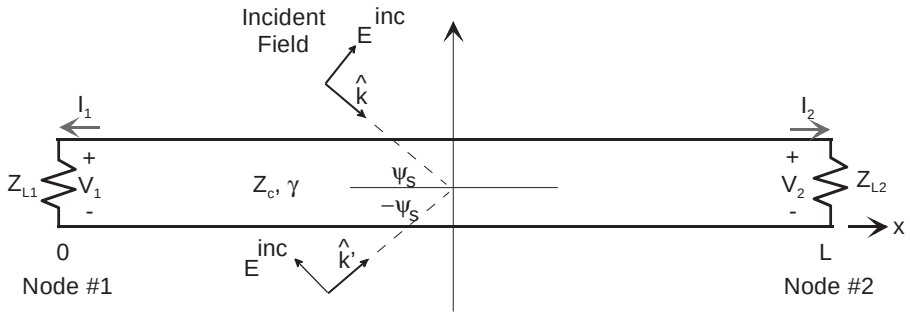

Figure 6. Line excitation for positive and negative angles of incidence, ψ_s.

The effect of this symmetry on the excitation of the differential (transmission-line) mode when the line is located next to a conducting ground plane is suggested in Figure 7. In this case, the reflected E field from the ground plane has a reversal of direction to satisfy the boundary condition that the tangential component of E is zero on the ground plane. This results in the ground-plane-reflected field, which arrives with a negative angle of incidence. This field affects the line exactly like the incident field in Figure 6, but with a different time delay. As a result, *both the incident and ground-reflected field components induce differential-mode responses on the transmission line that have the same sign*. In other words, the contributions from these E-field components to the differential mode are *additive*.

To extend Equation (1) to the case of *plane-wave* illumination of the transmission line located over the ground plane, we may superimpose the effects of the incident and ground-plane-reflected fields. This provides the following matrix expression:

$$\begin{bmatrix} V_{1,1}^{ref} \\ V_{1,2}^{ref} \end{bmatrix} = \begin{bmatrix} 0 & e^{\gamma L} \\ e^{\gamma L} & 0 \end{bmatrix} \bullet \begin{bmatrix} V_{1,1}^{inc} \\ V_{1,2}^{inc} \end{bmatrix}$$

$$- \begin{bmatrix} F_1(\psi_s)E^{inc} + F_1(-\psi_s)E^{gpref} \\ F_2(\psi_s)E^{inc} + F_2(-\psi_s)E^{gpref} \end{bmatrix} \qquad (6)$$

In this last equation, E^{inc} denotes the incident E-field strength evaluated at the midpoint of the transmission line, and E^{gpref} represents the ground-plane-reflected field strength at the same midpoint location.

Assuming that the line height over the ground plane is h, using the excitation symmetry, and taking the zero-phase reference to be at the midpoint of the line, we find that Equation (6) for the incident and reflected line voltages at nodes 1 and 2 for a plane-wave excitation becomes

$$\begin{bmatrix} V_{1,1}^{ref} \\ V_{1,2}^{ref} \end{bmatrix} = \begin{bmatrix} 0 & e^{\gamma L} \\ e^{\gamma L} & 0 \end{bmatrix} \bullet \begin{bmatrix} V_{1,1}^{inc} \\ V_{1,2}^{inc} \end{bmatrix}$$

$$- \begin{bmatrix} F_1(\psi_s)E^{inc}\left[1 + e^{-jk2h\sin(\psi_s)}\right] \\ F_2(\psi_s)E^{inc}\left[1 + e^{-jk2h\sin(\psi_s)}\right] \end{bmatrix}, \qquad (7)$$

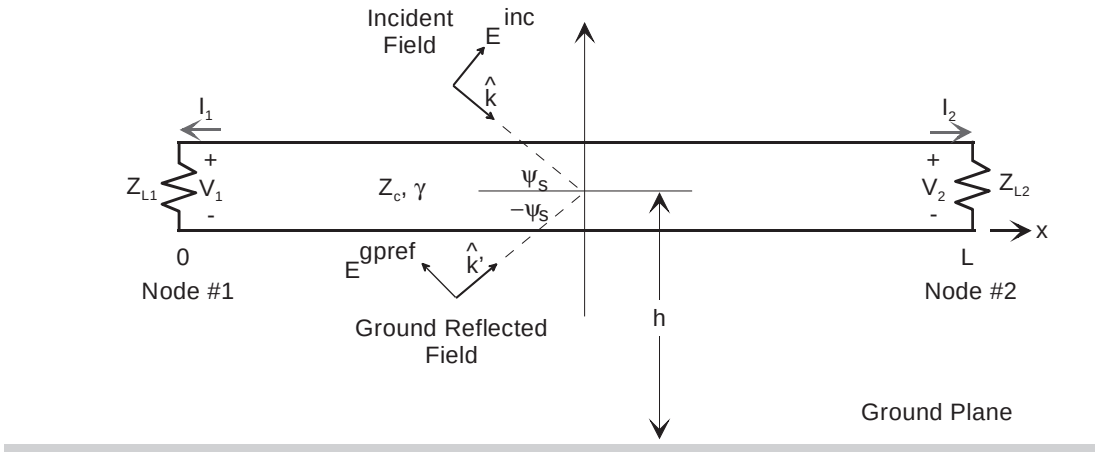

Figure 7. Transmission line located over a conducting ground plane and excited by an incident plane wave

where an effective excitation term, E^{excit}, has been defined as

$$E^{excit} = E^{inc}\left[1+e^{-jk2h\sin(\psi_s)}\right] \qquad (8)$$

Notice that the term E^{excit} is *not* the total excitation E field at the transmission line (which would be the sum of the incident and ground-plane-reflected field components, and written as $E^{tot} = E^{inc}\left[1-e^{-jk2h\sin(\psi_s)}\right]$), but rather it is given by Equation (8) with the *plus* sign for the exponential term. Since the assumed geometry of this problem involves only the *z* components of the E field (see Figure 2), the *z* component of the E field is identically zero on the ground plane ($h = 0$). The excitation term in Equation (8), with the positive sign for the exponential term, becomes $2E^{inc}$. This is a field boundary condition more akin to that for the tangential magnetic field on a perfect conductor than to that for the tangential E field.

Using the notation E^{excit} for the effective line excitation, we write Equation (7) as

$$\begin{bmatrix} V_{1,1}^{ref} \\ V_{1,2}^{ref} \end{bmatrix} = \begin{bmatrix} 0 & e^{\gamma L} \\ e^{\gamma L} & 0 \end{bmatrix} \bullet \begin{bmatrix} V_{1,1}^{inc} \\ V_{1,2}^{inc} \end{bmatrix} - \begin{bmatrix} F_1(\psi_s)E^{excit} \\ F_2(\psi_s)E^{excit} \end{bmatrix}. \qquad (9)$$

Thus, we see that the functional form of Equation (1) may be used to describe the relationships between the incident and reflected voltage waves at nodes 1 and 2 of the transmission line with the E^{inc} terms in the excitation being modified by the effects of the ground plane, as represented by the excitation term E^{excit}.

Of course, the expression for the excitation field in Equation (8) is valid only for an incident plane wave. In the case of the infinitesimal current-source excitation shown in Figure 1, a different form of this excitation function is required. Neglecting polarization effects and assuming that far-field conditions hold, one can express the incident E field on the transmission line by spherical waves from the current source Idl and possibly from a reflected field ($E_{2,3}^{ref}$) from the distant node 3 (see Figure 4) as

$$E^{inc} = \frac{e^{-jkr_o}}{r_0} a_3 E_{2,3}^{ref} + \frac{e^{-jkr_1}}{r_1} S_1(\psi_1). \qquad (10)$$

In this expression, the terms (e^{-jkr}/r) provide for the propagation of the spherical waves along tube 2. As discussed in reference [3], the parameter a_3 represents the nominal size of the scattering body at node 3, and is used as a normalizing constant for the E fields to provide dimensions of volts. In this manner, we obtain a BLT equation for all variables having the dimensions of volts.

The source term, $S_1(\psi_1)$, in Equation (10) describes the amplitude of the radiation from the elementary current source in the direction given by the angle ψ_1, as shown in Figure 8. For this simple example of a *z*-directed current source, the *z* component of the radiated E field at the transmission-line location is given as

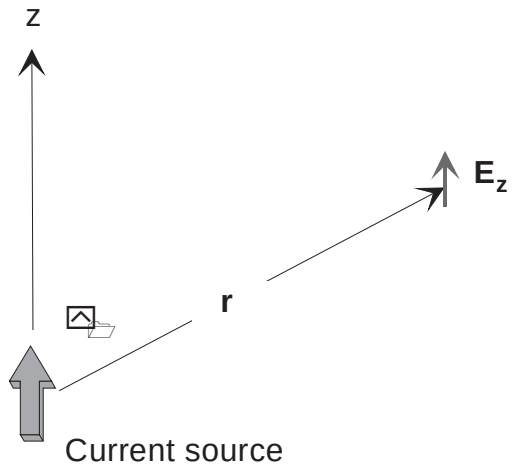

Figure 8. An elementary current source and the E_z field component at a distance r

$$E_z(\psi_1) = -\frac{j\omega\mu}{4\pi} Idl \sin^2(\psi_1) \frac{e^{-jkr_1}}{r_1} \qquad (11)$$

$$\equiv S_1(\psi_1) \frac{e^{-jkr_1}}{r_1}.$$

Equation (11) defines the source term, S, at an angle ψ_1 as $S(\psi_1) = -j\omega\mu\, Idl \sin^2(\psi_1)$. For the example we are considering in Figure 2, the source angle is $\psi_1 = \psi_s = \pi/2$, so that the source term in Equation (11) is

$$S_1 = -\frac{j\omega\mu}{4\pi} Idl. \qquad (12)$$

With the spherical wave of Equation (10) incident on the transmission line, another ground-plane-reflected spherical wave also will be present, and both will contribute to the excitation of the line. From Equation (10) and image theory, the following *z*-directed excitation E field acting on the transmission line can be determined:

$$E^{excit} = \left[\frac{e^{-jkr_0}}{r_0} + \frac{e^{-jk(r_0+2h)}}{r_0+2h}\right] a_3 E_{2,3}^{ref}$$

$$+ \left[\frac{e^{-jkr_1}}{r_1} + \frac{e^{-jk(r_1+2h)}}{r_1+2h}\right] S_1 \qquad (13)$$

$$\equiv K_1(r_0) a_3 E_{2,3}^{ref} + K_1(r_1) S_1$$

Here, the terms $K_z(r_0)$ and $K_1(r_1)$ amount to modified Green's functions representing the excitation functions for the transmission line in the presence of the ground plane. These are defined as

$$K_1(r) = \frac{e^{-jkr}}{r} + \frac{e^{-jk(r+2h)}}{r+2h}. \qquad (14)$$

With this excitation term for the transmission line, the tube 1 matrix propagation relation of Equation (9) for the spherical-wave excitation becomes[2]

$$\begin{bmatrix} V_{1,1}^{ref} \\ V_{1,2}^{ref} \end{bmatrix} = \begin{bmatrix} 0 & e^{\gamma L} \\ e^{\gamma L} & 0 \end{bmatrix} \bullet \begin{bmatrix} V_{1,1}^{inc} \\ V_{1,2}^{inc} \end{bmatrix}$$

$$- \begin{bmatrix} F_1 K_1(r_0) a_3 E_{2,3}^{ref} \\ F_2 K_1(r_0) a_3 E_{2,3}^{ref} \end{bmatrix} - \begin{bmatrix} F_1 K_1(r_1) S_1 \\ F_2 K_1(r_1) S_1 \end{bmatrix} \qquad (15)$$

3.1.2 Propagation on Tube 2 (the Field Propagation Path)

We now turn our attention to the behavior of the incident and reflected E fields at nodes 3 and 4 on tube 2: the field propagation path. Considering first the incident E field at node 4, $E_{2,4}^{inc}$, we note that it consists of a direct term like Equation (10) from the source and the reflected field at node 3, $E_{2,3}^{ref}$, together with the ground-plane image contributions. This results in an equation similar to Equation (13) for the excitation field of the transmission line, but with a *negative* sign for the image terms:

$$E_{2,4}^{inc} = \left[\frac{e^{-jkr_0}}{r_0} - \frac{e^{-jk(r_0+2h)}}{r_0+2h} \right] a_3 E_{2,3}^{ref}$$

$$+ \left[\frac{e^{-jkr_1}}{r_1} - \frac{e^{-jk(r_1+2h)}}{r_1+2h} \right] S_1 \qquad (16)$$

$$\equiv K_2(r_0) a_3 E_{2,3}^{ref} + K_2(r_1) S_1,$$

where the modified Green's function, $K_2(r)$, is given as

$$K_2(r) = \left[\frac{e^{-jkr}}{r} - \frac{e^{-jk(r+2h)}}{(r+2h)} \right] \qquad (17)$$

Similarly, *with the transmission line (tube 1) absent*, the E-field propagation relationship for the incident E field, $E_{2,3}^{inc}$, at node 3 (the field observation point) is expressed using image theory as

$$E_{2,3}^{inc} = \left[\frac{e^{-jkr_0}}{r_0} - \frac{e^{-j(kr_0+2h)}}{(r_0+2h)} \right] a_4 E_{2,4}^{ref}$$

$$+ \left[\frac{e^{-jkr_2}}{r_2} - \frac{e^{-jk(r_2+2r_1+2h)}}{r_2+2r_1+2h} \right] S_2(\psi_2) \qquad (18)$$

$$\equiv K_2(r_0) a_4 E_{2,4}^{ref} + K_3(r_2) S_2(\psi_2)$$

In this expression, a characteristic length of node 4 (a_4) is used for normalization of the field. Also, a third modified E field Green's function, $K_3(r)$, is introduced to account for the ground plane effects, as

$$K_3(r) = \left[\frac{e^{-jkr}}{r} - \frac{e^{-jk(r+2r_1+2h)}}{r+2r_1+2h} \right]. \qquad (19)$$

The source term, $S_2(\psi_2)$, in Equation (18) generally involves a different angle than does the source in Equation (16), as noted from Figure 1. However, for our example of Figure 2, this angle is the same as ψ_1, so that $S_2(\psi_2) = S_1(\psi_1) = -\frac{j\omega\mu}{4\pi} Idl$.

If the transmission line is inserted into the problem space, then the transmission-line mode currents flowing on the line also contribute to the incident E field at node 3. As noted in Appendix B of reference [3], the radiated E field at a distance r_0 and observation angle ψ_0 from the transmission-line currents flowing in the two-wire line of Figure 9 can be expressed in terms of the incident voltage waves at each node of the transmission line of the line (nodes 1 and 2) as

$$E_\xi = \frac{jk}{2\pi} \frac{Z_0}{Z_c} \frac{e^{-jkr_0}}{r_0} \left[V_1^{inc} F_1(\psi_0) + V_2^{inc} F_2(\psi_0) \right], \qquad (20)$$

where Z_0 is the free-space wave impedance ($Z_0 \approx 377\ \Omega$), Z_c is the characteristic impedance of the transmission line ($Z_c = 120 \ln(d/a)\ \Omega$ for wire radius a and separation d), and $k = 2\pi f / c$. The field radiation terms, F_1 and F_2 are the same as these derived for the reception case in Equation (4), but evaluated for the observation angle ψ_0.

Equation (20) is not the complete expression for the radiation from the transmission line, however, as the ground-plane effects have not yet been taken into account. Figure 10 shows the transmission line positioned near the ground plane and illustrates the fact that the wire currents of the transmission-line image are in the same direction as in the original transmission line. Thus, the radiation contribution

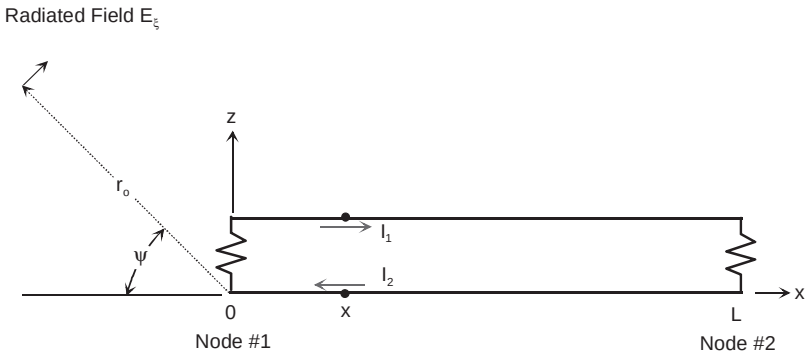

Figure 9. Illustration of a transmission line radiating an E_ξ-field component in a direction given by the angle ψ_o.

from the image transmission is expected to *add* to the original transmission-line radiation. Thus, the radiation at node 3 from the line located near the ground plane is given by the expression

$$E_\xi = \frac{jk}{2\pi}\frac{Z_0}{Z_c}\left[\frac{e^{-jkr_0}}{r_0} + \frac{e^{-j(kr_0+2h)}}{(r_0+2h)}\right]$$

$$\left[F_1\ (\psi_0)V_{1,1}^{inc} + F_2\ (\psi_0)V_{1,2}^{inc}\right] \qquad (21)$$

$$\equiv \frac{jk}{2\pi}\frac{Z_0}{Z_c}K_1(r_0)\left(F_1\ (\psi_0)V_{1,1}^{inc} + F_2\ (\psi_0)V_{1,2}^{inc}\right),$$

where the term K_1 is that defined in Equation (14) and the angle $\psi_0 = \pi/2$. Note that Equation (21) assumes that the observation angles ψ_0 from the physical and image transmission lines are equal, which is valid only for distant observation points.

With Equation (21) providing the contribution from the transmission-line currents to the incident field at node 3, we express the complete incident E field at this node as

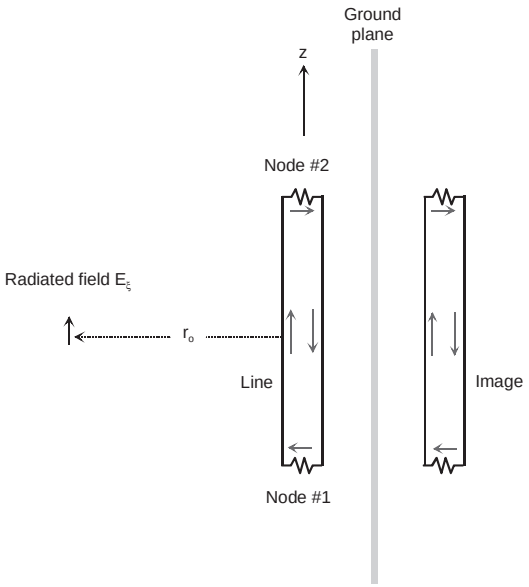

Figure 10. Radiation from the transmission line in the presence of the conducting ground

$$E_{2,3}^{inc} = K_2(r_0)a_4E_{2,4}^{ref} + K_3(r_2)S_2(\psi_2)$$

$$+\frac{jk}{2\pi}\frac{Z_0}{Z_c}K_1(r_0)\left[F_1\ (\psi_0)V_{1,1}^{inc} + F_2\ (\psi_0)V_{1,2}^{inc}\right] \quad (22)$$

Using the same procedure as in reference [3], we combine Equations (18) and (22) into a matrix equation for the incident and reflected E-field components at nodes 3 and 4, as

$$\begin{bmatrix}E_{2,3}^{inc}\\ E_{2,4}^{inc}\end{bmatrix} = \begin{bmatrix}0 & a_4K_2(r_0)\\ a_3K_2(r_0) & 0\end{bmatrix}\bullet\begin{bmatrix}E_{2,3}^{ref}\\ E_{2,4}^{ref}\end{bmatrix}$$

$$+\frac{jk}{2\pi}\frac{Z_0}{Z_c}K_1(r_0)\begin{bmatrix}F_1 & F_2\\ 0 & 0\end{bmatrix}\bullet\begin{bmatrix}V_{1,1}^{inc}\\ V_{1,2}^{inc}\end{bmatrix}+\begin{bmatrix}K_3(r_2)S_2\\ K_2(r_1)S_1\end{bmatrix} \quad (23)$$

and upon rearranging terms, this equation can be solved for the normalized *reflected* E fields at the nodes as

$$\begin{bmatrix}a_3E_{2,3}^{ref}\\ a_4E_{2,4}^{ref}\end{bmatrix} = \begin{bmatrix}0 & \dfrac{1}{a_4K_2(r_0)}\\ \dfrac{1}{a_3K_2(r_0)} & 0\end{bmatrix}\begin{bmatrix}a_3E_{2,3}^{inc}\\ a_4E_{2,4}^{inc}\end{bmatrix}$$

$$-\frac{jk}{2\pi}\frac{Z_0}{Z_c}\frac{K_1(r_0)}{K_2(r_0)}\begin{bmatrix}0 & 0\\ F_1 & F_2\end{bmatrix}\begin{bmatrix}V_{1,1}^{inc}\\ V_{1,2}^{inc}\end{bmatrix}-\begin{bmatrix}\dfrac{K_2(r_1)}{K_2(r_0)}S_1\\ \dfrac{K_3(r_2)}{K_2(r_0)}S_2\end{bmatrix}. \quad (24)$$

Equations (15) and (24) now can be combined into a larger matrix equation relating the reflected generalized voltage quantities at the nodes to the incident voltages and the source terms. See Appendix A of reference [4] for details. The resulting equation is

$$\begin{bmatrix} V_{1,1}^{ref} \\ V_{1,2}^{ref} \\ a_3 E_{2,3}^{ref} \\ a_4 E_{2,4}^{ref} \end{bmatrix} = \begin{bmatrix} 0 & e^{\gamma L} & 0 & -\dfrac{K_1(r_0)}{a_4 K_2(r_0)} F_1 \\ e^{\gamma L} & 0 & 0 & -\dfrac{K_1(r_0)}{a_4 K_2(r_0)} F_2 \\ 0 & 0 & 0 & \dfrac{1}{a_4 K_2(r_0)} \\ -\dfrac{jk}{2\pi}\dfrac{Z_0}{Z_c}\dfrac{K_1(r_0)}{K_2(r_0)} F_1 & -\dfrac{jk}{2\pi}\dfrac{Z_0}{Z_c}\dfrac{K_1(r_0)}{K_2(r_0)} F_2 & \dfrac{1}{a_3 K_2(r_0)} & 0 \end{bmatrix} \bullet \begin{bmatrix} V_{1,1}^{inc} \\ V_{1,2}^{inc} \\ a_3 E_{2,3}^{inc} \\ a_4 E_{2,4}^{inc} \end{bmatrix} - \begin{bmatrix} F_1 \left(\dfrac{K_1(r_1)K_2(r_0) - K_1(r_o)K_2(r_1)}{K_2(r_o)} \right) S_1 \\ F_2 \left(\dfrac{K_1(r_1)K_2(r_0) - K_1(r_o)K_2(r_1)}{K_2(r_o)} \right) S_1 \\ \dfrac{K_2(r_1)}{K_2(r_o)} S_1 \\ \dfrac{K_3(r_2)}{K_2(r_o)} S_2 \end{bmatrix} \quad (25)$$

3.2 Node Reflection Relationships

At nodes 1 and 2 on the transmission line, the voltage reflection coefficients, ρ_1 and ρ_2, are used to relate the reflected and incident voltage waves at the nodes as

$$V_{1,1}^{ref} = \rho_1 V_{1,1}^{inc} \text{ and } V_{1,2}^{ref} = \rho_2 V_{1,2}^{inc} , \qquad (26a)$$

where the reflection coefficients ρ_i are related to the terminating line impedance and the line characteristic impedance as

$$\rho_i = \frac{Z_{Li} - Z_c}{Z_{Li} + Z_c} . \qquad (26b)$$

Similarly, at node 3 we can define an E-field reflection coefficient between the field incident and reflected at this location – if there is a scattering body at this node. This relationship is

$$E_{2,3}^{ref} = \rho_3 E_{2,3}^{inc} . \qquad (27)$$

If we assume that this observation point is located in free space, there is no reflection of the field, and we have the condition that $\rho_3 = 0$.

At node 4, the field-coupling node, the effects of the transmission-line currents in producing a reflected field at this node have already been taken into account in Equation (22). However, the effects of the antenna-mode current flowing on the transmission line have yet to be included in the analysis. As shown in Figure 11, the two-wire line can be modeled as a single conductor of length L and effective radius $a_{eff} = \sqrt{2}\, a$, so that the equivalent cross-sectional area of the conductor is equal to the total area of the two-wire line.

For this line, an incident EM field with polarity as noted in the figure strikes the wire with an angle of incidence θ_i. This field induces a current $I(z)$ to flow in the wire and a scattered EM field results in such a way that the total tangential E field is zero along the wire. The $\hat{\theta}$ component of the scattered E field is observed at an angle θ_s, as shown in the diagram.

For use in the extended BLT equation, we need a relationship between the incident field at this wire to the scattered field to define the field reflection coefficient at node 4. The usual approach for determining this is to use an integral-equation solution. However, keeping with the spirit of performing a transmission-line analysis for this analysis, we can develop an approximate, transmission-line-like analysis for this scattering problem.

As noted in Chapter 4 of reference [2], the Hallén integral equation for the antenna-mode current for the conductor in Figure 11 can be approximated and a closed form of the incident-field-induced current results. For an incident field E^{inc} at angle θ_i, this current has the form

$$I(z) = \frac{j4\pi E^{inc}}{Z_c \Omega_0 k \sin\theta_i} \left[\left(\cos kz - e^{jkz\cos\theta_i} \right) + \left(e^{jkL\cos\theta_i} - \cos kL \right) \frac{\sin kz}{\sin kL} \right] \qquad (28)$$

In this expression, the term Ω_0 is the usual thin-wire antenna parameter, $\Omega_0 = 2\ln(L/a)$.

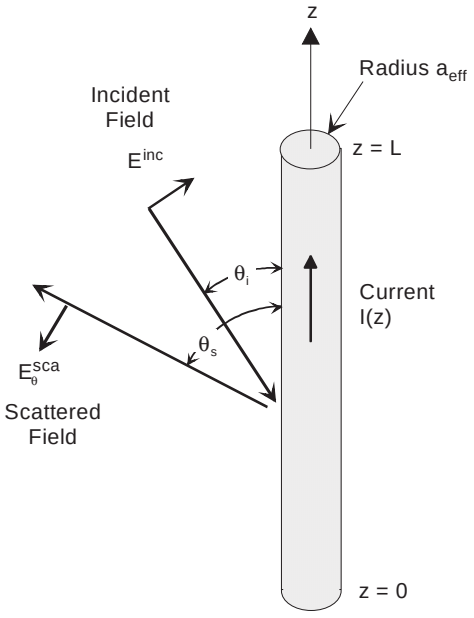

Figure 11. Illustration of a single conductor scatterer of length L and radius a_{eff}

The scattered E field at the angle θ_s can be determined from integration over the wire current distribution as

$$E_\theta^{sca} = \frac{jkZ_c \sin\theta_0}{4\pi} \frac{e^{-jkr_0}}{r_0} \int_0^L I(z) e^{jkz\cos\theta_0} dz$$

$$= -\frac{E^{inc}}{\Omega_0} \frac{\sin\theta_0}{\sin\theta_i} \frac{1}{\sin(kL)} \frac{e^{-jkr_0}}{r_0}$$

$$\int_0^L \Big[\Big(\cos kz - e^{jkz\cos\theta_i}\Big) \sin kL$$

$$- \Big(\cos kL - e^{jkL\cos\theta_i}\Big) \sin kz \Big] e^{jkz\cos\theta_0} dz \qquad (29)$$

where $k = \omega/c$. As noted in [2], the analytical expression for the scattered field for arbitrary angles θ_i and θ_s are very cumbersome. However, for $\theta_i = \theta_s = \pi/2$, the expression is rather simple:

$$E_\theta^{sca} = \frac{E^{inc}}{\Omega_0} \frac{e^{-jkr_0}}{kr_0} \frac{\{2[\cos(kL) - 1] + kL\sin(kL)\}}{\sin(kL)} \quad (30)$$

For the reflection coefficient at node 4, we wish to relate the z components of the fields. Noting that $E_\theta^{sca} = -E_z^{sca}$, we have from Equation (30)

$$E_z^{sca} = \frac{E^{inc}}{\Omega_0} \frac{e^{-jkr_0}}{kr_0} \frac{\{2[1 - \cos(kL)] - kL\sin(kL)\}}{\sin(kL)} \quad (31)$$

$$= E^{inc} \frac{e^{-jkr_0}}{r_0} \sigma(\omega) ,$$

where $\sigma(\omega)$ is the frequency-dependent *effective scattering length* of the wire, defined as

$$\sigma(\omega) \equiv \frac{c}{\Omega_0 \omega L} \frac{\{2[1 - \cos(\omega L/c)] - kL\sin(\omega L/c)\}}{\sin(\omega L/c)} \text{ (meters)} \qquad (32a)$$

The above expression for the effective scattering length is seen to have zeros in the denominator due to the term $\sin(\omega L/c)$. Frequencies for which $(\omega L/c) = n\pi$ correspond to the natural resonant frequencies of the antenna-mode current on the wire, and at these frequencies the scattering length given in Equation (32a) is infinite. This singularity arises because the radiation loss of the scatterer is not properly taken into account in the approximate scattering analysis.

In a numerical implementation of the extended BLT equation, these singularities in σ provide similar singularities in the spectrum of the computed E fields at the field nodes 3 and 4. Moreover, in the time domain, the FFT solution consists of an ever-repeating oscillating waveform with the frequency content of the various singularities.

To fix this problem, we can add artificial loss into the antenna-mode solution – not trying to model accurately the radiation resistance, but rather attempting to eliminate the singularities in the solution. Noting that the derivation of the antenna-mode response has involved a transmission-line-like equation, we can put Equation (32a) into a form resembling a transmission-line solution by expanding the $\sin(\omega L/c)$ term into complex exponentials. In this manner, Equation (32a) can be written as

$$\sigma(\omega) = \frac{-2je^{j\omega L/c}}{\Omega_0 \omega/c}$$

$$\frac{\{2[1 - \cos(\omega L/c)] - (\omega L/c)\sin(\omega L/c)\}}{e^{j2\omega L/c} - 1} \quad (32b)$$

In examining typical transmission-line solutions (see reference [2]), we see that the denominator term in Equation (32b) frequently appears as $e^{jk2\omega L/c} - \rho_1\rho_2$, where ρ_1 and ρ_2 correspond to voltage reflection coefficients. When ρ_1 and $\rho_2 = \pm 1$, there are zeros in the denominator and singularities in the response. However, when there is loss on the transmission line, the product of these reflection coefficients is $|\rho_1\rho_2| < 1$, with the result that there are no response singularities. Thus, a simple solution to eliminate these singularities is to rewrite the denominator in Equation (32b) as $e^{jk2\omega L/c} - \kappa$, where κ is a suitably chosen number close to, but less than, unity. A choice for this parameter for this study is $\kappa = 0.9$.

To determine the reflection coefficient at node 4, we evaluate Equation (31) at the node "boundary," which is defined by the parameter a_4 that was introduced in Equation (18). At a distance of a_4 from the node, the scattered E field is expressed in terms of the incident field as

$$E_z^{sca} = E^{inc} \frac{e^{-jka_4}}{a_4} \sigma(\omega)$$

$$\approx E^{inc} \frac{\sigma(\omega)}{a_4} \qquad (33)$$

$$\equiv E^{inc} \rho_4(\omega) \cdot$$

Hence, the reflection coefficient is $\rho_4 = \sigma/a_4$ at node 4.

Taking each of the reflected terms into account, we now can write the network reflection matrix as

$$\begin{bmatrix} V_{1,1}^{ref} \\ V_{1,2}^{ref} \\ E_{2,3}^{ref} \\ E_{2,4}^{ref} \end{bmatrix} = \begin{bmatrix} \rho_1 & 0 & 0 & 0 \\ 0 & \rho_2 & 0 & 0 \\ 0 & 0 & \rho_3 & 0 \\ 0 & 0 & 0 & \rho_4 \end{bmatrix} \cdot \begin{bmatrix} V_{1,1}^{inc} \\ V_{1,2}^{inc} \\ E_{2,3}^{inc} \\ E_{2,4}^{inc} \end{bmatrix} \quad (34a)$$

or in terms of the normalized voltage variables,

$$\begin{bmatrix} V_{1,1}^{ref} \\ V_{1,2}^{ref} \\ a_3 E_{2,3}^{ref} \\ a_4 E_{2,4}^{ref} \end{bmatrix} = \begin{bmatrix} \rho_1 & 0 & 0 & 0 \\ 0 & \rho_2 & 0 & 0 \\ 0 & 0 & \rho_3 & 0 \\ 0 & 0 & 0 & \rho_4 \end{bmatrix} \cdot \begin{bmatrix} V_{1,1}^{inc} \\ V_{1,2}^{inc} \\ a_3 E_{2,3}^{inc} \\ a_4 E_{2,4}^{inc} \end{bmatrix} \quad (34b)$$

3.3 The Extended BLT Equations

Equations (25) and (34b) can now be solved for the vector of incident waves at the nodes. This provides the following *extended* BLT equation for the incident voltages and E-fields at the nodes (equation 35):

Using Equation (34b) again in the above expression to compute the *total* voltage and E field, we can write the final expression for the extended BLT equation as (equation 36)

Note that this equation now contains the effects of both the transmission-line mode and the antenna-mode response of the two-wire line.

3.4 Solution to the Extended BLT Equation

For the case where there is no reflection at node 3 ($\rho_3 = 0$), it is possible to obtain a symbolic solution to Equation (36) for the total voltages and fields at the nodes. After a bit of manipulation, we can express these solutions as

$$V_{1,1} = (1+\rho_1)\frac{e^{\gamma L}F_2 + \rho_2 F_1}{e^{2\gamma L} - \rho_1\rho_2} K_1(r_1)S_1, \quad (37a)$$

$$V_{1,2} = (1+\rho_2)\frac{e^{\gamma L}F_1 + \rho_1 F_2}{e^{2\gamma L} - \rho_1\rho_2} K_1(r_1)S_1, \quad (37b)$$

$$E_{2,3} = K_3(r_2)S_2 + \sigma K_2(r_0)K_2(r_1)S_1 + \frac{jk}{2\pi}\frac{Z_0}{Z_c}K_1(r_0)K_1(r_1)\left(\frac{2F_1F_2e^{\gamma L} + F_1^2\rho_2 + F_2^2\rho_1}{e^{2\gamma L} - \rho_1\rho_2}\right)S_1 \quad (37c)$$

$$\begin{bmatrix} V_{1,1}^{inc} \\ V_{1,2}^{inc} \\ a_3E_{2,3}^{inc} \\ a_4E_{2,4}^{inc} \end{bmatrix} = \begin{bmatrix} -\rho_1 & e^{\gamma L} & 0 & -\frac{K_1(r_0)}{a_4K_2(r_0)}F_1 \\ e^{\gamma L} & -\rho_2 & 0 & -\frac{K_1(r_0)}{a_4K_2(r_0)}F_2 \\ 0 & 0 & -\rho_3 & \frac{1}{a_4K_2(r_0)} \\ -\frac{jk}{2\pi}\frac{Z_0}{Z_c}\frac{K_1(r_0)}{K_2(r_0)}F_1 & -\frac{jk}{2\pi}\frac{Z_0}{Z_c}\frac{K_1(r_0)}{K_2(r_0)}F_2 & \frac{1}{a_3K_2(r_0)} & -\rho_4 \end{bmatrix}^{-1} \cdot \begin{bmatrix} F_1\left(\frac{K_1(r_1)K_2(r_0)-K_1(r_0)K_2(r_1)}{K_2(r_0)}\right)S_1 \\ F_2\left(\frac{K_1(r_1)K_2(r_0)-K_1(r_0)K_2(r_1)}{K_2(r_0)}\right)S_1 \\ \frac{K_2(r_1)}{K_2(r_0)}S_1 \\ \frac{K_3(r_2)}{K_2(r_0)}S_2 \end{bmatrix} \quad (35)$$

$$\begin{bmatrix} V_{1,1} \\ V_{1,2}^{i} \\ a_3E_{2,3} \\ a_4E_{2,4} \end{bmatrix} = \begin{bmatrix} 1+\rho_1 & 0 & 0 & 0 \\ 0 & 1+\rho_2 & 0 & 0 \\ 0 & 0 & 1+\rho_3 & 0 \\ 0 & 0 & 0 & 1+\rho_4 \end{bmatrix} \times$$

$$\begin{bmatrix} -\rho_1 & e^{\gamma L} & 0 & -\frac{K_1(r_0)}{a_4K_2(r_0)}F_1 \\ e^{\gamma L} & -\rho_2 & 0 & -\frac{K_1(r_0)}{a_4K_2(r_0)}F_2 \\ 0 & 0 & -\rho_3 & \frac{1}{a_4K_2(r_0)} \\ -\frac{jk}{2\pi}\frac{Z_0}{Z_c}\frac{K_1(r_0)}{K_2(r_0)}F_1 & -\frac{jk}{2\pi}\frac{Z_0}{Z_c}\frac{K_1(r_0)}{K_2(r_0)}F_2 & \frac{1}{a_3K_2(r_0)} & -\rho_4 \end{bmatrix}^{-1} \cdot \begin{bmatrix} F_1\left(\frac{K_1(r_1)K_2(r_0)-K_1(r_0)K_2(r_1)}{K_2(r_0)}\right)S_1 \\ F_2\left(\frac{K_1(r_1)K_2(r_0)-K_1(r_0)K_2(r_1)}{K_2(r_0)}\right)S_1 \\ \frac{K_2(r_1)}{K_2(r_0)}S_1 \\ \frac{K_3(r_2)}{K_2(r_0)}S_2 \end{bmatrix} \quad (36)$$

$$E_{2,4} = \left(1 + \frac{\sigma}{a_4}\right) K_2(r_1) S_1 \qquad (37d)$$

The voltage solutions in Equations (37a) and (37b) have the form of the usual transmission-line solutions for the load voltages due to an incident field excitation. Note that the reflection coefficients ρ_1 and ρ_2 provide oscillations on the line, and the Green's function $K_1(r_1)$ contains the time delay and $1/r$ fall-off for the propagation of the excitation from the source and its image in the ground plane.

Equation (37c) for the total E field at the observation node 3 is seen to have three components. The first is a direct illumination by the source and its image. The second term arises from the antenna-mode scattering from node 4, which has been accounted for by the node 4 reflection coefficient, ρ_4. The last term in Equation (37c) arises from the differential-mode scattering from the line, and as such, it contains the influence of the transmission-line reflections. It is important to note that in this expression for the E field at node 3, the node dimension parameter, a_3, that was introduced for dimensional consistency in Equation (10) is not present. Clearly, the value of this parameter is not important when $\rho_3 = 0$. However, if there is a scattering body located at node 3, there will be a reflection at this node with the result that $\rho_3 \neq 0$. In this case, the parameter a_3 becomes important, since it represents the physical size of the scatterer at this node.

The final equation, Equation (37d), represents the solution for the total E field at the field coupling node 4. We see that the field expression at this point consists of an incident component from the source and its image (through the single $K_2(r_1)$ term) and another term arising from the scattering effects of the antenna current (the $(\sigma/a_4)K_2(r_1)$ term). Ideally, this total field should be zero, due to the boundary condition that the total E field on the scattering body is zero. However, we note that this approximate solution for the scattering from this wire does not provide a null field.

Furthermore, there have been no contributions to the E field at node 4 by the transmission-line currents. Had these contributions been included, the matrix of *F* terms in Equation (36) would have been full, with the traveling-wave currents providing incident wave contributions to node 4. Thus, the solution for the total field at node 4 is not obtainable from these approximate transmission-line and scattering solutions. However, it is known to be zero.

4. Numerical Verification

To check on the validity of this extended BLT solution, several numerical examples have been considered using the geometry of Figure 2. The following parameters have been chosen to define a *baseline* geometry for this comparison:

Line length $L = 1\,\text{m}$
Wire separation $d = 1\,\text{cm}$
Wire radius $a = 1\,\text{mm}$
Characteristic impedance $Z_c = 120\ln(d/a) = 276.3\ \Omega$
Load resistances $Z_L = Z_c/2 = 138.15\ \Omega$
Line-ground plane distance $h = 3\,\text{m}$
Source-line distance $r_1 = 10\,\text{m}$
Source-field point distance $r_2 = 10\,\text{m}$
All angles equal: $\psi_1 = \psi_2 = \psi_0 = \psi_s = \pi/2$.

4.1 Consideration of an Isolated Transmission Line

The first check for this solution involves examining an *isolated* transmission line. By adjusting the current excitation source of Equation (12) so that the incident E field on the line is $E^{inc} = 1\,\text{V/m}$, we can compute the load currents ($I_L = V_L/Z_L$) at each transmission-line load using the extended BLT solution for the voltages from Equation (36). For this isolated transmission line, the line length and wire radius given above were used, but a wire separation of $d = 2\,\text{cm}$ was used. Thus, the characteristic impedance of the line was $Z_c = 359.49\ \Omega$ and the load resistances were $Z_L = 179.74\ \Omega$.

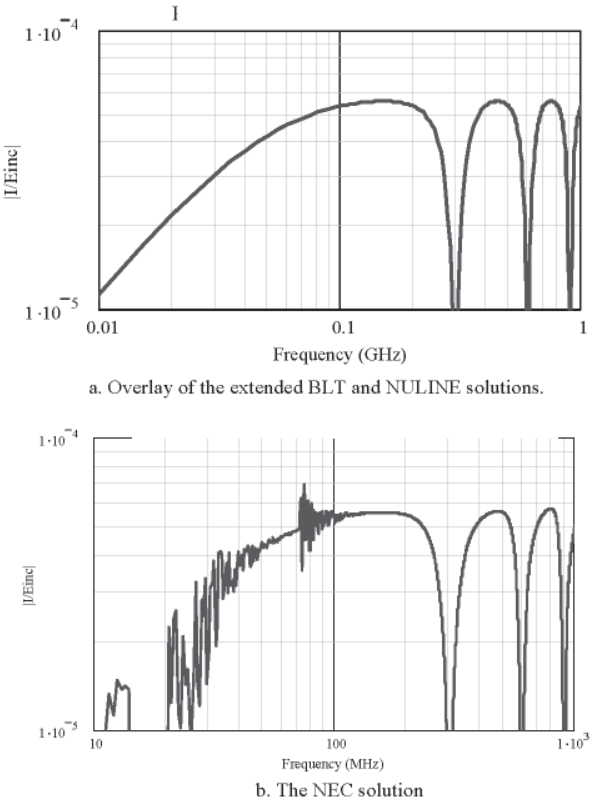

Figure 12. Comparison of the extended BLT, NULINE and NEC solutions for the plane-wave-induced load current spectrum |IL/Einc| *for an isolated transmission line.*

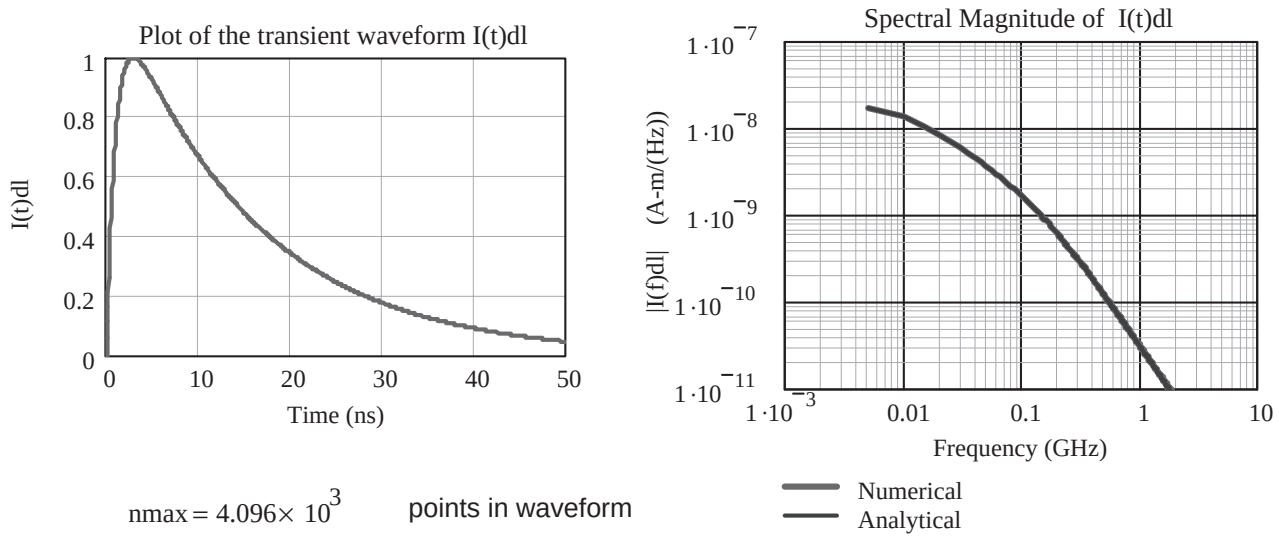

Figure 13.Plot of the transient behavior of the current moment i(t) dl *(left), and the corresponding spectral magnitude (right).*

Treating this transmission line as an incident-field excitation problem, we have developed an alternate transmission-line model, as discussed in [2]. The *NULINE* computer program was used to compute the current in load #1 on the transmission line, and the normalized response $\left|I_L/E^{inc}\right|$ is plotted in Figure 12a, overlaid with the extended BLT solution. The two curves are identical, as expected, because they are both formulated under the assumptions of transmission-line theory.

Figure 12b presents the results of calculating the load current on the same transmission-line structure using an integral-equation solution embodied in the *Numerical Electromagnetics Code* (*NEC*) [5]. Comparing the *a* and *b* parts of this figure, we note an excellent agreement between the transmission-line solutions and the *NEC* solution for frequencies above 100 MHz. Below this frequency, the *NEC* results were in error, due to the well-known code instability for loop structures at low frequencies.

4.2 Transmission Line Voltages at Nodes 1 and 2

The above check of the isolated-line case gives partial confidence in the validity of the extended BLT solution. To further examine the solution we included the ground plane in the problem and examined the responses in the time domain, where the times of arrival and polarity attributes of the response components could be easily seen. To this end, a simple unit-amplitude double-exponential waveform,

$$i(t)\,dl = \left[\left(\frac{\alpha}{\beta}\right)^{\frac{\alpha}{\beta-\alpha}} - \left(\frac{\alpha}{\beta}\right)^{\frac{\beta}{\beta-\alpha}}\right]^{-1}\left(e^{-\alpha t} - e^{-\beta t}\right)\Phi(t)\,, \quad (38)$$

was used to represent the time dependence of the current moment $i(t)dl$. For this waveform, the following parameters were used: $\alpha = 6.666\times10^{7}$ (1/s), $\beta = 1.0\times10^{9}$ (1/s). The term $\Phi(t)$ denotes the Heaviside

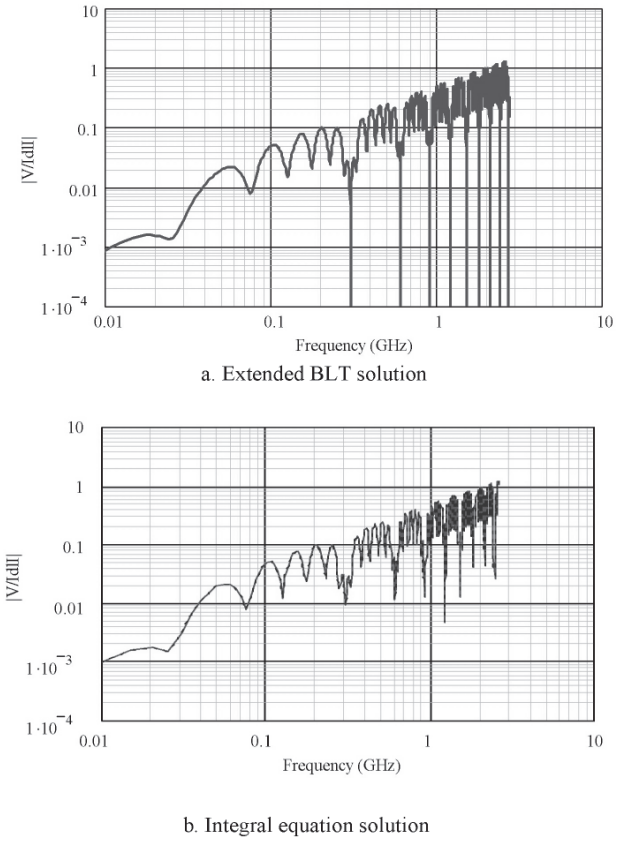

*Figure 14.Plots of the extended BLT equation solution (*a*) and an integral equation solution (*b*) for the load voltage transfer function spectra* $|V_L(f)/I(f)\,dl|$ *for the transmission line shown in Figure 2 (baseline configuration).*

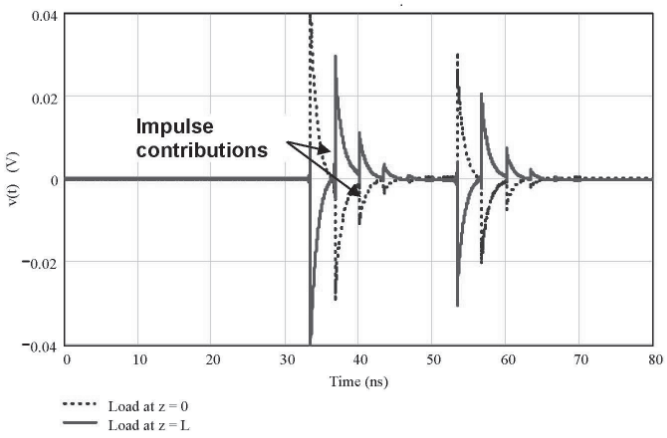

a. Extended BLT solution

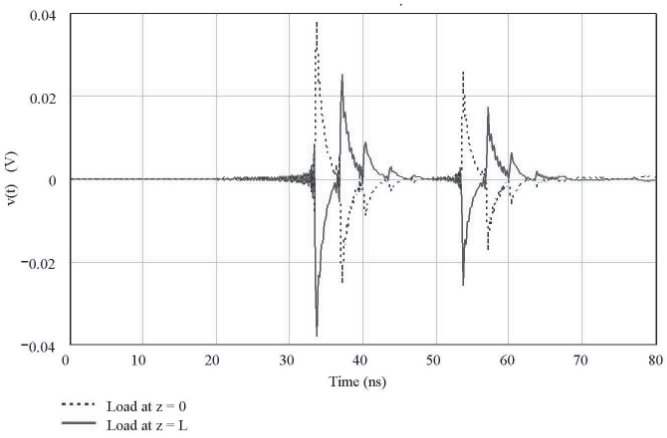

b. Integral equation solution

Figure 15.Plots of the transient BLT solution (a) and an integral equation solution (b) for the transient load voltages at both ends of the transmission line of Figure 2 (baseline configuration).

function: $\Phi(t) = 0$ for $t \le 0$, $= 1$ for $t > 0$. Figure 13 displays this source-excitation waveform and its spectral magnitude.

Calculating the load voltages from the extended BLT equation, Equation (36), for a unit excitation for the infinitesimal current element spectrum ($I(f)dl = 1$) yielded the voltage response transfer function shown in Figure 14. Part a of the figure presents the transfer function magnitude for both of the load voltages (they were identical in magnitude) as determined by the BLT equation, and part b shows the corresponding responses for an integral-equation solution – this time not using *NEC*, but rather another integral-equation solution developed by one of the authors (Jason Keen) for this comparison. As noted in this figure, the BLT transmission-line model and the integral-equation model yielded virtually identical spectral results.

The transient responses of the load voltages at nodes 1 and 2 of the transmission line is found by multiplying the transfer functions of Figure 14 by the excitation spectrum of Figure 13b and taking an inverse FFT3. These results are shown in Figure 15, with excellent agreement between the two methods being noted. While good agreement between these two results is noted in this case, it is to be expected that the agreement will be worse for cases where the transmission-line loads are either nearly short or open circuits.

4.3 E-fields at the Observation Node

In addition to the two transmission-line load voltages, the extended BLT equation provides the E fields at the observation nodes 3 and 4. As noted earlier, the BLT equation solution at node 4 is not valid, because it is located in the near field of the transmission line. Transmission-line theory is incapable of providing reliable information for the near fields.

However, the solution at node 3 is accurate. At this node, the BLT solution contains the effects of the direct radiation from the pulsed current source, the radiation of the antenna-mode current from the line, and the radiation effects of the transmission-line current (each having the ground-plane-image effects included). This partitioning of the responses into three components has been noted in Equation (37c).

For the baseline problem configuration, Figure 16a presents the complete E field at node 3. The first response that is observed occurs at a time $t = 10/c = 33.333$ ns, and is due to the incident wave propagating 10 m from the pulsed current source. The second pulse occurs at a time $t = \left[10 + (2 \times 3) + 20\right]/c$ = 120 ns, and is the reflection of

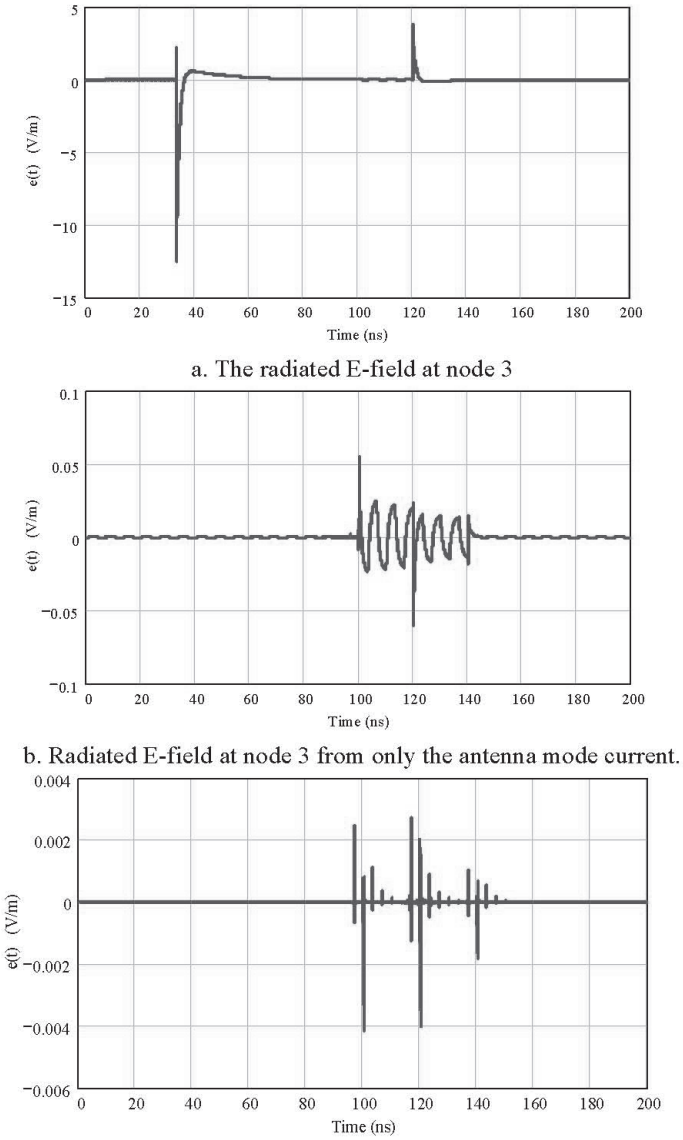

Figure 16.Illustration of the radiated E-field at node 3. Part (a) is the total solution, (b) is the solution with just the antenna mode contribution, and (c) is only the transmission line contribution to the field.

the incident field from the source in the ground plane. Of course, this waveform also contains the contributions from the antenna- and transmission-line-mode currents, but these latter components are much smaller than the direct incident-field component.

To illustrate the contributions from the antenna and transmission-line currents, we temporarily set the parameters K_3, F_1, and F_2 to zero in the BLT equation. This suppresses the incident field. (See Equation (37c) for the role that these parameters play in the solution.) This results in the E-field waveform of Figure 16b, which contains only the antenna-mode contributions. Note that this response is about a factor of 250 smaller than the complete solution: indicating that the scattered field from the line is not too important in determining the total field.

Similarly, by setting the parameters K_3 and σ to zero, we are able to compute the field response for just the transmission-line currents. This response component is shown in Figure 16c, and is a factor of 3500 smaller than the incident-field response. Clearly, this transmission-line component is unimportant in the total field solution.

5. Comments

This paper has illustrated the development and use of the extended BLT equation for analyzing a transmission line located near a conducting ground plane and illuminated by an EM field produced by a nearby point source emitting a spherical wave. The extended BLT equation includes the transmission line voltage responses as observables, as well as the E fields at observation nodes.

The solution of the transmission-line responses uses conventional transmission-line theory, with excitation being provided by the incident EM field from the source radiating in the presence of the ground plane. The ground-plane effect on the solution is taken into account through modified Green's functions.

The solution for the radiating field components likewise uses modified Green's functions for the ground-plane effect on the primary radiation from the point source. In addition, the radiation from the antenna-mode and transmission-line mode currents contribute to the E fields at the observation locations.

All of these effects are combined together into an extended BLT equation, and this equation can be solved either numerically or symbolically. The numerical results that have been shown here are both reasonable and they have been verified by an independent integral-equation analysis.

From the BLT analysis, it is clear that the E-field response computed at the transmission line is incorrect, because the transmission-line theory fails to provide accurate near-field results on the line. However, the transmission-line load responses and the distant scattered field are accurate – to within the limits afforded by the transmission-line approximation. As noted in the comparison of the "exact" and approximate transmission-line solutions, the agreement is very good. Future work in this area might include developing a rigorous EM scattering/radiation solution for complex systems using the BLT methodology. In addition, there are several other suggestions as to possible future work in the area of BLT analysis. These are as follows:

- Extend the analysis to permit near-field terms in the radiation and scattering terms of the BLT equation.
- Examine the use of the modified Green's function approach to consider a transmission line located within a rectangular cavity, for example, where the Green's function can be expressed analytically.
- Develop an analysis for the EM field coupling through an aperture in the ground plane (shield) that couples to a transmission line located on the opposite side of the shield.
- Extend the BLT formalism to be able to represent a general EM radiation and scattering problem, taking into account all aspects of EM coupling (e.g., integral-equation analysis), angle of incidence, and polarization issues.

Finally, it would be useful to employ the generalized BLT model for analyzing complex EM systems for which measurements can also be made, to further verify the accuracy of this modeling approach.

6. References

1. C. E. Baum, T. K. Liu, and F. M. Tesche, "On the Analysis of General Multiconductor Transmission Line Networks," *Interaction Notes*, Note 350, Kirtland AFB, NM, 1978.

2. F. M. Tesche et. al., *EMC Analysis Methods and Computational Models*, New York, John Wiley and Sons, 1997.

3. F. M. Tesche and C. M. Butler, "On the Addition of EM Field Propagation and Coupling Effects in the BLT Equation," *Interaction Notes*, Note 588, December 13, 2003.

4. F. M. Tesche, C. M. Butler, and J. M. Keen, "Example of the Use of the BLT Equation for EM Field Propagation and Coupling Calculations," *Interaction Notes*, Note 591, to be published.

5. G. J. Burke and A. J. Poggio, "Numerical Electromagnetic Code (NEC) – Method of Moments," NOSC Tech. Doc. 116, Naval Ocean Systems Center, San Diego, CA, January 1980.

1 Work conducted under the provisions of AFOSR MURI Grant F49620-01-1-0436. This work was originally submitted to Dr. Baum's note series as *Interaction Note 591*, Kirtland AFB, NM, to be published.

2 Note that the form of Equation (15) is different from the form of Equation (9) for the isolated transmission line. The source term for Equation (9) involves just the incident E field at the field coupling node (4), while in Equation (15) the effective excitation source involves both the E field reflected from node 3 *and* the radiated field from the current source. Both of these excitation fields are reflected in the ground plane (using the K_1 Green's functions), and then the original incident field components and the reflected fields are applied as excitation fields to the line, as indicated by Equation (6). This is done because the excitation of the transmission line is not determined by the total incident E field (e.g., the sum of the incident plus ground-plane-reflected field at node 4), but rather, the excitation depends on both the incident field strength *and* on the direction of incidence (see Figure 6). In this manner, the excitation of the line is constructed so that the signs of the incident and ground-reflected field components are correct.

3 Note that the choice of the excitation waveform in this example is unfortunate, in that the waveform has a discontinuous derivative at $t = 0$. As noted in Equation (12), the radiated E field from the Hertzian current source is proportional to $j\omega$ times the excitation spectrum, and the excitation function of the line in Equation (13) has another term involving $j\omega$ from the sums of the two exponential terms. These two factors of $j\omega$ multiplying the excitation waveform spectrum amount to taking a second time derivative of the waveform, which, for the double exponential function, provides a delta-function contribution when the waveform turns on. These impulse-function contributions are clearly evident in Figure 15.

Reciprocity Approach for EM Emission of Multiconductor Cable Networks in a 3D Geometry

J-P. Parmantier
S. Bertuol
F. Issac

Abstract

This paper concerns the modeling of multiconductor cable network emission in electromagnetic compatibility problems. The principle is based on a reciprocity formulation in order to substitute the resolution of the direct emission problem from the resolution of an EM susceptibility problem. The resolution of this second problem relies on the application of the field-to-transmission-line theory. After some canonical validations on a metallic ground plane, a more complex example is given, showing the application of the method on a satellite mockup with comparisons to measurements.

1. Introduction

In any electromagnetic compatibility (EMC) modeling-related problem, being able to correctly model cables is mandatory, since cables are essential contributors for EM coupling on complex systems. One of the most direct applications of EM Topology [1, 2] is for cable networks for which the multiconductor transmission-line-network theory naturally leads to the Baum-Liù-Tesche (BLT) equation [3]. Nowadays, despite the approximation of quasi-TEM modes on the cables, the relevance of this theory does not have to be proven anymore for modeling EM propagation and EM coupling on complex cable harnesses [4, 5]. Besides, through the application of field-to-transmission-line models, those transmission-line models are now currently linked with three-dimensional computer solvers used to calculate the incident fields scattered by the complex bodies hoisting the wiring [6-8].

However, one would say that three-dimensional computer solvers, based on the resolution of Maxwell's equations, are potentially capable of solving both types of EM coupling and EM emission problems. Nevertheless, those computer codes are not able to handle the description of the complex geometry of the scattering body and the description of the multiconductor wiring topology at the same time. On the contrary, the field-to-transmission-line method [9] offers an efficient operational methodology, consisting of solving the problem of the wiring coupling in two separate steps:

- Step 1: the calculation of the incident fields on the wiring routes with a three-dimensional code,
- Step 2: the calculation of the response of the wiring with a multiconductor cable network code.

The link between the two steps is made by the transmission-line generators (step 2), which are directly derived from the calculation of the incident fields on the cable routes (step 1). Here, the "incident" field stands for the field in the absence of the wire. From the modeling point of view, the field-to-transmission-line models offer several valuable advantages:

- The incident field can be calculated without meshing the wires, therefore avoiding cable topology description and possible instability problems with certain solvers;
- The calculations of the incident fields on the cable routes are made once for all, and several topologies of cable networks can be played with (modification of the connections, of the number of wires, terminal loads), provided that the routes of the cables are the same as the incident field routes;
- No source-code modification into the existing three-dimensional solver is required, except perhaps optimized routines for storing EM fields in the frequency domain along the cable routes (but this kind of signal processing remains achievable outside the three-dimensional software).

Among the field-to-transmission-line models, Agrawal's model presents several advantages (for example when compared to the well-known Taylor's model):

J-P. Parmantier, S. Bertuol, and F. Issac are with ONERA, 2 avenue Edouard Belin, 31055 Toulouse, France.

This invited paper is part of the special section honoring Carl E. Baum on his 65th birthday

- Only one component of the incident field is required – the component of the electric field tangent to the running path of the cable – which makes the calculation of the source wave vector easier in the BLT equation;

- The model does not require any notion of verticality with respect to the transmission-line reference surface, since the incident fields are collected along the paths where the cable runs;

- The per-unit-length equivalent generator to be applied in the multiconductor transmission-line model is directly equal to the tangential incident electric field, whereas it generally depends on the electrical parameters of the line in the other models.

Of course, Agrawal's model makes the reasonable approximation that the dielectric of the cables is negligible for the determination of the equivalent sources. However, the efficiency of this model in terms of precision and convenience of use has been demonstrated in various problems of EM coupling on wiring inside complex vehicles [6, 7, 10, 11].

As far as an EM emission problem is now concerned, one might intuitively think of applying the same field to transmission-line methodology in a reverse way, avoiding as much as possible any calculation development inside the existing three-dimensional solver. Therefore, one might think of decomposing the problem of the direct calculation of EM field emission into three main steps:

- Application of a driving interference source at the extremity of the wiring;

- Calculation of the current distribution all along the wires of the wiring harness, using a multiconductor transmission-line network model;

- "EM emission of those currents" with a full-wave three-dimensional solver.

For some specific geometry configurations, no real three-dimensional code is required. This occurs when the analytical expressions of the Green's functions can be analytically or numerically derived. This is the case for the generic configuration of a cable over an infinite ground plane [12]. Nevertheless, in the general case of any three-dimensional configuration solved by already available three-dimensional solvers, this approach is not operational, since the determination of the Green's function induces a large cost in CPU time and memory.

Consequently, one could think of directly applying the transmission-line current distributions as current-source terms directly into the three-dimensional solver. In the application described in this paper, the authors are particularly interested in using an FDTD code, because it is a widely spread technique in the EMC community. However, as far as direct methods are concerned for EM emission calculation, problems related to the positioning of current elements anywhere in the Cartesian grid may occur in this particular case of solvers, based on structured meshes. In an FDTD solver, for example, current generators are necessarily applied on wires, themselves positioned on the edges of the cells. Such a configuration barely fits with real cable routes. On the other hand, one might think that using solvers based on unstructured meshes (such as an integral-equation-based solver) would overcome those drawbacks. However, such solvers generally have more time and memory requirements than FDTD-like solvers. They require very large computer resources to handle such a large-dimension problem as the one considered at the end of this article with reasonable computer resources.

In addition, the application of current conditions in adjacent cells requires that Maxwell's equations be respected. This approach therefore presents real theoretical and technical difficulties. Any error or current approximation is likely to introduce undesirable and uncontrolled physical responses. In addition, such an approach would not be appropriate for a parametric study of the influence of the wiring topology on the field emission. Indeed, for any modification of the topology of the wiring driving the source, a three-dimensional calculation, generally requiring time and memory, would be required.

In order to avoid those various drawbacks, an appropriate reciprocity formulation of the problem is proposed. It offers the possibility of indirectly deriving the EM emission problem from the resolution of a related EM susceptibility problem. The way the reciprocity problem is formulated is exactly the way described by Tesche et al. in [9], generalized to a three-dimensional geometry[1]. After some recalling the reciprocity principle, the paper mainly focuses on the application of this formulation for building a methodology applicable to any complex system models. In this article, the validation of the methodology is first presented for canonical configurations, allowing the application of direct methods used as references. A demonstration is then made for a complex three-dimensional geometry on which reference measurements have been performed. This application is mainly inspired by a French paper, presented at a French conference in 2002 [13], and from *Interaction Note* 586 [14].

2. Reciprocity-Based Methodology

2.1 Reciprocity for a Two-Port Circuit Problem

Hereafter, how the EM field emitted by a transmission line can be expressed by solving a simple EM coupling problem is presented, derived from the reciprocity theorem applied on an equivalent two-port circuit [9]. We start from the general formulation of the reciprocity principle. We

Figure 1. A two-port electrical circuit.

consider two EM states, characterized by their sources, their current, and their magnetic current densities, respectively ($J^{(1)}, M^{(1)}$) for EM state 1 and ($J^{(2)}, M^{(2)}$) for EM state 2. Those sources radiate and generate EM fields, ($E^{(1)}, H^{(1)}$) for EM state 1 and ($E^{(2)}, H^{(2)}$) for EM state 2. In a supposedly infinite, linear, and isotropic medium, both EM states are related by the well-known integral equation:

$$\iiint_{volume} \left[E^{(1)} \bullet J^{(2)} - E^{(2)} \bullet J^{(1)} \right.$$

$$\left. - H^{(1)} \bullet M^{(2)} + H^{(2)} \bullet M^{(1)} \right] dv = 0 \qquad (1)$$

Different forms of equations can be derived, depending on the type of applications. In the case where electric and magnetic sources are localized in space at the level of electronic ports, the relationship of Equation (1), which relates EM fields, may be written in the form of a relationship combining currents and voltages of an *n*-port electrical circuit. In the particular case of a two-port circuit (Figure 1), in the absence of any nonlinear component, the reciprocity equation is given by

$$V_a^{(1)} I_a^{(2)} + V_b^{(1)} I_b^{(2)} = V_a^{(2)} I_a^{(1)} + V_b^{(2)} I_b^{(1)} \qquad (2)$$

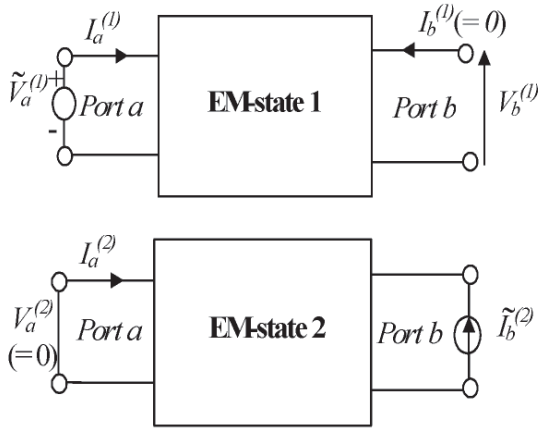

Figure 2. An application of the reciprocity principle to the two-port circuit, showing the choice of EM state 1 and EM state 2.

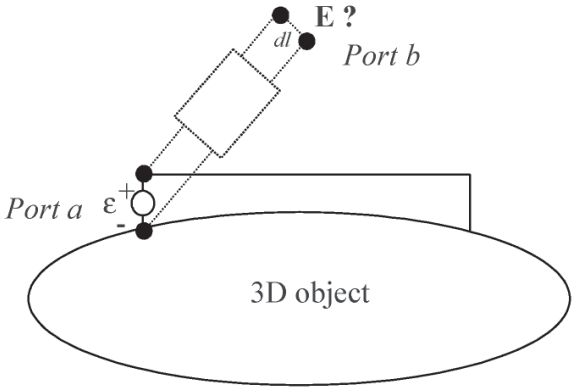

Figure 3. The identification of the three-dimensional problem with an equivalent two-port circuit.

By judiciously choosing EM state 1 and EM state 2 (Figure 2), Equation (2) can be simplified:

- EM state 1: a voltage generator, $\tilde{V}_a^{(1)}$, is applied to port "*a*" with port "*b*" left in open circuit. The current $I_b^{(1)}$ on port "*b*" is therefore equal to zero.
- EM state 2: a current generator, $\tilde{I}_b^{(2)}$, is applied to port "*b*" and port "*a*" is short-circuited. The voltage, $V_a^{(2)}$ on the port is therefore equal to zero.

The second reciprocity equation, Equation (2), is therefore reduced to

$$\tilde{V}_a^{(1)} I_a^{(2)} + V_b^{(1)} \tilde{I}_b^{(2)} = 0 \cdot \qquad (3)$$

2.2 Identification of the Emission Problem with a Two-Port Circuit Problem

In the case of a localized EM electric field radiated by a wire to which a voltage source is applied, we can imagine a fictitious two-port circuit, the two ports of which are defined as follows:

• Port "*a*" is located at the cable end, where the voltage source is applied;

• Port "*b*" is located on a localized element of length *dl*, where the electric field, *E*, is calculated (Figure 3).

2.3 Reciprocity Problem Formulation

In order to obtain a relation similar to Equation (3), the two EM states are defined in the following way:

- EM state 1 stands for the cable EM emission problem, to be solved with a driving source, $\tilde{V}_a^{(1)}$ (Figure 4);

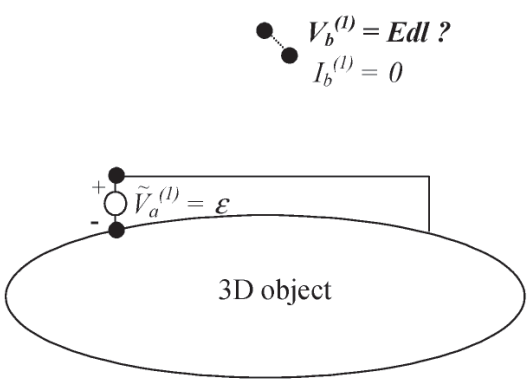

Figure 4. The reciprocity method: The definition of EM state 1

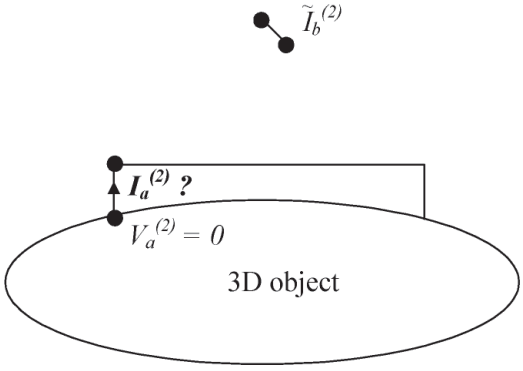

Figure 5. The reciprocity method: The definition of EM state 2.

- EM state 2 stands for the EM susceptibility problem of the same cable, submitted to the radiation of a current element on port "*b*" (Figure 5).

Consequently, the resolution of EM state 2 by a field-to-transmission-line technique and the application of Equation (3) allow a full derivation of EM state 1's solution from EM state 2's solution. We write

$$E\,dl = -\,\tilde{V}_a^{(1)}\frac{I_a^{(2)}}{I_b^{(2)}} = -\varepsilon\frac{I_{LT}}{I_{source}}\,. \qquad (4)$$

2.4 Application with a Three-Dimensional Solver

As mentioned in the introduction, an efficient method for solving EM state 2 is based on the chaining of a three-dimensional computer code and a cable-network computer code. In our application, we want to take advantage of the fact that this chaining is already entirely operational and fully validated [6, 15] between an FDTD computer code (*ALICE*), and a cable-network code based of the resolution of the BLT equation (*CRIPTE*). Both computer codes were developed at ONERA, France. The FDTD code (operating in the time domain) provides the calculated incident electric fields tangent to the wiring routes (in the absence of the cable), as required in Agrawal's formalism. In the EM state 2 problem, those fields are induced by the application of a current source, $I_b^{(2)}$ onto an element of length *dl* (port "*b*"). Those incident electric fields are then introduced into the cable-network computer code as voltage sources distributed along the cable models. The *CRIPTE* code operates in the frequency domain. A calculation of the current $I_a^{(2)}$, generated by the application of the tangent electric fields on the wiring, is made at the same position as the position of the voltage generator in EM state 1. The reciprocity relation, Equation (4), then gives the solution of the EM state 1 problem.

In this calculation, since a current is injected into the calculation domain, the electric fields produced by the current generator do not go to zero at late time. On the contrary, they stabilize around a constant value. This phenomenon can be explained by the charge of the capacitance existing between the injection-current element and the three-dimensional structure. Therefore, precautions are required in the chaining of the FDTD code and the cable-network code when the Fourier transforms of each electric-field component, tangent to the wiring routes, are made.

In past studies, the possibility of performing a time-domain filtering of the responses (Hanning windows) before performing FFTs has been studied extensively [15-18]. However, despite the increase of the calculation time, a discrete Fourier transform (DFT) provides more precise results, while offering the capability of removing by analytical calculation the problems related to Hanning windows. The technique used is presented in Figure 6. Unlike with the FFT technique, the constant part of the signal is now taken into account in a closed form by decomposing the signal into two parts (a time-varying part and a constant part). The Fourier transform is then obtained by

$$F(\omega) = \int_0^{t_0} f(t)e^{-j\omega t}dt + \frac{A}{j\omega}e^{-j\omega t_0}\,. \qquad (5)$$

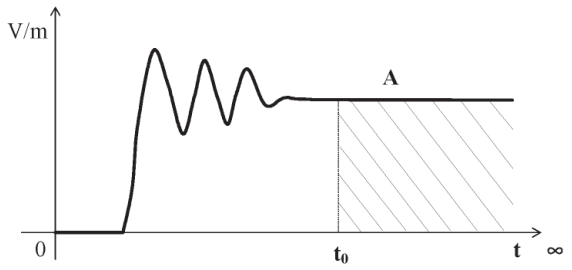

Figure 6. The decomposition of the field signal in order to account for the constant late-time part.

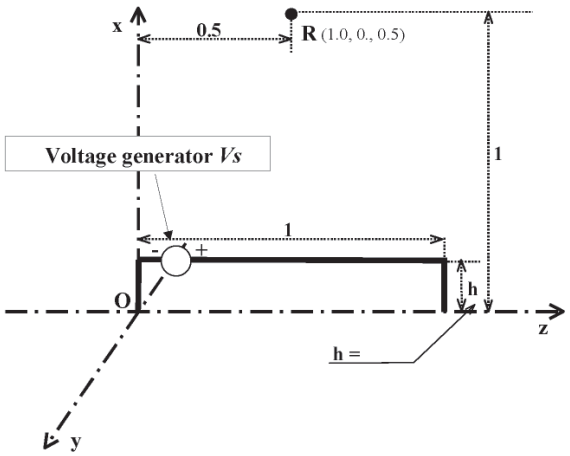

Figure 7a. The electric field radiated at one test point by a one-wire transmission line over an infinite ground plane: the dimensions of the transmission line over a ground plane

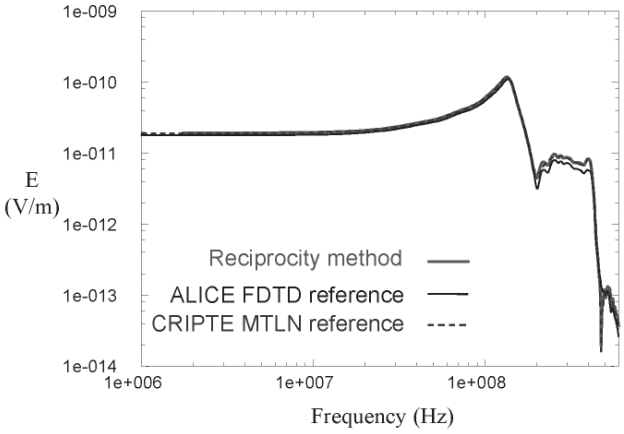

Figure 7b. Comparisons between the reciprocity method and the direct reference method for the problem of Figure 7a: the x component of the electric field at test point R in the frequency domain.

3. Results

3.1 Numerical Validations

As a first validation, the reciprocity method was compared with direct calculation methods (the treatment of the emission problem in a single three-dimensional solver calculation). The FDTD code, as with most of the three-dimensional codes, accounts for simple wire configurations (thin-wire models). In addition, the cable-radiation feature available in the cable-network code is valid only if the cable is considered on an infinite metallic ground plane [16-18]. Consequently, a first and natural validation case dealt with considering a one-wire transmission line on a ground plane, with the dimensions indicated in Figure 7a. The current on the line was driven by a Gaussian-pulse voltage generator,

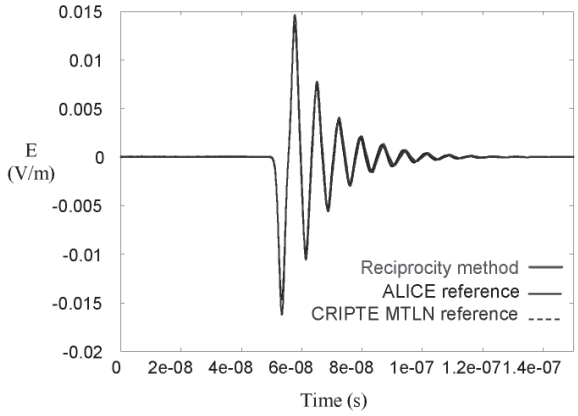

Figure 7c. Comparisons between the reciprocity method and the direct reference method for the problem of Figure 7a: the x component of the electric field at test point R in the time domain.

Vs at the end of the line. Figure 7b and Figure 7c present the calculations of the emitted electric field obtained in the frequency domain and in the time domain by the three methods at the test point *R*, located vertical to the line and at a one meter height. The superposition of the results obtained fully demonstrates the equivalence of the reciprocity approach.

3.2 Experimental Validations

As a second validation, the reciprocity calculation method was applied to a satellite mockup (Spacebus-300A type, Figure 8), for which the FDTD mesh is represented in Figure 9. *I*1 and *P*1 represent field test points, and *path 1* and *path 2* are wiring routes to which measurements will be referred. This mockup has already been used in past studies

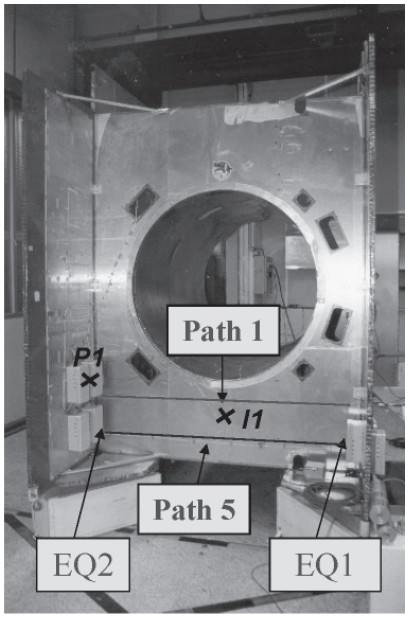

Figure 8. The Satellite mockup.

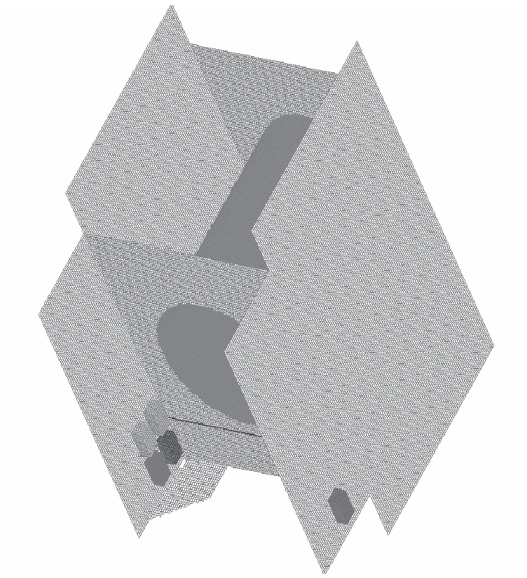

Figure 9. The mesh for the satellite mockup.

to analyze and model the susceptibility of electric wiring to electrostatic discharges (ESDs) [15, 17]. The volume of the satellite was approximately 16 m3. The number of cells was equal to 11 647 152 (calculation volume: $N_i = 228$, $N_j = 198$, $N_k = 258$) and 2 080 000 for the satellite mockup volume ($N_i = 130$, $N_j = 100$, $N_k = 160$). The size of a cubic mesh cell was equal to 2 cm. The three-dimensional calculation of EM state 2 was made on a Pentium III (550 MHz Xeon Dell PC) with 1 GB of memory, and took approximately 14 hours (for 8 192 iterations; time step = 3×10^{-11} s). The calculation time for the cable network was negligible compared to the three-dimensional calculation time. The calculated results were compared with the experimental results (Figures 10-12). The calculation of the incident fields having been made once and for all for a given location of the current-element injection, different types of cables could be tested on the same routes. In order to obtain good quality in the comparisons, all the characteristics of the measuring equipment used during the experiment had to be precisely calibrated or taken into account into the numerical models (amplifiers, measurement cables,...). The measurements were made with a network analyzer in the 300 kHz to 500 MHz frequency range. S_{21} parameters were measured between the injection port (with a driving source E on a 50 Ω internal load) and the field sensor (a small monopole, developing a voltage V on a 50 Ω internal load). Classically, this transfer function is given by

$$S_{21} = \frac{2V}{E}. \qquad (6)$$

Then, the calibration of the sensor in a TEM cell was used to relate the voltage, V, to the measured electric field.

Figures 10 to 12 describe configuration measurements where the driving-source voltage was located at the level of *EQ* 2. In the two first configurations of unshielded cables (a one-wire cable and an unshielded twisted pair, Figures 10 and 11), we verified that the orders of magnitude of the emitted field at test point $I1$ were higher than the emitted field at test point $P1$ by a shielded twisted pair (Figure 12). In this case, because of the lack of sensitivity of the measurement equipment at low frequencies,

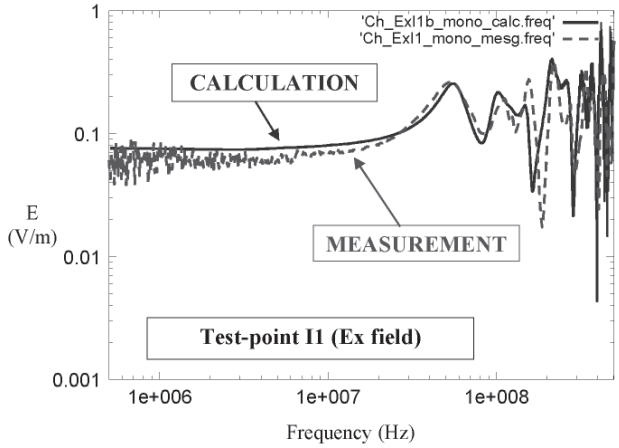

Figure 10. The electric field radiation of a one-wire cable on the satellite mockup at test point I1.

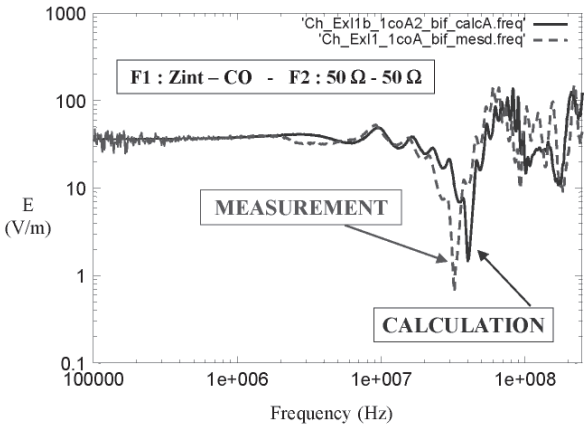

Figure 11. The electric field radiation of an unshielded twisted pair on the satellite mockup at test point I1.

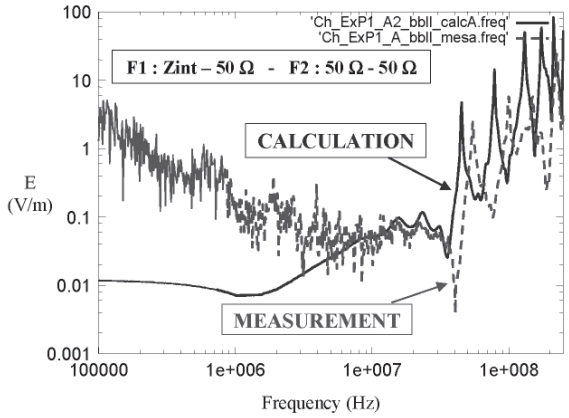

Figure 12. The electric field radiation of a shielded twisted pair on the satellite mockup at test point P1.

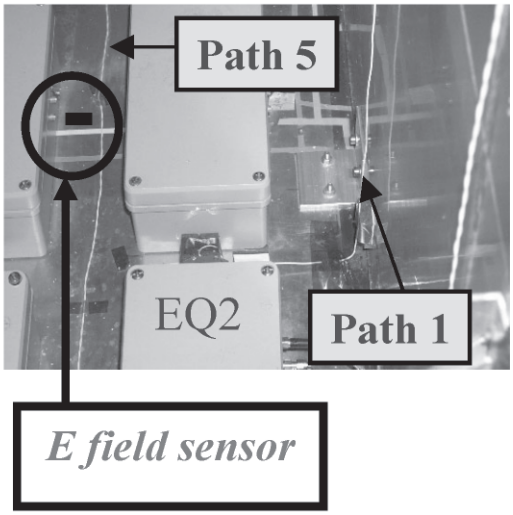

Figure 13a. The configuration for which the coupling is mainly due to neighboring cables: details of the electric field measurement at point P1.

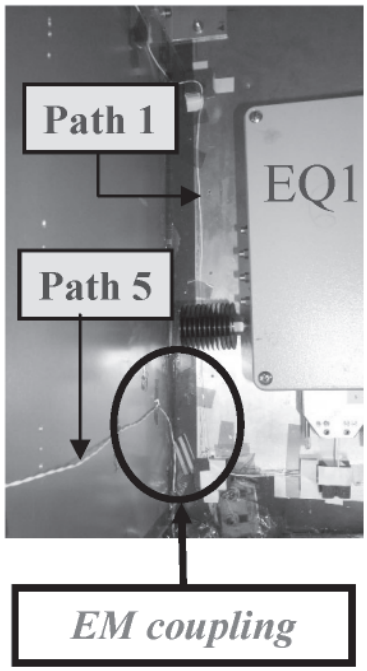

Figure 13b. The configuration for which the coupling is mainly due to neighboring cables: Details of the zone where EM cross-coupling occurs between path 1 and path 2.

only fields for frequencies higher than 10 MHz could be measured. The three results testified to the relevance of the reciprocity approach for handling the complexity of the three-dimensional geometry and the complexity of the cable topology in EM emission assessments at the same time.

4. Accounting for the Radiation of Neighboring Cables

Among the numerous measurements made extensively on this satellite mockup (different field test points, different cable types and cable routes) [16], several cases have outlined the importance of accounting for "neighboring" cables, that is to say, cables in the vicinity of the "emitting" cable, since those cables are themselves likely to participate significantly in the emitted field. Simultaneously, the combined EM coupling phenomena and the phenomena of radiation of neighboring cables have to be accounted for. As an example, Figure 14 describes the field obtained at point $P1$ (Figure 13a), when the injection was made on path 1 at the level of equipment *EQ* 2. The neighboring cable, on path 5, ran close to path 1 at the level of equipment *EQ* 1 (Figure 13b). The EM fields simulated were comparable to the measured fields only when the neighboring cable 5 was disconnected [16], which suggests that the entire topology should have to be considered as a whole in the case of more general emission-problem assessments.

In the satellite example, the topology of the entire wiring was not sufficiently controlled in order to enter it in the models. However, when the topology of the neighboring wires is controlled precisely enough (for instance, when a CAD model is available), such indirect coupling phenomenon can be numerically simulated.

In order to demonstrate this point, we took again the example of the EM emission of a one-wire cable on an infinite ground plane. The geometrical configurations of this cable – first alone, and then close to another perturbing cable – are given in Figure 15 (respectively, configurations A and B). In both cases, a Vs voltage generator equal to 1 volt was placed on the vertical wire of the line. The electric field at test point *P* was determined. The neighboring line had the same per-unit-length electrical parameters as the "emitting" line (length = 1.6 m). It ran along the emitting line on a 20 cm length. Along this length, the distance between the two lines was constant and equal to 0.5 mm. Then, towards its remote end, the neighboring cable ran close to test point *P* (at a 10 cm distance). Both lines were

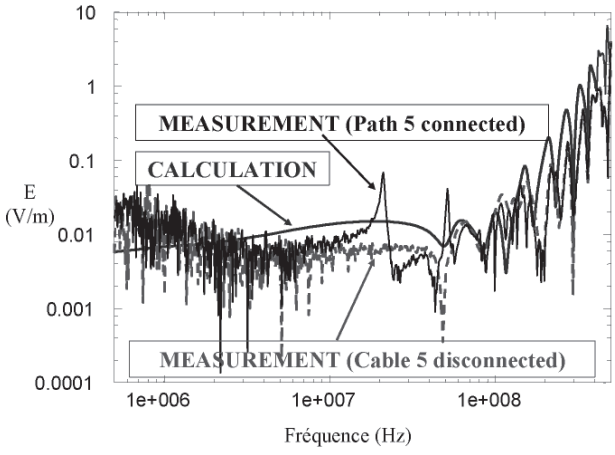

Figure 14. The radiation of the one-wire cable at test-point P1 on the satellite mockup: the influence of a neighboring cable.

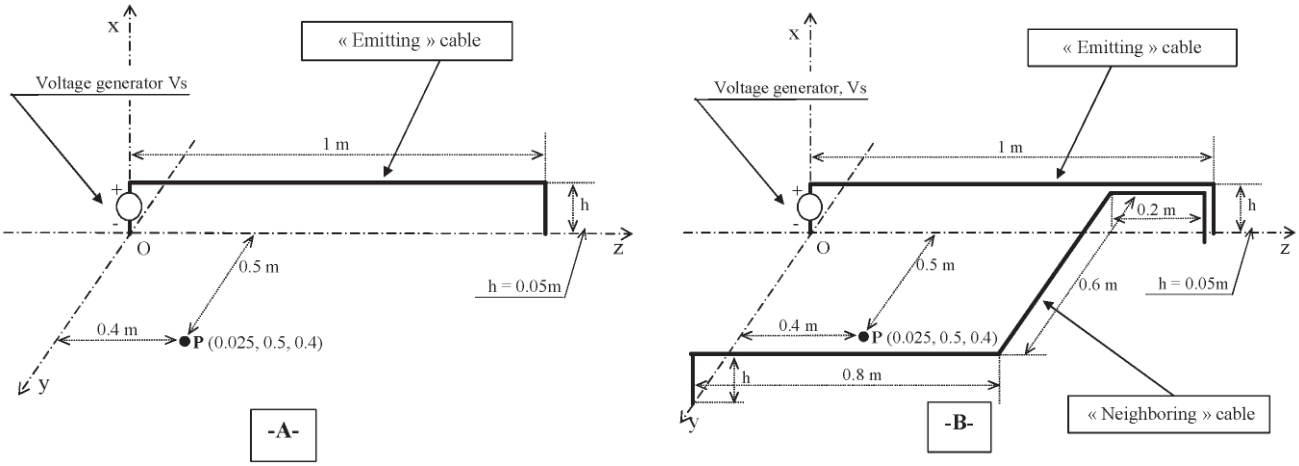

Figure 15. The one-wire line alone and in the presence of a neighboring line.

placed 5 cm above the ground plane. Their terminal loads were equal to 50 Ω.

In the reciprocity resolution of the problem, outlined in Figure 15, the whole wiring must be simulated. In the FDTD code, the tangent electric fields in EM state 2 were calculated on the routes of the two lines (the emitting line and the neighboring line). Then, those fields were introduced as distributed source terms in the *CRIPTE* code. Both lines were modeled in the same topological network, including the cross coupling along the 20 cm section. The electric fields resulting at test point *P* in the absence, or in the presence, of the "perturbing" line are presented in Figure 16. The amplitude of the emitted field was higher in the case of the presence of the "perturbing" line. Indeed, the current circulating on the emitting line coupled onto the neighboring line. This line also emitted significant EM fields, and therefore modified the E field produced by the "emitting" line alone at test point *P*.

5. Conclusion

The encouraging results obtained in this numerical and experimental investigation showed how the reciprocity method can be applied to large-dimension three-dimensional systems. The only calculation to perform concerns an EM susceptibility calculation. Therefore, already existing calculation chains, linking a three-dimensional solver and a multiconductor transmission-line computer code, previously designed for EM susceptibility applications, can also be used to study EM emission problems.

In the experimental validations, the importance of neighboring cables has clearly been demonstrated in several indirect cable-coupling configurations. Indeed, for several test points, neighboring cables may have had a significant influence on the emitted fields. So far, this interference phenomenon could only be reproduced numerically, in a configuration simpler than the satellite mockup.

In this article, only electric-field calculations have been shown. However, the proposed method can be extended to the determination of magnetic fields, as well. Indeed, in the resolution of EM state 2, the current-injection segment can easily be replaced by a current loop (the principle of magnetic sensors). Nevertheless, the numerical implementation and the validations of this configuration remain to be done.

Besides, the rectangular shape of the satellite presented in this paper is appropriate for the use of an FDTD computer code. However, in the case of a more conformal geometry, it would be more appropriate to apply a hybrid technique, allowing better management of the surface of the object while maintaining FDTD performance in most of the calculation volume, and to make the description of the cable routes easier, as done in [8] for EM susceptibility applications.

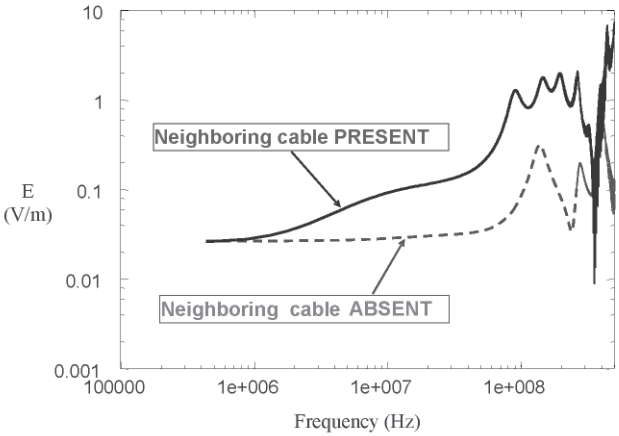

Figure 16. The electric field radiated at test point P by a one-wire cable installed on an infinite metallic ground plane in the absence or in the presence of a neighboring cable (calculation with the reciprocity approach).

Finally, the reciprocity relation applied in the article between cable ports and field-sensor ports could be easily generalized to a "multiple-port multiple-field" problem. Nevertheless, this problem would require minor modifications to the currently available calculation chains. The use of a frequency-domain three-dimensional technique, allowing one to solve a linear system with several right-hand-side source configurations, would be especially clearly indicated for future applications of this kind of problem.

6. Acknowledgement

The authors want to acknowledge Messrs. Catani and Panh from the French Aerospace Agency (CNES) for supporting the validation work carried out on the satellite mockup. This work was originally published under Dr. Baum's *Interaction Note* series as Note 586, Kirtland AFB, NM.

7. References

1. C. E. Baum, "The Theory of the Electromagnetic Interference Control," in J. Bach Andersen (ed.), *Modern Radio Science 1990*, Oxford University Press, 1990, pp. 87-101.

2. C. E. Baum, "The Theory of the Electromagnetic Interference Control," *Interaction Notes*, Note 478, December 1989.

3. C. E. Baum, T. K. Liù, F. M. Tesche, "On the Analysis of General Multiconductor Transmission-Line Networks," *Interaction Notes*, Note 350, November 1978.

4. J-P. Parmantier, V. Gobin, F. Issac, I. Junqua, Y. Daudy, J. M. Lagarde, "An Application of the Electromagnetic Topology Theory on the Test-bed Aircraft, EMPTAC," *Interaction Notes*, Note 506, November 1993.

5. J-P. Parmantier, V. Gobin, F. Issac, I. Junqua, Y. Daudy, J-M. Lagarde, L. Paletta, "ETE III: Application of Electromagnetic Topology on EMPTAC," *Interaction Notes*, Note 527, May 1997.

6. L. Paletta, J-P. Parmantier, F. Issac, P. Dumas, J-C. Alliot, "Susceptibility Analysis of Wiring in a Complex System Combining a 3D Solver and a Transmission-Line Network Simulation," *IEEE Transactions on EMC*, **EMC-44**, 2, May 2002, pp. 309-317.

7. M. D'Amore, M. Sarto, A. Scarlatti, "Radiated Susceptibility of Wiring System Aboard Lightning Struck Aircraft. Part I: Sensitivity to the Distributed Sources," *Proc. 2002 IEEE Int. Symp. EMC*, Minneapolis, MN, August 200.

8. X. Ferrieres, J-P. Parmantier, S. Bertuol, A. Ruddle, "Application of Hybrid Finite Difference/Finite Volume to Solve an Automotive Problem," *IEEE Transactions on EMC*, **EMC-46**, 4, November 2004, pp. 624, 634 .

9. F. M. Tesche, M. V. Ianoz, T. Karlsson, *EMC Analysis Methods and Computational Models*, New York, John Wiley & Sons, 1997, pp. 247-266.

10. I. Junqua, "Contribution of ONERA to EMAZ, task 2.3. Application of Electromagnetic Models and Modelling Techniques on a BK117 Helicopter," *ONERA report* RT.3/03755 DEMR, February 2003.

11. I. Junqua and J-P. Parmantier, "Application de Techniques de Modélisation Numérique Coopératives à un Hélicoptère BK117," *Proceedings of the 12th French EMC Conference*, Toulouse, Mars 2004, pp. 95-98 (in French).

12. J-P. Parmantier, F. Issac, S. Bertuol, F. Boulay, "Modèle Unifié d'un Câble Multiconducteur Blindé : Application à la Susceptibilité et à l'Émission Électromagnétique," *Proceedings of the 10th French EMC Conference*, Clermont-Ferrand, March 2000, pp 131-136 (in French).

13. S. Bertuol, J-P. Parmantier, F. Issac, J-P. Catani, J. Panh, "Approche Réciproque pour l'Étude de l'Émission Électromagnétique de Câbles: Application à un Câblage de Satellite," *Proceedings of the 11th French CEM Conference*, Grenoble, March 2002, pp. 217-222 (in French).

14. S. Bertuol, J-P. Parmantier, F. Issac, "Reciprocity Approach for EM Emission of Cables in a 3D Geometry," *Interaction Notes*, Note 586, October 2003.

15. F. Issac, S. Bertuol, F. Boulay, J. P. Parmantier, "Etude Approfondie du Couplage d'une ESD sur un Câblage à Partir d'une Méthodologie de Couplage Champ-Câble," *Proceedings of the 10th French CEM Conference*, Clermont-Ferrand, March 2000, pp. 124-129, (in French).

16. S. Bertuol, F. Issac, J-P. Parmantier, F. Boulay, "CEM des Véhicules Spatiaux: Simulation des Modes Rayonnés sur Satellite," *ONERA report*, RF 3/03073 DEMR - November 2000, (in French).

17. S. Bertuol, "Modélisation des Perturbations Induites par une Décharge Électrostatique sur un Satellite," *ONERA report* RTI 1/05511 DEMR - February 2001 (in French).

18. S. Bertuol, F. Issac, J-P. Parmantier, F. Boulay," Etude de la Modélisation du Rayonnement d'un Réseau de Câbles sur Plan de Masse et du Couplage d'une Décharge Électrostatique sur un Câblage de Satellite," *ONERA report*, RT 23/6727 DEMR/Y, May 1999 (in French).

1 In this paper, we intentionally do not speak of "radiated" fields, which implicitly suppose far-field considerations and refer to antenna theory. As far as EMC problems are concerned, we are more interested in near fields. Therefore, we will speak of "emitted" EM fields, in order to avoid any confusion with antenna theory.

Enabling RF/Microwave Devices using Negative-Refractive-Index Transmission-Line Metamaterials

G.V. Eleftheriades

Abstract

Metamaterials are artificially engineered structures with unusual electromagnetic properties. In this article, we review the implementation of isotropic metamaterials that exhibit a negative permittivity and a negative permeability, thus leading to a negative index of refraction. Specifically, the article focuses on transmission-line metamaterials, which are planar structures comprising a network of distributed transmission lines loaded periodically in a dual (high-pass) configuration with lumped inductors, *L*, and capacitors, *C*. The periodic unit cell is much smaller than the wavelength, thus leading to an effective medium in which the lumped loading elements can be either chip or printed. Based on this transmission-line method, a number of RF/microwave devices are presented, including lenses that can overcome the diffraction limit, compact phase-shifting lines, small antennas, antenna feed networks and baluns, backward leaky-wave antennas and high-directivity coupled-line couplers.

1. Introduction

Broadly speaking, the term "metamaterials" refers to artificial media with electromagnetic properties that transcend those of natural media ("meta" means "beyond" in Greek). Most researchers in this field restrict metamaterials to be artificially structured periodic media in which the periodicity is much smaller than the wavelength of the impinging electromagnetic wave. These periodic inclusions act as artificial "molecules" that scatter back the impinging electromagnetic field in a prescribed manner. This scattering process can be macroscopically characterized by means of effective material parameters, such as a permittivity, a permeability, and a refractive index. Yet, others do not impose strict limits on the size of the constituent unit cells, thus extending the definition of metamaterials to include periodic structures, such as photonic crystals. This article adopts the former definition, which establishes a direct relationship with artificial dielectrics [1]. Moreover, we will limit our discussion to planar isotropic metamaterials in which the permittivity and permeability are simultaneously negative, hence leading to a negative refractive index [2].

Bulk "left-handed" or "negative-refractive-index" (NRI) media supporting two-dimensional wave propagation were first implemented using periodic arrays of thin wires to synthesize negative permittivity, and split-ring resonators to synthesize negative permeability [3]. A different approach for implementing negative-refractive-index media that also supports two-dimensional wave propagation has been proposed in [4, 5] by loading a planar network of printed transmission lines (TL) with series capacitors and shunt inductors in a dual (high-pass) configuration. Such a planar negative-refractive-index medium was interfaced with a commensurate conventional dielectric, arguably leading to the first experimental demonstration of focusing from a left-handed metamaterial [5, 6]. This transmission-line methodology for making negative-refractive-index media leads to wide operating bandwidths over which the refractive index remains negative. For example, [6] reported focusing due to negative refraction over an octave bandwidth. More recently, a three-region lens arrangement was used to observe focusing beyond the diffraction limit [7, 8] as was predicted by J. B. Pendry [9]. A similar transmission-line approach was followed by Itoh and Caloz, and led to interesting circuits [10, 11]. This article is limited to planar isotropic negative-refractive-index metamaterials synthesized using loaded transmission lines. However, intriguing and useful planar anisotropic transmission-line metamaterials have been developed by Balmain et al. [12, 13]. Further developments in the general area of metamaterials can be found in two recent special issues: the October, 2003, issue of the *IEEE Transactions on Antennas and Propagation* (guest Editors R. W. Ziolkowski and N. Engheta), and the April, 2003, issue of *Optics Express* (**11**, 7, guest Editor J. B. Pendry).

George V. Eleftheriades is with the Department of Electrical and Computer Engineering, University of Toronto, 10 King's College Road, Toronto, ON M5S 3G4, Canada; Tel: +1 (416) 946-3564; Fax: +1 (416) 971-2286; E-mail: gelefth@waves.utoronto.ca.

This is one of the invited *Reviews of Radio Science*, from Commission B.

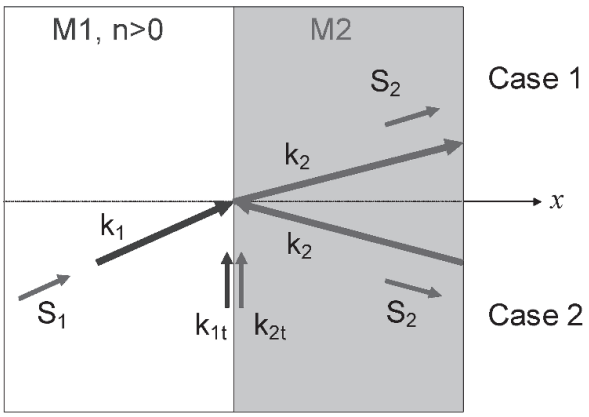

Figure 1. The negative refraction of a plane wave incident from a regular dielectric to another regular dielectric (Case 1) or to a negative-refractive-index medium (Case 2). The arrows on the rays represent the propagation vectors; observe the underlying phase matching of the tangential components of these vectors in Case 2. Another implied principle is that the Poynting Vector, $\bar{S}$, should point away from the interface in the second medium.

In this article, we are presenting the latest results on a number of RF/microwave passive devices and antennas that have been developed at the University of Toronto, based on transmission-line negative-refractive-index metamaterials. This includes a brief exposition of the effective medium theory for such transmission-line negative-refractive-index media, followed by the presentation of a class of metamaterial phase-shifting lines that offer phase shifts around the 360° mark with small length, wide bandwidth, and high linearity. Applications of these phase-shifting lines are also presented, including small antennas and antenna feed networks. Subsequently, a planar transmission-line negative-refractive-index lens is presented that overcomes the diffraction limit, offering sub-wavelength resolution at microwave frequencies. This is followed by a peculiar planar coupled-line coupler, in which the phase flow is co-directional but the power flow is contra-directional. This coupler supports complex modes that vary exponentially with distance along the lines, thus leading to high coupling levels and low isolation, and, hence, a high directivity. Finally, a unique backward-wave leaky-wave antenna is presented, which radiates its fundamental spatial harmonic.

2. Fundamental Properties

Veselago was the first to examine in the open literature the feasibility of media characterized by simultaneously negative permittivity and permeability [2]. He concluded that such media are allowed by Maxwell's equations, and that plane waves propagating in them would have their electric field, $\bar{E}$, magnetic field, $\bar{H}$, and propagation constant, $\bar{k}$, form a left-handed triplet. Therefore, he coined the term "left-handed" to describe these hypothetical media. Also, Veselago realized that one has to choose the negative branch of the square root to properly define the corresponding refractive index, i.e., $n = -\sqrt{\varepsilon\mu}$. Thus, such left-handed media support negative refraction of electromagnetic waves, something that was demonstrated experimentally more than three decades later by Shelby, Smith, and Schultz [3]. Moreover, due to the fact that $\bar{E}$, $\bar{H}$, and $\bar{k}$ form a left-handed triplet, whereas the $\bar{E}$, $\bar{H}$ vectors and the Poynting vector, $\bar{S}$, form a right-handed triplet, Veselago concluded that in left-handed media, the propagation constant, $\bar{k}$, is anti-parallel to the Poynting vector, $\bar{S}$. In retrospect, what Veselago was describing were backward waves. For this reason, some researchers use the term "backward-wave" media to describe left-handed materials [14].

Certainly, one-dimensional backward-wave lines are not new to the microwave community, and there is an interesting connection to familiar concepts and structures. However what is remarkable and surprising in Veselago's work is his realization that two- or three-dimensional isotropic and homogeneous media supporting backward waves should be characterized by a negative refractive index. Consequently, when such media are interfaced with conventional dielectrics, Snell's law is reversed, leading to the negative refraction of an incident electromagnetic plane wave. One way to understand negative refraction is through the notion of phase matching, as explained in Figure 1. Since Snell's law is a manifestation of phase matching of the transverse propagation vector at the interface between two dielectrics, Figure 1 readily suggests that the left-handed medium should be characterized by a negative refractive index. Another way to show this is by invoking the radiation condition, as discussed in the next section.

An issue worth clarifying here is the terminology "negative group velocity," which was used by Veselago in his original paper to characterize left-handed media [2]. Apparently, what Veselago had in mind were backward waves in which the phase velocity is anti-parallel to the group velocity (although he never mentioned backward waves explicitly in [2]). Hence, if we define the phase velocity to be negative, then in left-handed media, the group velocity should be positive to describe power flowing away from the source. In this context, negative group velocity would indicate anomalous dispersion, which prevails in conventional dielectric media close to absorption lines. Such left-handed media exhibiting negative phase velocity and anomalous negative group velocity have recently been realized by deliberately inserting lossy resonators in transmission-line metamaterials [15].

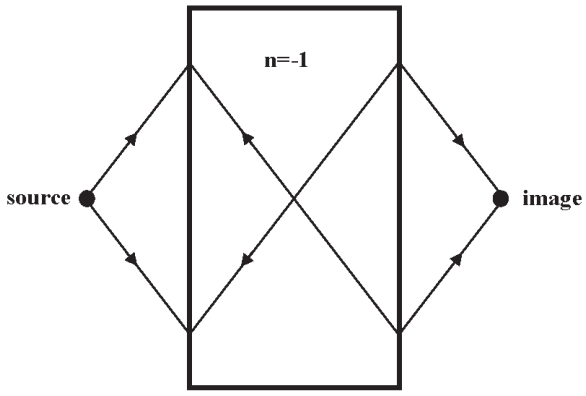

Figure 2. Veselago's lens in a vacuum. As shown, negative refraction is utilized in order to focus a point to a point. This leads to a lens with flat surfaces and no optical axis. The rays converge to the same point when $n=-1$, thus leading to aberration-free focusing and no reflections from the lens surfaces. The thickness of the lens is half the distance from the source to the image.

Harnessing the phenomenon of negative refraction, entirely new refractive devices can be envisioned, such as a flat lens without an optical axis, also proposed by Veselago, as shown in Figure 2. Other intriguing possibilities predicted by Veselago include the reversal of Cherenkov radiation [16] and of the Doppler shift [17]. Each of these new phenomena can be utilized to make interesting new devices. For example, the reversal of Cherenkov radiation inspired the development of backward-wave antennas radiating their fundamental spatial harmonic [16, 18] whereas the reversal of the Doppler shift can be exploited for making wideband millimeter-wave sources [17]. Other interesting potential applications of metamaterials can be found in [19].

Before we finish this section, it is perhaps useful to summarize the various names used in the literature for characterizing the metamaterials under consideration. The most frequently used terms are "left-handed," "negative-refractive-index," "backward-wave" and "doubly-negative" media [20, 21]. We have already mentioned all names and justified their origin, except the last. The term "doubly-negative" media originates from the fact that these materials are characterized by a simultaneously negative permittivity and permeability. In our opinion, all four names are justified, and have their advantages and disadvantages. However, we will not engage here in a further discussion of the nomenclature. The author's research group uses the term "negative-refractive-index" metamaterials because this term conveys one of the most fundamental and surprising aspects of these media, which can capture the imagination of the non-specialist; moreover, this name is self-contained. Nevertheless, we also liberally use the term "left-handed" metamaterials for historical reasons.

3. Effective Medium Theory

A practical, periodic two-dimensional transmission-line based negative-refractive-index metamaterial can be realized using an array of unit cells, each as depicted in Figure 3. A host transmission-line medium (e.g. a microstrip) is periodically loaded using discrete series capacitors and shunt inductors [4, 5]. From the onset, the key observation is that there is a correspondence between negative permittivity and a shunt inductor (L), as well as between negative permeability and a series capacitor (C). This allows synthesizing artificial media (metamaterials) with a negative permittivity and a negative permeability and, hence, a negative refractive index. When the unit cell dimension, d, is much smaller than a guided wavelength, the array can be regarded as a homogeneous effective medium, and, as such, can be described by effective constitutive parameters $\mu_N(\omega)$ and $\varepsilon_N(\omega)$, which are determined through a rigorous periodic analysis to be of the form shown in Equation (1) (assuming two-dimensional TM_y wave propagation in Figure 3):

$$\varepsilon_N(\omega) = 2\varepsilon_p - \frac{g}{\omega^2 L_0 d}, \qquad (1)$$

$$\mu_N(\omega) = \mu_p - \frac{1/g}{\omega^2 C_0 d}$$

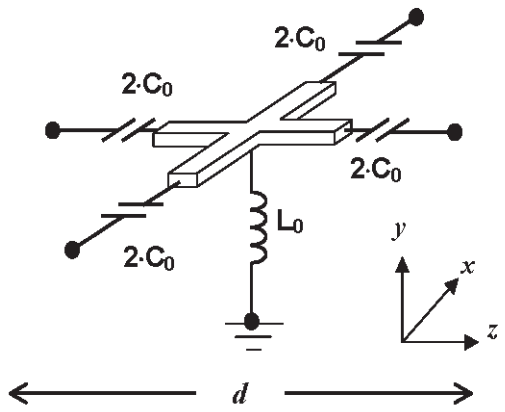

Figure 3. The unit cell for the two-dimensional transmission-line-based negative-refractive-index metamaterial. A host transmission line is loaded periodically with series capacitors and shunt inductors in a dual (high-pass) configuration.

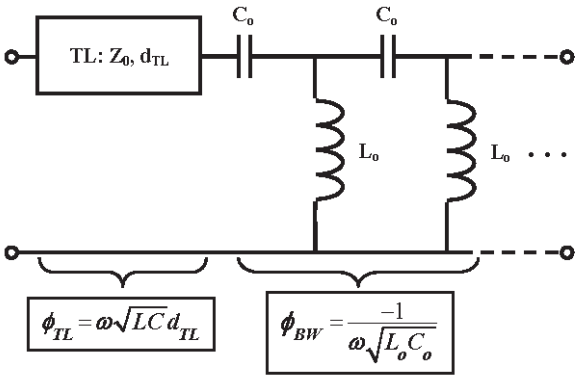

Figure 4. A phase-compensating structure based on a conventional transmission line and a negative-refractive-index (backward-wave) line

Here, ε_p and μ_p are positive constants describing the host transmission-line medium, and they are proportional to the per-unit-length capacitance and inductance of this host transmission-line medium, respectively. The geometrical factor, g, relates the characteristic impedance of the transmission-line network to the wave impedance of the effective medium. Moreover, the factor of two in front of the effective permittivity of the two-dimensional medium is necessary to properly account for scattering at the edges of the unit cell (this factor becomes unity for one-dimensional media). Naturally, the practically realizable unit cell of Figure 3 contains both a positive- as well as a negative-refractive-index response, as was originally stipulated in [4, 5, 6] and [16]. This particular arrangement of the inclusions L_0 and C_0 provides the desired negative material contribution that diminishes with frequency, ω, and ensures compatibility with the Poynting theorem for dispersive media [1, 2]. When the parameters are simultaneously negative, these structures exhibit a negative effective refractive index and have experimentally demonstrated the predicted associated phenomena, including negative refraction, focusing, and focusing with sub-wavelength resolution [4-8].

In practical realizations, the sub-wavelength unit cell of Figure 3 is repeated to synthesize artificial two-dimensional materials with overall dimensions that are larger than the incident electromagnetic wavelength. Therefore, the resulting structures are by definition distributed. However, the loading lumped elements could be realized either in chip [4, 5] or in printed form [16, 18, 22, 23].

Once it is established that a negative permittivity and permeability characterizes these media, then the refractive index is given by $n = \pm\sqrt{\varepsilon_N \mu_N}$, where one has to choose the correct branch of the square root. For this purpose, consider low-loss propagation in which the permeability is slightly complex, such that $\mu_N = \mu_N' - j\mu_N''$ with $\mu_N' < 0$ and $\mu_N'' > 0$. In the limit of low-loss propagation, the refractive index can be approximated by

$$n \cong \pm\sqrt{\varepsilon_N \mu_N'}\left(1 - j\frac{\mu_N''}{2\mu_N'}\right). \qquad (2)$$

A plane wave propagating along the positive z axis, $e^{-jk_0 nz}$, should decay with distance. Hence, the imaginary part of the refractive index $n = n' - jn''$ should be positive, i.e., one has to choose the negative branch of the square root in Equation (2) to satisfy the radiation condition.

4. Compact, Broadband Phase-Shifting Lines and Applications

In conventional positive-refractive-index (PRI) transmission lines (TLs), the phase lags in the direction of positive group velocity, implying that the phase incurred is negative. It therefore follows that phase compensation can be achieved at a given frequency by cascading a section of a negative-refractive-index line (i.e., a backward-wave line) with a section of a positive-refractive-index line to synthesize positive, negative, or zero transmission phase at a short physical length (see Figure 4) [24].

The structure of Figure 4 can be rearranged to form a series of symmetric metamaterial unit cells, as proposed in [5, 24]. Such a unit cell is shown in Figure 5, and it is nothing but a transmission line of characteristic impedance Z_0, periodically loaded with series capacitors, C_0, and shunt inductors, L_0 (see Figure 3). A representative dispersion diagram for typical host transmission-line and loading parameters is shown in Figure 6.

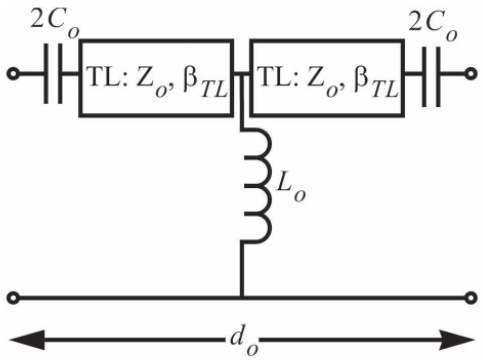

Figure 5. A unit cell of a metamaterial phase-shifting line comprising a host transmission line periodically loaded with series capacitors and shunt inductors.

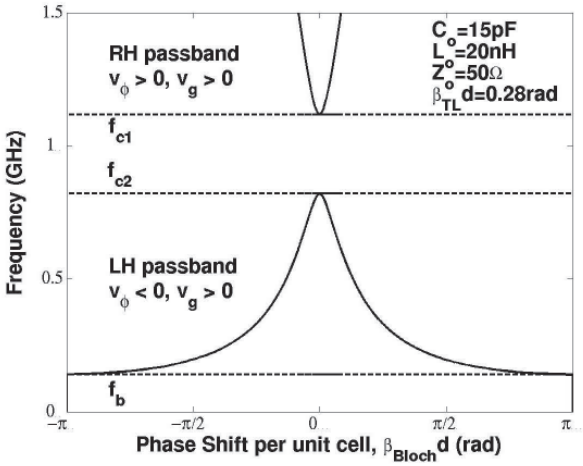

Figure 6. The dispersion diagram for the periodic structure of Figure 5 with typical line and loading parameters. The edges of the stop-band are designated by f_{c1} and f_{c2}.

The metamaterial phase-shifting lines can then be constructed by cascading a series of these unit cells. The edges of the stop-band, f_{c1} and f_{c2}, in Figure 6 are determined at the series resonance between the inductance of the transmission-line section and the loading capacitor, C_0, and the shunt resonance between the capacitance of the transmission-line section and the loading inductance, L_0, respectively. Alternatively, these are the frequencies at which the effective permeability, $\mu_N(\omega)$, and the effective permittivity, $\varepsilon_N(\omega)$, vanish: $\varepsilon_N(\omega)=0$, $\mu_N(\omega)=0$.

Hence, by setting the effective material parameters of Equation (1) to zero, these cutoff frequencies are readily determined to be

$$f_{c1} = \frac{1}{2\pi}\sqrt{\frac{1/g}{\mu_p C_0 d}}, \tag{3}$$

$$f_{c2} = \frac{1}{2\pi}\sqrt{\frac{g}{\varepsilon_p L_0 d}}, \tag{4}$$

where the characteristic impedance of the host transmission line is

$$Z_o = g\sqrt{\frac{\mu_p}{\varepsilon_p}} = \sqrt{\frac{L}{C}}.$$

By equating f_{c1} and f_{c2}, the stop-band in Figure 6 can be closed, thus allowing access to phase shifts around the zero mark. The condition for a closed stop-band is therefore determined to be

$$Z_0 = \sqrt{\frac{L_0}{C_0}}. \tag{5}$$

This condition also implies that the transmission line of Figure 4 is matched to the negative-refractive-index line. The closed stop-band condition, Equation (5), was originally derived in [5] (Equation (29)), and later also reported in [25]. Under this condition, it has been shown in [24] that the total phase shift per unit cell is

$$\beta_{eff} \approx \omega\sqrt{LC} + \frac{-1}{\omega\sqrt{L_0 C_0}}. \tag{6}$$

This expression can be interpreted as the sum of the phase incurred by the host transmission line and a uniform backward wave *L-C* line, as shown in Figure 4.

Various one-dimensional phase-shifting lines were constructed in co-planar waveguide (CPW) technology at 0.9 GHz, as shown in Figure 7. The simulated and measured phase responses for two-stage and four-stage 0° phase-shifting lines are shown in Figure 8, compared to the phase response of a conventional $-360°$ transmission line. Also shown are the magnitude responses of the two-stage and four-stage 0° lines.

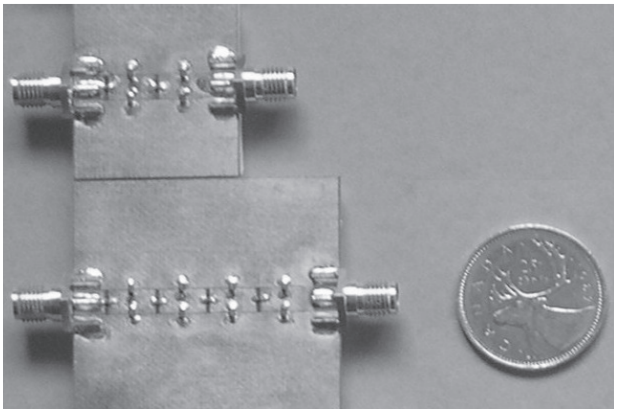

Figure 7. (Top) A two-stage phase-shifting line (16 mm). (Bottom) A four-stage phase-shifting line (32 mm) at 0.9 GHz. Note that the reference $-360°$ transmission line was 283.5 mm (not shown).

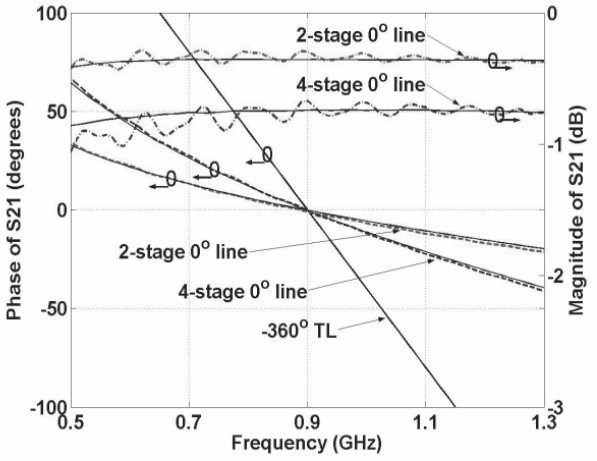

Figure 8. The phase responses of one, four, and eight-stage 0° phase-shifting lines compared to a conventional $-360°$ transmission line at 0.9 GHz: The dashed line is measured data; the solid line is from an Agilent ADS *simulation. Also shown are the amplitude responses for the two- and four-stage devices.*

It can be observed that the experimental results correspond very closely to the simulated results, highlighting the broadband nature of the phase-shifting lines and their small losses.

It can be concluded that the metamaterial phase-shifting lines offer some significant advantages when compared to conventional delay lines. They are compact in size, can be easily fabricated using standard etching techniques, and exhibit a linear phase response around the design frequency. They can incur *either* a negative *or* a positive phase, as well as a 0° phase, depending on the values of the loading elements, while maintaining a short physical length. In addition, the phase incurred is independent of the length of the structure. Due to their compact, planar design, they lend themselves easily towards integration with other microwave components and devices. The metamaterial phase-shifting lines are therefore ideal for broadband applications requiring small, versatile, linear devices.

An example of harnessing these phase-shifting lines to feed printed dipole antennas in series has been reported in [26]. The main idea is to use zero-degree phase-shifting lines to feed the dipoles in phase in a series-fed array. Due to the broadband nature of these lines, the resulting array patterns squint much less with frequency when compared to their conventional series-fed counterparts using meandered one-wavelength lines.

Another application of these lines is the implementation of a metamaterial balun, as shown in

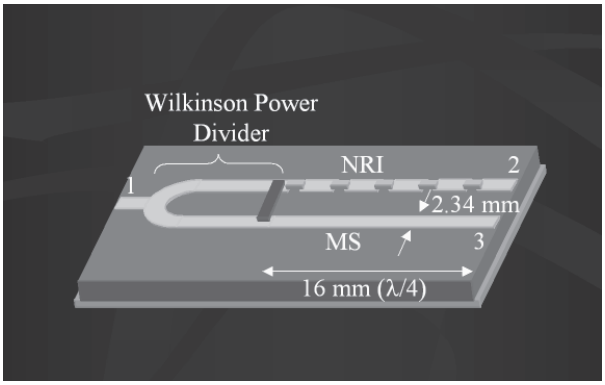

Figure 9a. A metamaterial balun. An example design in microstrip at 2.55 GHz on a TMM4 substrate ($\varepsilon_r = 4.6$, height = 50 mil) corresponds to a microstrip line 16 mm long and 2.34 mm wide (positive-refractive-index line); the negative-refractive-index line comprises five unit cells loaded with 1.1 pF series capacitors and 5.6 nH shunt inductors with a length and width equal to the positive-refractive-index (microstrip) line.

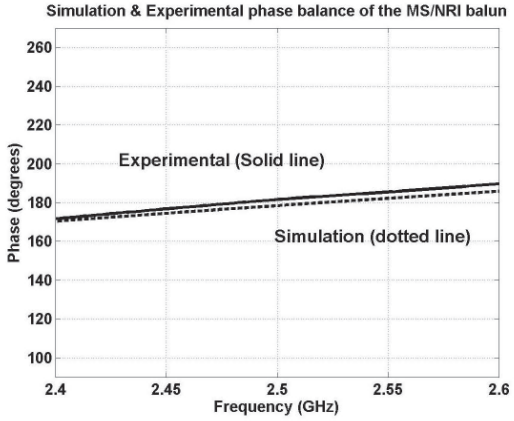

Figure 9b. The measured phase-balance response for the case of Figure 9a.

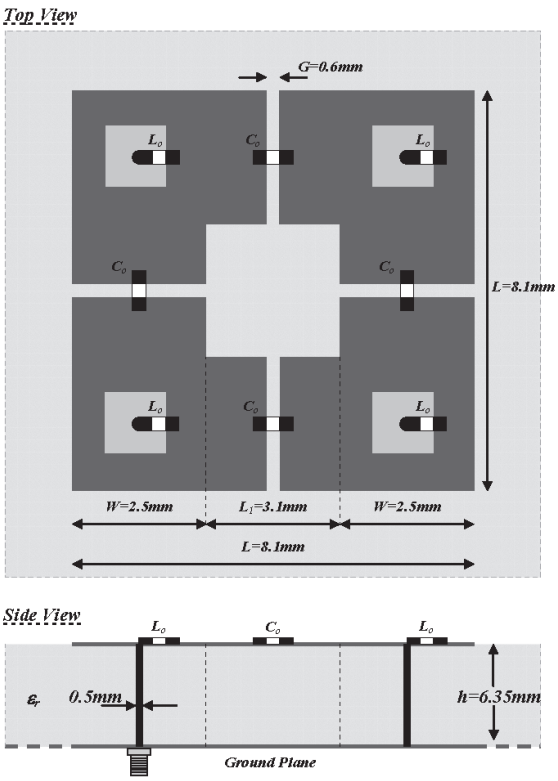

Figure 10. A diagram of a metamaterial ring antenna at 1.5 GHz. The loading capacitance and inductance required to feed the vias in phase were $C_0 = 3.70\,pF$ *and* $L_0 = 71.08\,nH$.

Figure 9. Specifically, a zero-degree phase-shifting microstrip line is tapped at its center. If the phase shift of the negative-refractive-index line is $-90°$ and that of the positive-refractive-index line is $+90°$, then the output ports #2 and #3 are 180° out of phase.

As shown in Figure 9b, there is a very good phase balance between 2.4 GHz and 2.6 GHz. Moreover, the measured isolation between the output ports maintains an average value of about 30 dB throughout the same band.

A final example of harnessing the phase-shifting lines of [24] is to wrap around a zero-degree phase-shifting line to implement a small printed antenna. This is shown in Figure 10 for a realization at 1.5 GHz. As shown, there are four metamaterial phase-shifting sections arranged in a square ring. Each constituent section comprises a negative-refractive-index (NRI) microstrip transmission line (TL), designed to incur a zero insertion phase at the antenna's operating frequency. This allows the inductive posts to ground – which act as the main radiating elements – to be fed in phase. Hence, the antenna operates as a two-dimensional array of closely spaced monopoles that are fed in phase through a compact feed network. This leads to a ring antenna with a small footprint (a diameter of $\lambda/25$) and a low profile (a height of $\lambda/31$), capable of radiating vertical polarization.

The measured return loss obtained indicates a good matching of greater than 25 dB at 1.51 GHz, with a -10 dB bandwidth of approximately 2%. This bandwidth can be increased to 3%-4% if the dielectric substrate is reduced to about the size of the ring, or if the via height is increased. Figure 11 shows the measured versus the simulated E- and H-plane patterns obtained from Ansoft's *HFSS*, which demonstrates good agreement. It can be observed that the antenna exhibits a radiation pattern with a vertical linear electric field polarization, similar to a short monopole on a finite ground plane. The radiation in the back direction is reduced compared to the forward direction due to the effect of the finite ground plane used; however, it is not completely

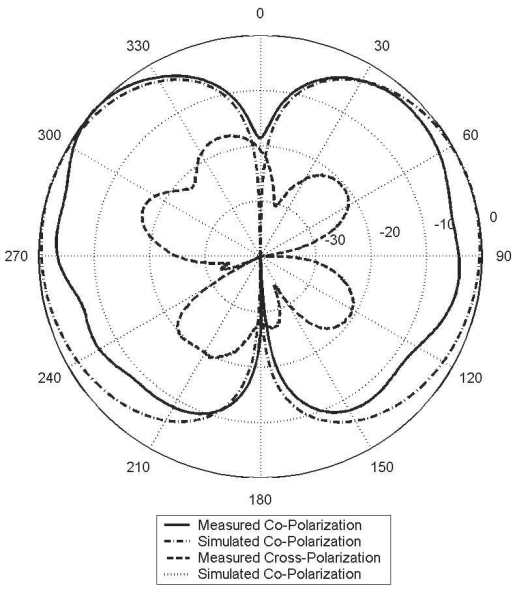

Figure 11a. The measured and simulated (Ansoft's HFSS*) E-plane antenna patterns at 1.51 GHz.*

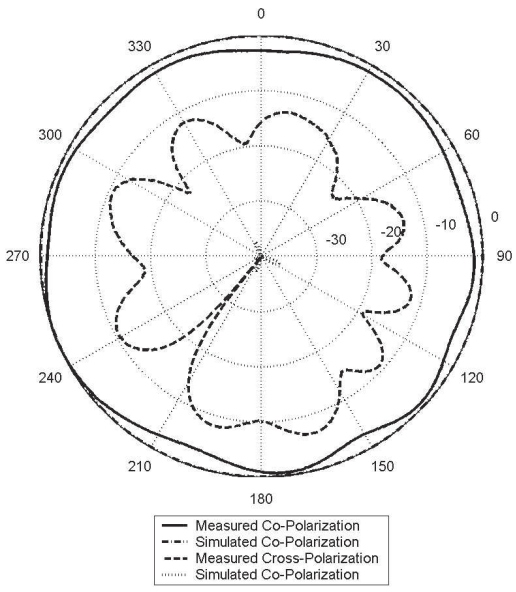

Figure 11b. The measured and simulated (Ansoft's HFSS*) H-plane antenna patterns at 1.51 GHz.*

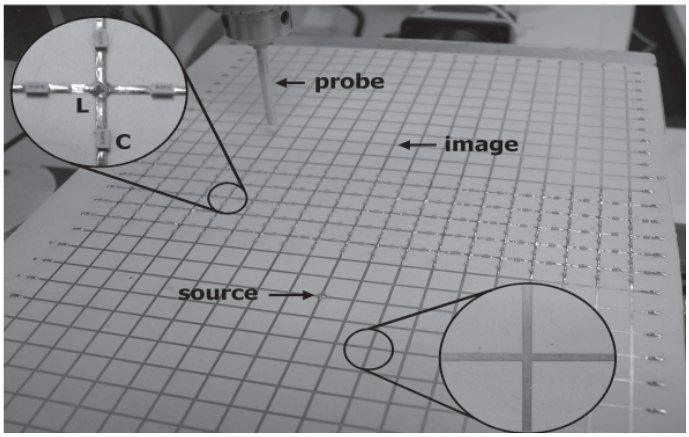

Figure 12. A photograph of a planar superresolving Veselago lens around 1 GHz [8].

eliminated. Moreover, there is good cross-polarization purity in the E plane, with a maximum measured electric field cross-polarization level of -17.2 dB. In the H plane, the maximum electric field cross-polarization level is only -6.6 dB.

The loading with chip passive lumped elements is effective at RF and low microwave frequencies. At higher frequencies, these can be replaced by printed lumped elements. For example, a fully printed version of this antenna at 30 GHz, in which the loading lumped-element chip capacitors and inductors were replaced by gaps and vias, respectively, was reported in [27]. A further interesting application of metamaterials for the design of small and efficient antennas can be found in [28].

5. A Super-Resolving Negative-Refractive-Index Transmission-Line Lens

Classical electrodynamics imposes a resolution limit when imaging using conventional lenses. This fundamental limit, called the "diffraction limit" in its ultimate form, is attributed to the finite wavelength of electromagnetic waves. The electromagnetic field emanating from an illuminated object, lying over the *x*-*y* plane, consists of a continuum of plane waves $\exp(-jk_x x - jk_y y)\exp(-jk_z z)$. Each plane wave has a characteristic amplitude and propagates at an angle with the optical *z* axis given by the direction cosines k_x/k_0, k_y/k_0, where k_0 is the propagation constant in free space. The plane waves with real-valued direction cosines ($k_x^2 + k_y^2 < k_0^2$) propagate without attenuation, while the evanescent plane waves with imaginary direction cosines ($k_x^2 + k_y^2 > k_0^2$) attenuate exponentially along the optical *z* axis. A conventional lens focuses only the propagating waves, resulting in an imperfect image of the object, even if the lens diameter is infinite. The finer details of the object, carried by the evanescent waves, are lost due to the strong attenuation these waves experience ($\exp\left(-z\sqrt{k_x^2 + k_y^2 - k_0^2}\right)$) when traveling from the object to the image through the lens. The Fourier transform uncertainty relation $k_{t\_\max}\Delta\rho \sim 2\pi$, relating the maximum transverse wavenumber, $k_{t\_\max}$, to the smallest transverse spatial detail, $\Delta\rho$, implies that spatial details smaller than a wavelength are eliminated from the image ($\Delta\rho \sim 2\pi/k_0 = \lambda$). This loss of resolution, which is valid even if the diameter of the lens is infinite, constitutes the origin of the diffraction limit in its ultimate form. For the typical case of imaging a point source, the diffraction limit manifests itself as an image smeared over an area approximately one wavelength in diameter.

In 2000, John Pendry extended the analysis of Veselago's lens to include evanescent waves, and observed that such lenses could overcome the diffraction limit [9]. Pendry suggested that Veselago's lens would allow "perfect imaging" if it were completely lossless and its refractive index was exactly equal to $n = -1$ relative to the surrounding medium. The left-handed lens achieves imaging with super-resolution by focusing propagating waves as would a conventional lens (see Figure 2), but in addition it supports growing evanescent waves, which restore the decaying evanescent waves emanating from the source. This restoration of evanescent waves at the image plane extends the maximum accessible wavenumbers, $k_{t\_\max} > k_0$, and allows imaging with superresolution. The physical mechanism behind the growth of evanescent waves is quite interesting: within the negative-refractive-index slab, multiple reflections result in both growing and attenuating evanescent waves. However, $n = -1$ corresponds to a resonant phenomenon in which the attenuating solution is cancelled out, thus leaving only the growing wave present. In a sense, one may think of Veselago's lens as an inverse system that exactly restores propagation in free space.

A picture of a planar version of Veselago's lens that was constructed at the University of Toronto is shown in Figure 12. The negative-refractive-index lens is a slab consisting of a 5×19 grid of printed microstrip strips, loaded with series capacitors (C_0) and shunt inductors (L_0). This negative-refractive-index slab is sandwiched between two unloaded printed grids that act as homogeneous media with a positive index of refraction. The first unloaded grid is excited with a monopole (point source), which is imaged by the negative-refractive-index lens to the second unloaded grid. The vertical electric field over the entire structure is measured using a detecting probe (for details, see [6]).

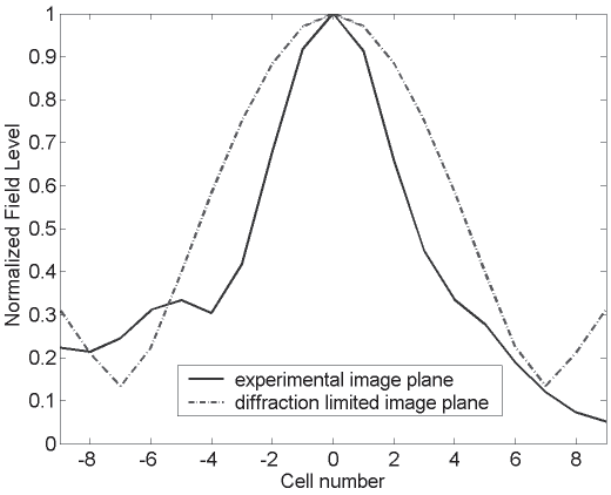

Figure 13. Experimental verification of sub-wavelength focusing.

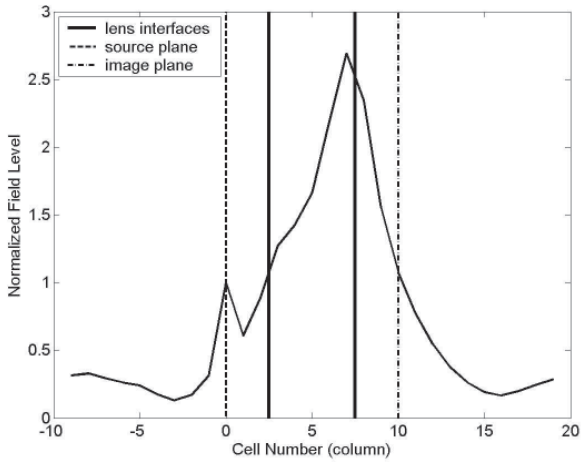

Figure 14. Experimental verification of growing evanescent waves in a super-resolving transmission-line negative-refractive-index lens.

The measured half-power beamwidth of the point-source image at 1.057 GHz is 0.21 effective wavelengths, which is appreciably narrower than that of the diffraction-limited image corresponding to 0.36 wavelengths (see Figure 13). The enhancement of evanescent waves for the specific structure under consideration was demonstrated in [29]. Figure 14 shows the measured vertical electric field above the central row of the lens, which verifies the exponential growth of the fields inside the negative-refractive-index medium predicted in [29]. Since there is some controversy regarding losses in negative-refractive-index metamaterials, we hereby report that the loss tangent of the negative-refractive-index medium at 1.05 GHz was estimated to be $\tan(\delta) = 0.062$, which attests to the low-loss nature of the negative-refractive-index transmission-line lens. However, even such a slight loss is sufficient to deteriorate the growth of evanescent waves to $k_{t\_\max} = 3k_0$ [8]. The super-resolving imaging properties of the structure shown in Figure 12 have been theoretically investigated by means of a rigorous periodic Green's function analysis in [30]. Furthermore, the corresponding dispersion characteristics for these distributed structures were derived in [31] using periodic two-dimensional transmission-line theory. In the case where the loading is achieved using printed instead of chip loading lumped elements – e.g., microstrip gaps and vias, or coils to implement series capacitors and inductors, respectively [22] – the corresponding dispersion characteristics have been examined using finite-element electromagnetic simulations in [23].

6. A High-Directivity Backward NRI/Microstrip Coupler

A peculiar coupled-line coupler (see Figure 15) can be realized using a regular microstrip (MS) line that is edge coupled to a negative-refractive-index (NRI) line [32, 33]. Such a coupler exhibits co-directional phase but contra-directional Poynting vectors on the lines, thus leading to backward power coupling.

Using coupled-mode theory, it can be shown that *complex-conjugate coupled modes* are excited in this coupler

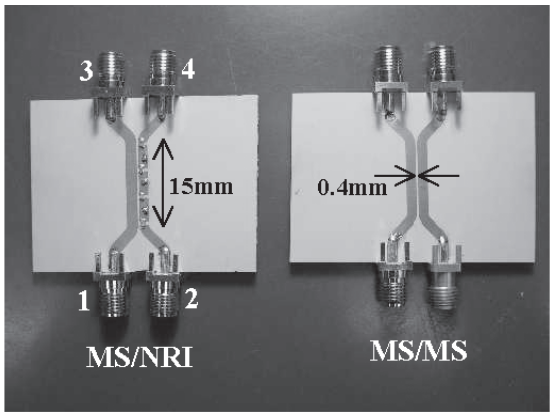

Figure 15. Microstrip/negative-refractive-index and microstrip/microstrip ($\lambda/4$) couplers of equal length, line spacing, and propagation constants, designed for operation at 2.8 GHz.

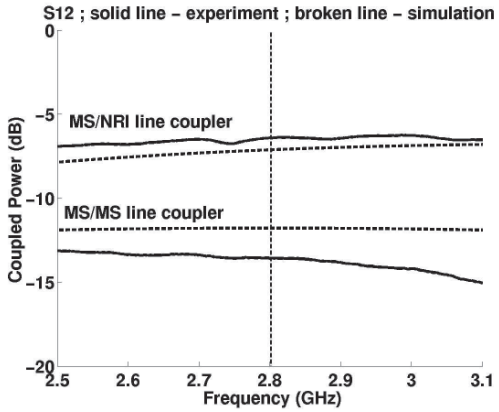

Figure 16. A comparison of the coupled power levels for the microstrip/negative-refractive-index and the microstrip/microstrip couplers.

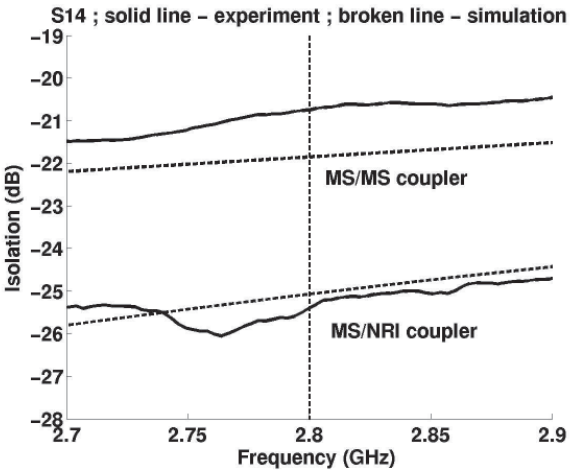

Figure 17. A comparison of the isolation for the microstrip/negative-refractive-index and the microstrip/microstrip couplers.

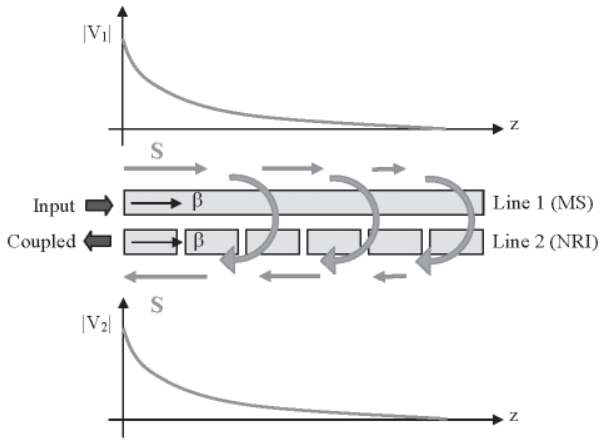

Figure 18. The physical mechanism by which power continuously leaks from the microstrip line to the negative-refractive-index line.

at the frequency where the propagation constants of the two isolated lines become equal [33]. For a sufficiently long coupler operated at this frequency, the exponentially increasing modes can be discarded, and the line voltage/current expressions take the following form:

$$\begin{bmatrix} V_1 \\ V_2 \\ I_1 \\ I_2 \end{bmatrix} = \begin{bmatrix} 1 & 1 \\ j & -j \\ 1/Z & 1/(-Z^*) \\ j/(-Z) & -j/Z^* \end{bmatrix} \begin{bmatrix} V_c^+ e^{-\gamma_c z} \\ V_\pi^+ e^{-\gamma_\pi z} \end{bmatrix} \qquad (7)$$

Here, γ_c and γ_π are complex-conjugate eigenvalues, $\gamma_c = \alpha + j\beta$, and Z is the impedance of the symmetric p-mode on the microstrip line. If port 1 (see Figure 15) is excited, it can be shown from Equation (7) that

$$\frac{1}{2}\mathrm{Re}\left(V_1 I_1^*\big|_{z=0}\right) = \frac{\mathrm{Re}(Z)}{2|Z|^2}\left(|V_c|^2 - |V_\pi|^2\right) \qquad (8)$$

$$= -\frac{1}{2}\mathrm{Re}\left(V_2 I_2^*\big|_{z=0}\right).$$

Equation (8) demonstrates that there is complete backward transfer of power from port 1 to port 2 (see Figure 15). In order to compare the performance of a microstrip/negative-refractive-index coupler to its regular counterpart of equal length, line spacing, and propagation constant, a benchmark microstrip coupler was designed and is shown in Figure 15. This benchmark microstrip/negative-refractive-index coupler was constructed with unit cells 5 mm long and loading elements of 2.7 nH shunt inductors and 0.9 pF series capacitors for the negative-refractive-index line. The line widths were 2.45 mm (microstrip) and 2 mm (negative-refractive index), and the transverse line separation was 0.4 mm. The performance of a three-unit cell microstrip/negative-refractive-index coupler was compared to that of a quarter-wavelength regular microstrip/microstrip coupler at 2.8 GHz when the isolated propagation constants of the two lines were similar. From Figures 16 and 17 it is evident that compared to its conventional counterpart of the same length and line spacing, this new microstrip/negative-refractive-index coupler exhibited better performance in terms of coupled power (higher coupling), lower return loss, and isolation, without any bandwidth degradation or significant change in insertion loss. This resulted in improved directivity. An experimental 3 dB device was reported in [33]. Typical directivity figures for these couplers are of the order of 20 dB, although couplers with a measured directivity of over 30 dB have been constructed and tested in the author's laboratory.

As was noted in [33], at the frequency where the isolated $\omega - \beta$ dispersion diagrams of the microstrip and negative-refractive-index lines meet, strong electromagnetic coupling between the lines takes place, leading to complex-conjugate propagation constants for the resulting symmetric and anti-symmetric modes. Around this point, one could think that the microstrip mode continuously "leaks" power backwards to the negative-refractive-index line, as suggested in Figure 18. This leakage effect has to be described in terms of a complex propagation constant. Quantitatively, for a finite coupler of length d, terminated to the symmetric-mode characteristic impedance, it can be shown that the coupling coefficient $|S_{21}|$ is given by the following equation:

$$|S_{21}| = \frac{2}{1 + e^{-2\alpha d}} - 1. \qquad (9)$$

This equation indicates that a coupler of a length on the order of a few times $1/\alpha$ will direct almost all the input power to the coupled port. Moreover, the attenuation constant, α, is larger with a smaller physical separation between the coupled lines.

It should be pointed out that the related phenomenon of contra-directional power but co-directional phase coupling between a negative-refractive-index and a regular dielectric

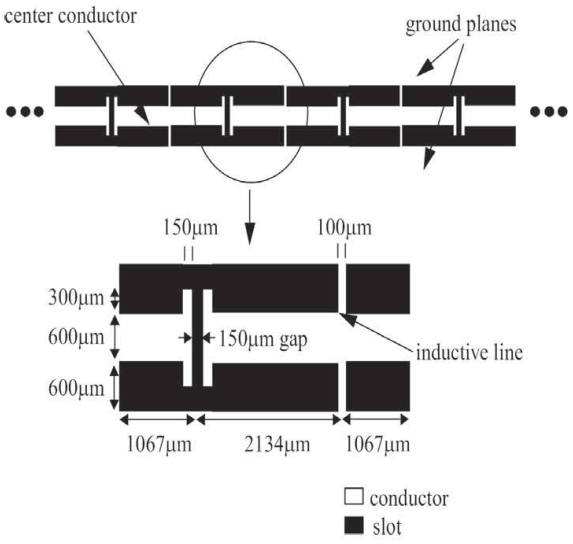

Figure 19. A backward leaky-wave antenna based on the dual transmission-line model at 15 GHz.

slab has also been reported in [34]. Moreover, a different backward-wave coupler comprising two negative-refractive-index lines has been described in [35].

7. A Leaky-Wave Backward Antenna Radiating its Fundamental Spatial Harmonic

The transmission-line (TL) approach to synthesizing negative-refractive-index metamaterials has led to the development of a new kind of leaky-wave antenna (LWA). By appropriately choosing the circuit parameters of the dual transmission-line model, a fast-wave structure can be designed that supports a fundamental spatial harmonic, which radiates toward the backward direction [16, 18].

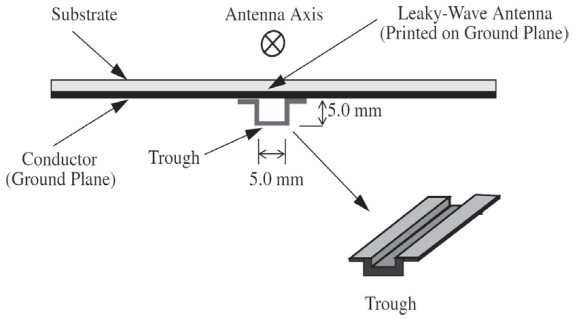

Figure 20. A unidirectional backward leaky-wave antenna design at 15 GHz.

The proposed coplanar waveguide (CPW) implementation of the leaky-wave antenna is shown in Figure 19. The gaps in the coplanar waveguide feed line serve as the series capacitors of the dual transmission-line model, while the narrow lines connecting the center conductor to the coplanar ground planes serve as the shunt inductors. The capacitive gaps are the radiating elements in this leaky-wave antenna, and excite a radiating transverse magnetic (TM) wave. Due to the anti-parallel currents flowing on each pair of narrow inductive lines, the shunt inductors remain non-radiating. Simulated and experimental results for this bi-directional leaky-wave antenna were reported in [16]. Simulation results for a unidirectional leaky-wave antenna design were also presented in [18]. The unidirectional design is simply the leaky-wave antenna described in [16] backed by a long metallic trough, as shown in Figure 20. Since the leaky-wave antenna's transverse dimension is electrically small, the backing trough can be narrow (below resonance). The trough used was a quarter wavelength in height and width, and covered the entire length of the antenna on the conductor side of the substrate. It acted as a waveguide below cutoff and recovered

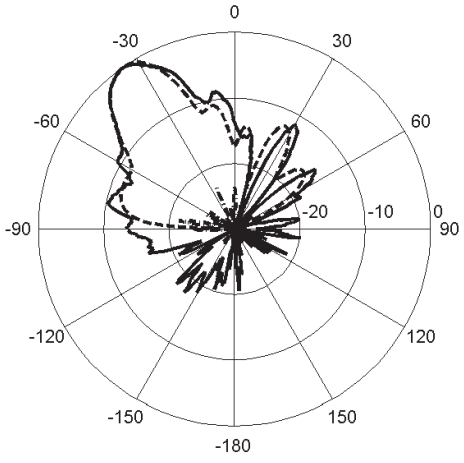

Figure 21. The E-Plane pattern for the unidirectional leaky-wave antenna. The solid line is the experimental co-polarization, the dash-dotted line is the experimental cross-polarization, and the dashed line is the simulated co-polarization using Agilent ADS*;* $f = 15$ *GHz.*

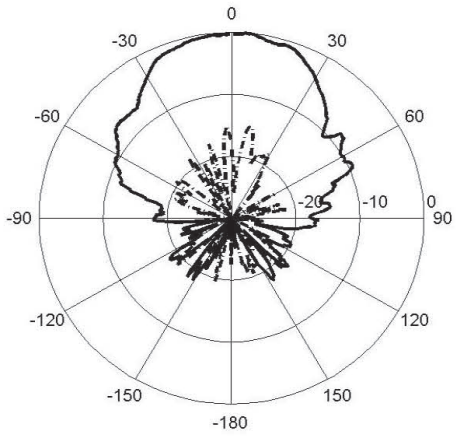

Figure 22. The H-plane pattern for the unidirectional leaky-wave antenna. The solid line is the experimental co-polarization, the dash-dotted line is the experimental cross-polarization, and the dashed line is the simulated co-polarization using Agilent ADS*;* $f = 15$ *GHz.*

the back radiation, resulting in unidirectional far-field patterns.

A complementary forward unidirectional leaky-wave antenna was also reported in [36]. The periodic structure of [36] also operated on the fundamental spatial harmonic and, hence, can be thought of as a metamaterial with a positive phase velocity. Here, we describe experimental results for the unidirectional design proposed in [18]. As noted in [18], a frequency shift of 3%, or 400 MHz, was observed in the experiments, compared to the Method-of-Moments simulations of the leaky-wave antenna using Agilent's *Advanced Design System*. As a result, the experimental unidirectional radiation patterns are shown at 14.6 GHz, while the simulation patterns are shown at 15 GHz. The E-plane and H-plane patterns are shown in Figures 21 and 22, respectively. A gain improvement of 2.8 dB was observed for the unidirectional design over the bi-directional design, indicating that effectively all of the back radiation was recovered with the trough.

8. Conclusion

The emerging field of negative-refractive-index metamaterials is very exciting for two interrelated reasons. On the one hand, there is new science being developed, associated with fascinating phenomena and their interpretation. These intriguing phenomena include negative refraction, growing evanescent waves and surpassing the classical diffraction limit, reversal of the Cerenkov and Doppler effects, and others yet to be discovered! On the other hand, these new phenomena are being harnessed to make RF/microwave passive devices, including antennas and their feed networks, offering unique properties in terms of functionality, size reduction, and performance. In this article, we have demonstrated a number of these devices based on negative-refractive-index transmission-line metamaterials. Specifically, we have presented lenses that can overcome the diffraction limit, compact and broadband phase-shifting lines, backward leaky-wave antennas, and high-directivity coupled-line couplers. This article was limited to the transmission-line methodology for implementing negative-refractive-index metamaterials. For other alternative realizations and their applications, the reader is referred to a couple of recent review articles [37, 38].

9. Acknowledgements

The author would like to thank his graduate students at the University of Toronto, who carried out all the hard work, and for their dedication and enthusiasm. For the material presented in this article, the author specifically thanks Tony Grbic, Ashwin Iyer, Marco Antoniades, and Rubaiyat Islam. He also would like to thank his colleagues at the University of Toronto, notably Prof. Keith G. Balmain and Profs. Mo Mojahedi, Costas Sarris, and Stewart Aitchison.

Financial support from the Natural Sciences and Engineering Research Council of Canada (NSERC), through Discovery and Strategic grants, as well as more recently through a Steacie Fellowship, are gratefully acknowledged. Moreover, the author thanks the Department of National Defence (DRDC/Ottawa) for financial support and for a wonderful collaboration.

10. References

1. R. E. Collin, *Field Theory of Guided Waves, Second Edition*, Toronto, Wiley-IEEE Press, Chapter 12, 1990.

2. V. G. Veselago, "The Electrodynamics of Substances with Simultaneously Negative Values of e and m," *Soviet Physics Usp*., **10**, 4, January 1968, pp. 509-514.

3. R. A. Shelby, D. R. Smith, and S. Schultz, "Experimental Verification of a Negative Index of Refraction," *Science*, **292**, April 6, 2001, pp. 77-79.

4. A. K. Iyer and G. V. Eleftheriades, "Negative Refractive Index Metamaterials Supporting 2-D Waves," *IEEE MTT-S International Microwave Symposium Digest*, **2**, June 2-7, 2002, Seattle, WA, pp. 1067-1070.

5. G. V. Eleftheriades, A. K. Iyer, and P. C. Kremer, "Planar Negative Refractive Index Media using Periodically L-C Loaded Transmission Lines," *IEEE Transactions on Microwave Theory and Techniques*, **MTT-50**, 12, December 2002, pp. 2702-2712.

6. A. K. Iyer, P. C. Kremer, and G. V. Eleftheriades, "Experimental and Theoretical Verification of Focusing in a Large, Periodically Loaded Transmission Line Negative Refractive Index Metamaterial," *Optics Express*, **11**, April 2003, pp. 696-708; http://www.opticsexpress.org/abstract.cfm?URI=OPEX-11-7-696.

7. A. K. Iyer, A. Grbic, and G. V. Eleftheriades, "Sub-Wavelength Focusing in Loaded Transmission Line Negative Refractive Index Metamaterials," *IEEE MTT-S International Microwave Symposium Digest*, June 8-13, 2003, Philadelphia, PA, pp. 199-202.

8. A. Grbic and G. V. Eleftheriades, "Overcoming the Diffraction Limit with a Planar Left-Handed Transmission-Line Lens," *Physical Review Letters*, **92**, 11, March 19, 2004, pp. 117403.

9. J. B. Pendry, "Negative Refraction Makes a Perfect Lens," *Physical Review Letters*, **85**, 18, October 2000, pp. 3966-3969.

10. L. Liu, C. Caloz, C. Chang, and T. Itoh, "Forward Coupling Phenomenon between Artificial Left-Handed Transmission Lines," *J. Appl. Phys.*, **92**, 9, November 2002, pp. 5560-5565.

11. C. **Caloz and T. Itoh, "Novel Microwave Devices and Structures Based on the Transmission Line Approach of Meta-Materials,**" *2003 IEEE Intl. Microwave Symposium Digest*, June 2003, pp. 195-198.

12. K. G. Balmain, A. A. E. Lüttgen, and P. C. Kremer, "Power Flow for Resonance Cone Phenomena in Planar Anisotropic Metamaterials," *IEEE Transactions on Antennas and Propagation*, **AP-51**, 10, October 2003, pp. 2612-2618.

13. K. G. Balmain, A. A. E. Lüttgen, and P. C. Kremer, "Resonance Cone Formation, Reflection, Refraction, and Focusing in a Planar Anisotropic Metamaterial," *IEEE Antennas and Wireless Propagation Letters*, **1**, 7, 2002, pp. 146-149.

14. S. Tretyakov, *Analytical Modeling in Applied Electromagnetics*, Norwood, MA, Artech House, 2003.

15. O. Siddiqui, M. Mojahedi, and G. V. Eleftheriades, "Periodically Loaded Transmission Line with Effective Negative Refractive Index and Negative Group Velocity," *IEEE Transactions on Antennas and Propagation*, **AP-51**, 10, October 2003, pp. 2619-2625.

16. A. Grbic and G. V. Eleftheriades, "Experimental Verification of Backward-Wave Radiation from a Negative Refractive Index Metamaterial," *Journal of Applied Physics*, **92**, 10, November 2002, pp. 5930-5935.

17. N. Seddon, and T. Bearpark. "Observation of the Inverse Doppler Effect," *Science*, **302**, November 28, 2003, pp. 537-1540.

18. A. Grbic and G. V. Eleftheriades, "A Backward-Wave Antenna Based on Negative Refractive Index L-C Networks," *IEEE International Symposium on Antennas and Propagation Digest*, **4**, San Antonio, TX, June 16-21, 2002, pp. 340-343.

19. N. Engheta, "Ideas for Potential Applications of Metamaterials with Negative Permittivity and Permeability," in S. Zouhdi, A. H. Sihvola, and M. Arsalane (eds.), *Advances in Electromagnetics of Complex Media and Metamaterials*, NATO Science Series, the Proceedings of NATO Advanced Research Workshop in Marrakech (Bianisotropics'2002), Kluwer Academic Publishers, Inc., 2002, pp. 19-37.

20. **R. W. Ziolkowski and E. Hayman, "Wave Propagation in Media Having Negative Permittivity and Permeability**," *Phys. Rev. E*, **64**, 2001, p. 056625.

21. R. W. Ziolkowski and A. D. Kipple, "Causality and Double-Negative Metamaterials," *Phys. Rev. E*, **68**, Part 2, 2003, pp. 026615.

22. G. V. Eleftheriades, "Planar Negative Refractive Index Metamaterials Based on Periodically L-C Loaded Transmission Lines," Workshop of Quantum Optics, Kavli Inst. of Theoretical Physics, University of Santa Barbara, July 2002; http://online.kitp.ucsb.edu/online/qo02/eleftheriades/ (slide #12).

23. A. Grbic and G. V. Eleftheriades, "Dispersion Analysis of a Microstrip Based Negative Refractive Index Periodic Structure," *IEEE Microwave and Wireless Components Letters*, **13**, 4, April 2003, pp. 155-157.

24. M. A. Antoniades and G. V. Eleftheriades, "Compact, Linear, Lead/Lag Metamaterial Phase Shifters for Broadband Applications," *IEEE Antennas and Wireless Propagation Letters*, **2**, 7, July 2003, pp. 103-106.

25. A. Sanada, C. Caloz, and T. Itoh, "Characteristics of the Composite Right/Left-Handed Transmission Lines," *IEEE Microwave and Wireless Components Letters*, **14**, February 2004, pp. 68-70.

26. G. V. Eleftheriades, M. A. Antoniades, A. Grbic, and R. Islam, "Electromagnetic Applications of Negative-Refractive-Index Transmission-Line Metamaterials," 27th ESA Antenna Technology Workshop on Innovative Periodic Antennas, Santiago, Spain, March 2004, pp. 21-28.

27. G. V. Eleftheriades, A. Grbic, and M. Antoniades, "Negative-Refractive-Index Metamaterials and Enabling Electromagnetic Applications," *2004 IEEE International Symposium on Antennas and Propagation Digest*, Monterey, CA, June 2004.

28. **R. W. Ziolkowski and A. D. Kipple, "Application of Double Negative Materials to Increase the Power Radiated by Electrically Small Antennas**," *IEEE Transactions on Antennas and Propagation*, **AP-51**, 10, October 2003, pp. 2626-2640.

29. A. Grbic and G. V. Eleftheriades, "Growing Evanescent Waves in Negative-Refractive-Index Transmission-Line Media," *Applied Physics Letters*, **82**, 12, March 24, 2003, pp. 1815-1817.

30. A. Grbic and G. V. Eleftheriades, "Negative Refraction, Growing Evanescent Waves and Sub-Diffraction Imaging in Loaded-Transmission-Line Metamaterials," *IEEE Transactions on Microwave Theory and Techniques*, **MTT-51**, 12, December 2003, pp. 2297-2305; "Erratum," *IEEE Transactions on Microwave Theory and Techniques*, **MTT-52**, 5, May 2004, p. 1580.

31. A. Grbic and G. V. Eleftheriades, "Periodic Analysis of a Two-Dimensional Negative Refractive Index Transmission Line Structure," *IEEE Transactions on Antennas and Propagation*, **AP-51**, 10, October 2003, pp. 2604-2611.

32. R. Islam and G. V. Eleftheriades, "A Planar Metamaterial Co-Directional Coupler that Couples Power Backwards," *2003 IEEE International Microwave Symposium Digest*, Philadelphia, June 8-13, 2003, pp. 321-324.

33. R. Islam, F. Elek and G. V. Eleftheriades, "A Coupled-Line Metamaterial Coupler Having Co-Directional Phase but Contra-Directional Power Flow," *Electronics Letters*, **40**, 5, March 04, 2004.

34. A. Alu and N. Engheta, "Anomalous Mode Coupling in Guided-Wave Structures Containing Metamaterials with Negative Permittivity and Permeability," *Proceedings of the 2002 IEEE Conference on Nanotechnology (IEEE-Nano'2002)*, August 26-28, 2002, Washington DC, pp. 233-234.

35. C. Caloz, A. Sanada, and T. Itoh, "A Novel Composite Right-/Left-Handed Coupled-Line Directional Coupler with Arbitrary Coupling Level and Broad Bandwidth," *IEEE Transactions on Microwave Theory and Techniques*, **MTT-52**, March 2004, pp. 980-992.

36. A. Grbic and G. V. Eleftheriades, "Leaky CPW-Based Slot Antenna Arrays for Millimeter-Wave Applications," *IEEE Transactions on Antennas and Propagation*, **AP-50**, 11, November 2002, pp. 1494-1504.

37. J. B. Pendry, "Negative Refraction," *Contemporary Physics*, **45**, 3, May-June 2004, pp. 191-202.

38. D. R. Smith, J. B. **Pendry**, and M. C. K. Wiltshire, "**Metamaterials and Negative Refractive Index,"** *Science*, 305, 6 August 2004, pp. 788-792.

IUCAF Annual Report for 2004

1. Introduction

The Scientific Committee on Frequency Allocations for Radio Astronomy and Space Science, IUCAF, was formed in 1960 by URSI, IAU, and COSPAR. Its brief is to study and coordinate the requirements of radio frequency allocations for passive (i.e., non-emitting) radio sciences, such as radio astronomy, space research and remote sensing, in order to make these requirements known to the national and international bodies that allocate frequencies. IUCAF operates as a standing inter-disciplinary committee under the auspices of ICSU, the International Council for Science.

2. Membership

At the end of 2004 the composition of membership for IUCAF was:

URSI	Y. Gupta	India
	A. Tzioumis	Australia
	W. van Driel (Chair)	France
	G. Wannberg	Sweden
IAU	H. Chung	Korea
	R.J. Cohen	United Kingdom
	D.T. Emerson	USA
	M. Ohishi	Japan
	K.F. Tapping	Canada
COSPAR	S. Gulkis	USA
	J. Romney	USA
at large:	W.A. Baan	The Netherlands
	K. Ruf	Germany

IUCAF also has a group of Correspondents, in order to improve its global geographic representation and for issues on spectrum regulation concerning astronomical observations in the optical and infrared domains.

3. International Meetings

During the period of January to December 2004, its Members and Correspondents represented IUCAF in the following international meetings:

March:	ITU-R Working Party 7C (Earth exploration-satellite systems and meteorological elements) in Geneva, Switzerland
	ITU-R Working Party 7D(radioastronomy) in Geneva, Switzerland
April:	ITU-R Task Group 1/9 (Compatibility between passive and active services) in Geneva, Switzerland
May:	"Exploring the Cosmic Frontier" Conference in Berlin, Germany
June:	ITU-R Task Group 1/8 (Compatibility between ultra-wideband devices (UWB) and radiocommunication services) in Boston, USA
July:	RFI2004 Workshop on Mitigation of Radio Frequency Interference in Radio Astronomy in Penticton, Canada
	17th Wroclaw Symposium on Electromagnetic Compatibility in Wroclaw, Poland
	34th COSPAR Scientific Assembly in Paris, France
September:	Space Frequency Coordination Group meeting SFCG-24 in Perros-Guirec, France
October:	ESF/RadioNet Workshop on Active protection of passive services in Cagliari, Italy
	ITU-R Working Party 7C (Earth exploration-satellite systems and meteorological elements) in Geneva, Switzerland
	ITU-R Working Party 7D (radio astronomy) in Geneva, Switzerland
November:	ITU-R Task Group 1/8 (Compatibility between ultra-wideband devices (UWB) and radiocommunication services) in Geneva, Switzerland

Additionally, many IUCAF members and Correspondents participated in numerous national or regional meetings (including CORF, CRAF, RAFCAP, the FCC etc.), dealing with spectrum management issues.

3.1 IUCAF Business Meetings

During the year 2004 IUCAF had a face-to-face meeting as a committee before each of the ITU meetings of Working Parties and Task Groups of relevance to IUCAF, with the purpose of discussing important issues on the agenda of the respective meetings in preparation for the public sessions. During these ITU sessions, typically lasting a week to 10 days, a number of ad-hoc meetings of IUCAF are held to discuss further the IUCAF strategy. Other IUCAF business such as action plans for future workshops and summer schools or initiatives, and future contributions to international spectrum meetings were also discussed at these meetings.

Although such face-to-face meetings at the ITU venues and elsewhere have been convenient and effective, throughout the year much IUCAF business is undertaken via e-mail communications between the members and correspondents.

4. Contact with the Sponsoring Unions and ICSU

IUCAF keeps regular contact with the supporting Unions and with ICSU. The Unions play a strong supporting role for IUCAF and the membership is greatly encouraged by their support.

IUCAF members actively participated in national URSI meetings, in IAU Colloquia and Symposia and in the 2004 COSPAR Scientific Assembly.

IUCAF participates actively in the work of the URSI Scientific Commission on Telecommunication (SCT), whose first priority is to communicate results of research by scientists active in URSI for use by "user" organisations such as the ITU, needing to apply such information.

ICSU completed its first ever review of IUCAF in May, within the framework of its Priority Area Assessment on Scientific Data and Information. In its written input document for this review, IUCAF stressed its aim to fulfill its brief and to operate as a truly inter-disciplinary committee within ICSU. COSPAR, the IAU and URSI also submitted their comments on the value of IUCAF to ICSU.

In its review, ICSU recommends that "ICSU should encourage the three main partners of IUCAF - IAU, URSI and COSPAR, to organize a joint meeting to define specific procedures and actions that will ensure that IUCAF becomes a truly interdisciplinary committee that has the necessary expertise to coordinate the efforts of *all* the passive radio sciences in frequency management matters."

In 2004, IUCAF has been working actively towards strengthening its links with other passive radio science communities and defining a concerted strategy in common spectrum management issues, as detailed in Section 5.

5. Protecting the Passive Radio Science Services

At the International Telecommunication Union (ITU), the work in the various ITU-R Working Parties and Task Groups of interest to IUCAF was focused largely on the preparations for WRC-07, the World Radiocommunication Conference to be held in 2007.

Of particular concern to IUCAF in ITU-R Working Parties 7C and 7D, specializing in Earth exploration and in radio astronomy, respectively, is the protection of the 1400-1427 MHz passive band from unwanted emissions from fixed-satellite service feeder links in the nearby bands 1 390-1 392 MHz and 1 430-1 432 MHz. This frequency band contains the heavily observed interstellar 21-cm neutral hydrogen line, and is used by the Earth exploration satellite service to measure soil moisture and ocean salinity.

ITU-R Task Group 1/8 deals with the introduction of unregistered low power ultra-wide bandwidth (UWB) devices (including vehicular anti-collision radars) transmitting across large parts of the radio spectrum, into bands that are already allocated to a variety of other services and in some of which "all emissions are prohibited" according to the ITU Radio Regulations. Preliminary studies show that the operation of such devices would be very harmful to the passive radio services.

ITU-R Task Group 1/9 deals with the protection of passive services, specifically the radio astronomy service and the Earth exploration-satellite (passive) service, from unwanted emissions of active services in adjacent and nearby bands. Its goal is to review and update, if appropriate, the tables of threshold levels used for consultation between the passive radio services and active services that appear in Recommendation ITU-R SM.1633, which was adopted at WRC-03 and in whose redaction IUCAF played an active role. TG1/9 is also charged with providing proposals on how to solve two related agenda items of WRC-07.

Within the Space Frequency Coordination Group, IUCAF worked towards a Resolution on the sharing of the band 94-94.1 GHz between the radio astronomy service and Space agencies operating powerful satellite-borne cloud profile radars, which can potentially damage, and even destroy, receivers in radio telescopes observing in the direction of such radars. The mutual planning procedure defined Resolution SFCG 24-2 is aimed at preventing this.

At the Workshop on "Active protection of Passive Services: towards a concerted strategy", representatives of radio astronomy and remote sensing communities (space research, meteorology, aeronomy and geodesy) recognized their common interests, as all depend on the frequency bands allocated uniquely to passive radio services to be free of interference. Action items were defined to work towards closer synergy, in which IUCAF will play a key role, as per its brief – an example is a concerted approach towards an agenda item on the allocation of frequencies in the range 275-3000 GHz for WRC-10

6. IUCAF-sponsored Meetings

IUCAF sponsored the RFI2004 Workshop on Mitigation of Radio Frequency Interference in Radio Astronomy, which was held in Penticton, Canada, on 16-18 July; the first such IUCAF-sponsored Workshop was held in Bonn, Germany, in 2001.

The emphasis of the Workshop was on technical aspects of radio interference mitigation, in particular concepts applicable to the Square Kilometre Array (SKA), a future giant radio telescope towards whose design and construction a large community of radio astronomers is working. The number of participants (80),the quality and diversity of the presentations and the methods described showed the

importance that the astronomical community attributes to making radio telescopes more robust towards man-made interference.

7. Publications and Reports

IUCAF has a permanent web address, http://www.iucaf.org , where the latest updates on the organization's activities are made available. The Proceedings of IUCAF's first Summer School in Radio Astronomy and Spectrum Management was made available on the IUCAF website. All contributions to the IUCAF-sponsored RFI2004 Workshop on Mitigation of Radio Frequency Interference in Radio Astronomy were also made available on this website.

8. Conclusion

IUCAF interests and activities range from preserving what has been achieved through regulatory measures or mitigation techniques, to looking very far into the future of high frequency use and giant radio telescope use. Current priorities, which will certainly keep us busy through the next years, include band-by-band studies for cases where allocations are made to satellite down-links close in frequency to the radio astronomy bands, to satellite up-links and terrestrial radio services in the vicinity of bands allocated to the Earth Exploration Satellite Service(passive), the possible detrimental effects of ultra-wide band transmissions on all passive services, and studies on the operational conditions that will allow the successful operation of future giant radio telescopes.

IUCAF is thankful for the moral and financial support that has been given for these continuing efforts by ICSU, URSI, the IAU, and COSPAR during the recent years. IUCAF also recognizes the support given by radio astronomy observatories, universities and national funding agencies to individual members in order to participate in the work of IUCAF.

Wim van Driel, IUCAF Chair
Meudon, France
March 29th 2004
IUCAF website: http://www.iucaf.org
IUCAF contact: iucafchair@iucaf.org

Radio-Frequency Radiation Safety and Health

James C. Lin

Mobile Phone Use and Benign Tumors of the Auditory Nerve

The potential of elevated cancer risks from exposure to wireless radiation has been a major source of concern for many mobile-phone users. In common usage, about 50% of the radiated radio-frequency (RF) energy is absorbed by tissues on the side of the head close to the handset. Cancer in the central nervous system thus has snagged the attention of the general public, scientific investigators, and the mobile-phone industry, almost since the introduction of the popular invention into contemporary society.

In a recently reported study, an increased risk of acoustic neuroma was found among persons in Sweden with 10 or more years of mobile-phone use [1]. There was no association with use less than 10 years, nor for other measures of use such as total hours of use or total number of calls made.

Acoustic neuromas are slow-growing benign tumors of the auditory nervous system. Left unchecked, continued growth of the tumor can be life threatening. According to the Acoustic Neuroma Association [2], asymptomatic acoustic neuromas have been found perhaps to be in as few as 0.01% of the general population, and about one person in 100,000 is diagnosed with symptomatic acoustic neuromas. The worldwide incidence rates of acoustic neuroma vary from one to 20 cases per million population per year [3]. Most acoustic neuromas are diagnosed in patients between the ages of 30 and 60, and it is rarely diagnosed in persons less than 30 years of age. Acoustic neuromas appear to occur spontaneously from causes that are mostly unknown.

Acoustic neuromas are benign tissue growths that appear on the eighth cranial nerve, or auditory nerve, leading from the inner ear to the brain. This nerve pathway goes through a bony internal auditory canal that is approximately 2 cm long, and it is here that acoustic neuromas originate from the sheath surrounding the eighth nerve. As it grows, it displaces normal brain tissues and it pushes against the brain. But it doesn't spread into the brain: brain tissues are not invaded by the tumor. The slowly enlarging tumor protrudes from the internal auditory canal into an area behind the temporal bone, on the side of the head. Vital functions to sustain life can be threatened when a large tumor causes severe pressure on the brainstem and cerebellum part of the brain. Many sensory and motor nerves are located in the lateral and medial regions of the brainstem.

Signs and symptoms pointing to an acoustic neuroma include hearing loss in one ear, often accompanied by ear ringing or tinnitus in the affected ear. These early signs and symptoms are sometimes mistaken for normal changes associated with aging. Moreover, acoustic neuromas usually grow slowly over a period of years. Thus, they are easily overlooked, and diagnosis is often delayed. Since the pathway for the nerve fibers sending balance signals to the brain from the inner ear lie adjacent to the auditory nerve fibers, and they pass through the same bony internal auditory canal, dizziness and loss of balance may occur as the mass of the acoustic neuroma enlarges.

Authors of the Lönn, et al. study [1] employed a population-based, case-controlled epidemiological approach. The study ascertained an elevated risk of acoustic neuroma among persons in Sweden with 10 or more years of mobile-phone use, with an odds ratio (OR) of 1.9 (95% confidence interval, 0.9 to 4.1). There was no association with use of less than 10 years. The risk estimates did not increase with the amount of use estimated as either cumulative number of hours or cumulative number of calls. When the data analysis was restricted to acoustic neuromas on the same side of the head where mobile phones were normally used – ipsilateral mobile-phone use – the odds ratio was 3.9 (1.6 to 9.5) for acoustic neuroma. The corresponding result was 0.8 (0.2 to 2.9) for contralateral use.

The study included all persons between 20 and 69 years of age who were residents of three geographical areas covered by the regional Cancer Registries in Stockholm, Goteborg, and Lund, which have a population totaling 3.1 million. The cases consisted of all subjects diagnosed with

James C. Lin is with the University of Illinois at Chicago
851 South Morgan Street (M/C 154),
Chicago, Illinois 60607-7053 USA;
Tel: +1 (312) 413-1052 (direct); +1 (312) 996-3423 (main office); Fax: +1 (312) 996-6465;
E-mail: lin@uic.edu

Portions of this contribution also appeared in the *IEEE Antennas and Propagation Magazine*, **47**, 1, February 2005, pp. 183-185.

acoustic neuroma from September, 1999, to August 2002. A total of 160 eligible acoustic neuroma cases was identified; controls ($n = 838$) were randomly selected from the study base stratified on age in five-year groups, sex, and residential area covered by the regional cancer registry areas. Participation rates were 93% ($n = 148$) for cases and 72% for controls ($n = 604$).

Since RF exposure from a mobile phone is directly related to the output power used by the phone to communicate with the base station, separate analyses showed that for subjects using mobile phones mainly in rural areas, the risk estimate was 0.7 (0.3 to 1.6), mainly in urban areas 1.4 (0.9 to 2.3), and in both urban and rural areas 0.7 (0.4 to 1.2). It is commonly recognized that the output power from mobile phones varies with the geographic location of the user, and output powers have been shown to be higher in rural areas compared to urban areas.

In the reported study, an increased risk was found only for long-term use (> 10 years), and not for other measures of use, such as cumulative hours of use or cumulative number of calls. Note that most subjects, if not all, who had used analog phones ten years ago likely have switched to digital phones since. Clearly, the results are based on mixed use of analog and digital phones, and do not indicate the relative risk of using an analog or digital phone alone. Moreover, acoustic neuromas grow slowly over a period of years, and the average time to diagnosis has been estimated to be more than five years. Given the recent introduction and popularization of digital phones – this study used five years as the time since first regular use – these results provide only limited guidance with regard to the risk of short-term use of mobile phones and exposure to wireless radiation.

It should be noted that the Lönn, et al. study [1] was not the only study of its kind, nor the first. But it does stand apart by the relatively large number of cases. An earlier report by Christensen et al. [4] from Denmark used the same study protocol. The results from the two studies are very similar for short-term mobile-phone use. Christensen et al. reported an overall estimated relative risk for acoustic neuroma of 0.90 (0.51 to 1.57). They found that use of a mobile phone for 10 years or more did not increase the risk of acoustic neuroma over that of short-term users. Furthermore, tumors did not occur more frequently on the side of the head on which the mobile phone was typically used. However, the Danish study had very few users with at least 10 years since first exposure. Thus, the study did not have sufficient statistical power to study effects of long-term mobile-phone use.

Among the general population, there appears to be a slight unevenness in the distribution of acoustic neuromas occurring on the right or left side. Thus, the finding of an elevated risk associated with long-term, ipsilateral mobile-phone use is noteworthy. It is the side of the head where the head receives the highest quantity of absorbed RF energy. In this case, the odds ratio for acoustic neuroma was 3.9 (1.6 to 9.5), in contrast to a corresponding odds ratio for the contralateral side of 0.8 (0.2 to 2.9): indicating a strong correlation between the laterality of phone use and laterality of tumors.

Laterality was investigated in several prior publications [5-8]. In addition to the limitations of small numbers of cases and short latencies since first use of the mobile phones, there were identifiable flaws in the assumptions made and methodologies applied in these studies. Consequently, the robustness of some of these results had been challenged, especially for long-term users.

As always, there may be potential confounding factors which merit special attention: are alternative causes likely for the positive findings? Early signs or symptoms that are indicative of an acoustic neuroma include ear ringing or tinnitus, and hearing loss in the affected ear. One possibility is that the symptom would solicit greater attention if it happens on the side of the head on which the mobile phone was most often used. Also, assessment of true exposure is an obvious issue, since mobile-phone use is self-reported, and recall bias could be a potential problem in all such studies.

Nevertheless, it should be noted that the Lönn, et al. study [1] was characterized by fastidious execution, through analysis, and attention to methodological details. Aside from the factors listed above, the analyses were adjusted for age, sex, residential area, educational level, and hands-free operation. Moreover, adjustments for hearing loss or tinnitus did not change any of the risk estimates.

References

1. S. Lönn, A. Ahlbom, P. Hall, and M. Feychting, "Mobile Phone Use and the Risk of Acoustic Neuroma," *Epidemiology*, 15, 2004, pp. 653-659.
2. http://www.anausa.org/an-faq.htm.
3. M. F. Howitz, C. Johansen, M. Tos, S. Charabi, and J. H. Olsen, "Incidence of Vestibular Schwannoma in Denmark, 1977-1995," *Am. J. Otol*., 21, 2000, pp. 690-694.
4. H. C. Christensen, J. Schuz, M. Kosteljanetz, H. S. Poulsen, J. Thomsen, and C. Johansen, "Cellular Telephone Use and Risk of Acoustic Neuroma," *Am. J. Epidemiol*., 159, 2004, pp. 277-283.
5. P. D. Inskip, R. E. Tarone, E. E. Hatch, T. C. Wilcosky, W. R. Shapiro, R. G. Selker, H. A. Fine, P. M. Black, J. S. Loeffler, and M. S. Linet, "Cellular Telephone Use and Brain Tumors, *New England Journal of Medicine*, 344, 2001, pp. 79-86.
6. L. Hardell, K. H. Mild, and M. Carlberg, "Case-Control Study on the Use of Cellular and Cordless Phones and the Risk for Malignant Brain Tumours," *Int. J. Radiat. Biol*., 78, 2002, pp. 931-936.
7. L. Hardell, A. Hallquist, K. H. Mild, M. Carlberg, A. Pahlson, and A. Lilja, "Cellular and Cordless Telephones and the Risk for Brain Tumours," *Eur. J. Cancer Prev*., 11, 2002, pp. 377-386.
8. J. E. Muscat, M. G. Malkin, R. E. Shore, S. Thompson, A. I. Neugut, S. D. Stellman, and J. Bruce, "Handheld Cellular Telephones and Risk of Acoustic Neuroma." *Neurology*, 58, 2002, pp. 1304-1306.

Conferences

CONFERENCE ANNOUNCEMENTS

CLIMDIFF 2005

Cleveland, Ohio, USA, 26 - 27 September 2005

General

A two-day specialist symposium is planned in the tradition of previous Climpara meetings (Moscow 1994, Oslo 1996, Ottawa 1998 and Budapest 2001) and the Climdiff meeting in Fortaleza, 2003. Once again, the scope of the meeting includes both Climatic and Diffraction effects (see below). This URSI Commission F meeting will immediately precede parallel meetings of ITU-R Working Parties: WP 3J (Propagation fundamentals), 3K (Point-to-area propagation), 3L (Ionospheric propagation) and 3M (Point-to-point and Earth-space propagation), in the same venue 28 September to 7 October 2005. Participants in the Climdiff symposium are encouraged to attend the ITU-R meetings as members of their national delegation, and vice versa.

Topics

The "Clim" part (on the *use of climatic parameters in the prediction of radiowave propagation*) covers (i) clear air modelling and climatic parameters needed, data available, measurements still needed and instruments, and (ii) precipitation modelling and climatic parameters needed, measurements still needed and instruments. In both cases, mapping processes are very relevant.

The "Diff" part addresses any *aspects of diffraction for the prediction of radiowave propagation* and includes (i) hill tops and hairy hill tops, (ii) propagation over, between and through buildings and vegetation (iii) ray tracing, parabolic equation and integral equation methods, and (iv) derivation and application of high-resolution topographic maps, land-use maps and 3D urban maps. It could also include coverage modelling and results, vegetation effects, new techniques and data sources, and indoor, and short-range propagation.

Abstracts

Abstracts for contributions should be emailed attachments to be received **BEFORE 17 JUNE 2005** at the address below. Abstracts should be one sheet of A4 paper or less, but give sufficient information to enable an objective assessment to be made by referees. As well as the title of the paper, submissions should indicate the appropriate topic, as listed above, and include the name(s) of author(s), organisation(s), email address(es), phone and fax number(s) and full postal address(es). The meeting and all papers will be in English.

Deadlines

Notification of acceptance of paper: **13 July 2005**
Full paper required for publication: **5 September 2005**

Contact

Mrs Carol Wilson
CSIRO ICT Centre,
PO Box 76 Epping NSW 1710 Australia
Fax: +61 2 9372 4490
Email: climdiff@csiro.au
http://spectrum.nasa.gov/climdiff/

MRRS 2005
International Workshop on Microwaves, Radar and Remote Sensing

Kiev, Ukraine, 19 - 21 September 2005

Objectives

The Workshop is planned to be a forum of ideas exchange and results discussion in the field of electromagnetic theory and applications; radar technology, systems and signal processing; remote sensing methods and data processing. Both passive and active methods and systems of all frequency bands are welcome. The only specific demand of MRRS-2005 suggests that aerospace application of the results or their influence to aviation safety or security is desired to be indicated in the submissions. Aerospace systems always were the application field of the newest achievements of microwave and electronic theory, methods and technologies. That is why this demand does not limit the range of conference topics essentially.

Suggested topics

- Math modeling and simulation
- Electromagnetic fields and guided waves
- Antenna theory and techniques
- Scattering and RCS
- Polarimetric and Doppler techniques
- Signal processing
- Primary radar systems
- Secondary radar systems
- Passive radar systems
- Millimeter and sub-millimeter wave systems
- Ultra-wideband radar
- Target classification and identification
- Airborne and spaceborne surveillance systems
- Remote sensing of land
- Weather radar
- Meteorological phenomena identification
- Remote sensing of atmosphere
- Biomedical applications
- Data and image processing and representation
- Origin of radar and remote sensing
- Education in microwave, radar and remote sensing

Deadlines

Deadline for Abstracts: May 27, 2005
Notification of Acceptance: June10, 2005
Submission of final paper: June 30, 2005
Early registration deadline: June 30, 2005

Authors are invited to submit abstracts, including the author's full contact information by E-mail to yanovsky@nau.edu.ua

Contact

For further information about this Workshop as well as detailed instruction for submitting the final paper, please visit our web page at http://congress.org.ua or contact us by e-mail yanovsky@i.com.ua

URSI CONFERENCE CALENDAR

An up-to-date version of this Conference Calendar, with links to various conference web sites can be found at www.ursi.org/ Calendar of supported meetings

April 2005

Commission F Specialist Meeting on Microwave Remote Sensing of the Earth, Ice, and Atmosphere
Ispra, Italy, 20-21 April 2005
cf. Announcement in RSB December 2004, pp. 116-117
Contact : Ms. Marta Garotta, DG Joint Research Centre, I-21020 Ispra (VA), Italy, Tel. +39 0332 785339, Fax. +39 0332 785469, e-mail : Marta.Garotta@cec.eu.int, http://ursi-f-2005.jrc.it/

May 2005

IES 2005 - 11th International Ionospheric Effects Symposium
Alexandria, Virginia, USA, 3-5 May 2005
Contact : JMG Associates Ltd., IES2005 Symposium Managers, 8310 Lilac Lane, Alexandria, VA 22308, USA, Fax: +1-703-360-3954, jm_good@cox.net, Web site : http://www.ies2005.com

4th European Workshop on Conformal Antennas
Stockholm, Sweden, 23-24 May 2005
Contact : Dr. Patrik Persson, Royal Institute of Technology, Alfvén Laboratory, Division of Electromagnetic Theory, SE-100 44 Stockholm, Sweden, E-mail : patrik.persson@alfvenlab.kth.se , http://www.ewca-home.org/

June 2005

IWWCUCA - First International Workshop on Wireless Communications in Underground and Confined Areas
Val d'Or, Quebec, Canada, 6-7 June 2005
Contact : Laboratoire de recherche Télébec Mobilité en communications souterraines, 450, 3e Avenue, Local 103, Val-d'Or, Québec J9P 1S2, Canada, Phone: (819) 874-7400, ext. 221, Fax: (819) 874-7166, E-mail: lrcs@uqat.ca, http://lrcs.uqat.ca/

ETTC'05 - European Test and Telemetry Conference
Toulouse, France, 7-9 June 2005
Contact : SEE, Société de l'Electricité, de l'Electronique et des Technologies de l'Information et de la Communication, 17, rue Hamelin, F-75783 Paris Cedex 16, FRANCE, Tel: +33 1 56 90 37 05, Fax: +33 1 56 90 37 08, e-mail : ettc2005@see.asso.fr, http://www.ettc2005.org/

ANTEM 2005
Saint Malo, France, 15-17 June 2005
Contact : Antem 2005 - IETR Université de Rennes 1, campus Beaulieu, Bât. 11D 35042 Rennes Cedex, France, Tel. +33 2 23 23 62 17 and +33 2 23 23 69 56, Fax +33 2 23 23 69 69, http://antem2005.ietr.org/home/index.htm

EMC2005 - VIth International Symposium on Electromagnetic Compatibility and Electromagnetic Ecology
St. Petersburg, Russia, 21-24 June 2005
Contact : Dr. Pavel Asovich, Prof. Popov Str. 5, St. Petersburg 197376, Russia, Fax +7 812 234-4840, E-mail: discone@vilan.spb.ru , http://www.eltech.ru/emc2005

IRI Workshop 2005 - New Satellite and ground data for IRI, and comparison with regional models
Roquetes, Spain, 27 June - 1 July 2005
Contact : IRI 2005 WORKSHOP "New satellite and ground data for IRI, and comparison with regional models", Observatori de l'Ebre, Roquetes, Spain, secretaria@obsebre.esn ,http://www.obsebre.es/w3/wsiri/

July 2005

CEFBIOS 2005 - Coherence and Electromagnetic Fields in Biological Systems
Prague, Czech Republic, 1-4 July 2005
cf. announcement in RSB September 2004, p. 118
Contact : Dr. Jiri Pokorny, Inst. of Radioengineering and Electronics, Academy of Sciences of the Czech Republic, Chaberska 57, CZ-182 51 PRAGUE 8, Czech Republic, phone : +420 266 773 432, fax +420 284 680 222, pokorny@ure.cas.cz , http://www.ure.cas.cz/events/cefbios2005/

August 2005

ISAP'05 - International Symposium on Antennas and Propagation
Seoul, Korea, 3-5 August 2005
cf. announcement in RSB December 2004, p. 117
Contact : Prof. H.J. Eom, Department of Electrical Engineering and Computer Science, Korea Advanced Institute of Science and Technology (KAIST), 373-1, Guseong-dong, Yuseong-gu Daejeon, 305-701 Korea, Tel. +82 42-869 3436, Fax : +82 42-869 8036, E-mail : hjeom@ee.kaist.ac.kr, http://www/isap05.org

MAPE 2005 - International Symposium on Microwave, Antenna, Propagation, and EMC Technologies for Wireless Communications
Beijing, China, 8-12 August 2005
cf. announcement in RSB September 2004, p. 118
Contact : Mr. Mengqi Zhou, Secretary of IEEE Beijing Section, P.O. Box 165, Beijing 100036, China, E-mail : mqzhou@public.bta.net.cn , http://www.cie-china.org/mape2005/temp/main.html

ISMOT 2005 - 10th International Symposium on Microwave and Optical Technology
Fukuoka, Japan, 22-25 August 2005
Contact : Prof. Kiyotoshi YASUMOTO, Dpt. Comp. Sci. & Comm. Eng., Kyushu University, 6-10-1 Hakozaki, Higashi-ku, Fukuoka 812-8581, Japan, Phone: +81-92-642-4045, Fax: +81-92-632-5204, E-mail: yasumoto@csce.kyushu-u.ac.jp , http://ismot2005.fit.ac.jp

September 2005

ICEAA'05 - International Conference on Electromagnetics in Advanced Applications
Torino, Italy, 12-16 September 2005
Contact : COREP- ICEAA 05, Politecnico di Torino, C.so Duca degli Abruzzi, 24, I-10129 Torino, Italy, Tel.: +39 011 564 5103, Fax: +39 011 564 5199, info@iceaa.polito.it, http://www.iceaa.polito.it

CAOL 2005 - Int. Conference on Advanced Optoelectronics and Lasers
Yalta, Crimea, Ukraine, 12-17 September 2005
Contact : Prof. Dr.Sc. Igor A. Sukhoivanov, CAOL Organizer, e-mail i.sukhoivanov@ieee.org , http://caol.kture.kharkov.ua/eng/caol/caol_eng.html

Microwave, Radar and Remote Sensing
Kiev, Ukraine, 19-21 September 2005
cf. announcement in RSB March 2005, p. 72
Contact : Microwave, Radar and Remote Sensing, c/o Dr. Felix Yanovsky, NAU, Prospect Komarova 1, Kiev 03058, Ukraine, Fax +380 44-408 2278, E-mail: yanovsky@i.com.ua , http://congress.nau.edu.ua/mrrs/

ClimDiff 2005
Cleveland, Ohio, USA, 26-27 September 2005
cf. announcement in RSB March 2005, p. 71
Contact : Mrs Carol Wilson, CSIRO ICT Centre, PO Box 76, Epping NSW 1710, Australia, Fax: +61 2 9372 4490, Email: climdiff@csiro.au, http://spectrum.nasa.gov/climdiff

October 2005

XXVIIIth URSI General Assembly
New Delhi, India, 23-29 October 2005
Contact : URSI Secretariat, c/o INTEC, Sint-Pietersnieuwstraat 41, B-9000 Ghent, Belgium, Tel. : +32 9 264 3320, Fax : +32 9 264 4288, E-mail : info@ursi.org http://www.ursiga2005.org

May 2006

EUSAR 2006 - 6th European Conference on Synthetic Aperture Radar
Dresden, Germany, 16-18 May 2006
Contact : VDE CONFERENCE SERVICES, Stresemann-allee 15, D-60596 Frankfurt am Main, Germany, Tel. : +49 69-63 08-275 / 229, Fax: +49 69-96 31 52 13, vde-conferences@vde.com , http://www.eusar.de

If you wish to announce your meeting in this meeting in this calendar, you will gind more information at www.ursi.org URSI cannot held responsible for any errors contained in this list of meetings

News from the URSI Community

NEWS FROM THE MEMBER COMMITTEES

FRANCE
Médaille du CNFRS

Le 24 février lors des Journées scientifiques du Comité National Français de Radioélectricité Scientifique, la Médaille du CNFRS a été remise à Pierre Degauque par Alain Orszag. Cette médaille est « destinée à honorer des personnes qui ont œuvré pour le renom de la Science en Radioélectricité et/ou participé d'une manière très significative à la vie et au renom du CNFRS/URSI ». Le CNFRS souhaite ainsi souligner l'importance de la contribution de Pierre Degauque aux méthodes électromagnétiques en relation avec la prospection géophysique et la compatibilité électromagnétique.

Pierre Degauque, né le 19 septembre 1946, après avoir obtenu un diplôme d'Ingénieur de l'Institut Supérieur d'Électronique du Nord (maintenant de Nanotechnologies), rejoint en 1967 l'Université de Lille, plus précisément le Laboratoire de Radio Propagation et Électronique, Unité CNRS, dirigée par le Professeur Robert Gabillard. Il y soutient une thèse de Docteur Ingénieur, puis de Doctorat es Sciences en 1974. Nommé Assistant à l'IUT Génie Électrique en 1968, il devient professeur en 1976. Directeur adjoint de l'Unité CNRS en 1986, il en assure ensuite la direction de 1993 à 2004. Au 1er janvier 2004 cette Unité, baptisée TELICE, pour Télécommunications, Interférences et Compatibilité Électromagnétique, intègre l'UMR IEMN (Institut d'Électronique, Microélectronique et Nanotechnologies) en tant que Groupe de recherches.

Après une thèse sur la caractérisation et le rayonnement d'antennes enterrées ou immergées, la propagation dans le guide d'ondes terre-ionosphère, il poursuit ses travaux en étudiant les méthodes électromagnétiques en relation avec la prospection géophysique. Le domaine couvert s'étend de la mise en évidence de gisement d'hydrocarbures, à la détection de veines dans des blocs de marbre avant leur extraction ou leur découpe. Il s'intéresse ensuite à la Compatibilité Électromagnétique et plus particulièrement au couplage entre l'onde électromagnétique générée par la foudre ou une explosion nucléaire et les structures filaires.

Dans le domaine de la compatibilité électromagnétique, il a joué un véritable rôle de catalyseur auprès de la communauté scientifique française puisque, après de premiers séminaires organisés dès 1976 sous l'égide du CNET, il organise à Lille, deux ans plus tard, les premières « Journées Scientifiques » sur la « Compatibilité Électromagnétique » et développe en France la nouvelle Commission E : Bruit et Brouillage Électromagnétique de l'Union Radio Scientifique International (URSI) et devient représentant français de cette Commission, puis Président du Comité français de l'URSI. En 1996, il organise à Lille l'Assemblée Générale de l'URSI. Enfin en 2002, il devient Président au niveau international de la Commission E de l'URSI.

POLAND

XI National Polish Symposium of Radio Science - URSI 2005

On April 7-8, 2005, a scientific event with more than a thirty-year-old tradition took place in Poznañ, Poland, at the Poznan Center of Science, Wieniawskiego street 15/17. The XI National Symposium of Radio Science URSI 2005 was especially significant to researchers, professionals, and enterprises working in the area of radio science.

The XI URSI 2005 symposium was organized by the Institute of Electronics and Telecommunications, Poznan University of Technology, under the joint auspices of the National Committee of the International Union of Radio Science (URSI) and the Polish Academy of Sciences. The Chair of Honor became Prof. Jerzy Dembczyñski, the Rector Magnificus of Poznan University of Technology. The main sponsors of the symposium were the following enterprises: Lucent Technologies Poland, Idea Centertel, and Alma S.A.

The Program Committee consisted of Stefan Hahn (Chair), Daniel J. Bem, Hanna Bogucka, Andrzej Dobrogowski, Marek Domanski, Stanislaw Gorgolewski, Jolanta Karpowicz, Tomasz Kosilo, Bohdan Mroziewicz, Jozef Pawelec, Wiktor Pawlowski, Marian Piekarski, Karol Radecki, Iwona Stanislawska, Andrzej Turski, Andrzej Wernik, and Krzysztof Wesolowski. The Organizing Committee consisted of Andrzej Dobrogowski (Chair), Hanna Bogucka (Vice Chair), Adrian Langowski, Anna Pawlaczyk, and Barbara Wagrowska

International sessions in English were organized within the conference, with the participation of guests from Germany, Norway, Belgium, Austria, France, United Kingdom, Italy, Spain, Greece, and Turkey. The following topics of interest were the most significant problems considered in the papers:

- Mobile Communications,
- Electromagnetic Metrology,
- Satellite Systems,
- Electromagnetic Fields and Waves,
- Radio Astronomy,
- Radio Wave Propagation,
- Signals and Systems,
- Electromagnetic Noise and Interference,
- Electromagnetic Field in Biology and Medicine.

During the first day of the conference, Prof. Kristian Schlegel, the President of the International Union of Radio Science, gave an address on "Modern Radio Science." The following plenary papers were delivered in English:

- Prof. Hubert Trzaska, "Electromagnetic Environment Protection"
- Prof. Lajos Hanzo, "The Myth and Realities of Interference-Immune Spreading Codes: Time- and Frequency-Domain Spreading Aided MC-DS-CDMA Transceivers"
- Prof. Andrzej Dobrogowski, "Impact of Relativistic Effects on Synchronization of Clocks"
- Prof. Hermann Rohling, "OFDM – A Flexible and Adaptive Air Interface for a 4G Communication System."

In addition, three international sessions were held within the framework of the URSI Symposium, and under the auspices of the European Network of Excellence NEWCOM (Network of Excellence in Wireless Communications). The purpose of the NEWCOM project, realized within the IST 6th Framework Programme of the European Union, is to establish a European network of cooperation, uniting a substantial number of leading research centers and groups. The thematic area of the NEWCOM sessions was focused on advanced technologies in wireless communications and flexible radio.

There were 146 participants, including guests from Poland, Germany, Norway, Belgium, Austria, France, Great Britain, Italy, Spain, Greece, and Turkey. Researchers from Poland and from abroad delivered 85 papers. They also had the possibility to exchange experience and ideas during 18 thematic sessions as well, and outside the conference rooms during informal and long-lasting heated discussions. Renowned scientists from top-rated Polish research centers and groups participated in the symposium, including the following, among others: Jagiellonian University (Krakow), Warsaw University of Technology (Warsaw), Gdansk University of Technology (Gdansk), Wroclaw University of Technology (Wroclaw), Silesian University of Technology (Gliwice), AGH University of Science and Technology (Krakow), National Institute of Telecommunications (Warsaw), Military University of Technology (Warsaw), Maritime Academy (Gdynia). Representatives of the Polish digital cellular telephony operators were also present at the conference.

The organizers of the XI Symposium of Radio Science URSI 2005 wish to thank all the participants for taking part in the conference, for interesting papers, engaging discussions, and a warm, friendly atmosphere. The organizers hereby wish to invite all potential participants to the next edition of this URSI symposium.

Hanna Bogucka
Vice Chair of the Organizing Committee
Poznan University of Technology
Institute of Electronics and Telecommunications
ul. Piotrowo 3A, 60-965 Poznan, Poland
Tel: 61-6652614; Fax: 61-6652572
E-mail: hbogucka@ET.PUT.Poznan.PL

URSI Publications

Modern Radio Science 1999

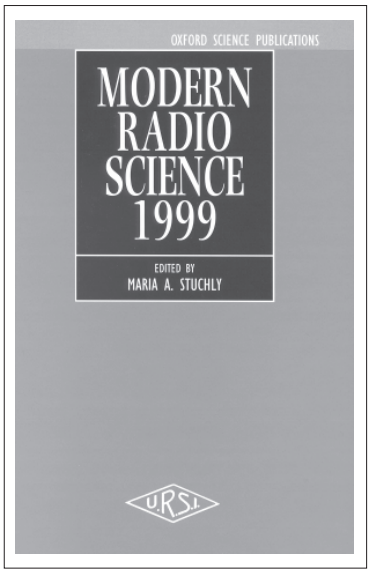

Editor: Maria Stuchly
ISBN 0-7803-6002-8
List Price : USD 49.95 Member Price : USD 45.00
IEEE Product No. PC5837

Published by Oxford University Press
in cooperation with URSI and IEEE Press
Order 24 hours a day, 7 days a week :
1-732-981 0060 (Worldwide)
1-800-678 4333 (USA & Canada)
Fax 1-732 981 9667
E-mail : customer-service@ieee.org

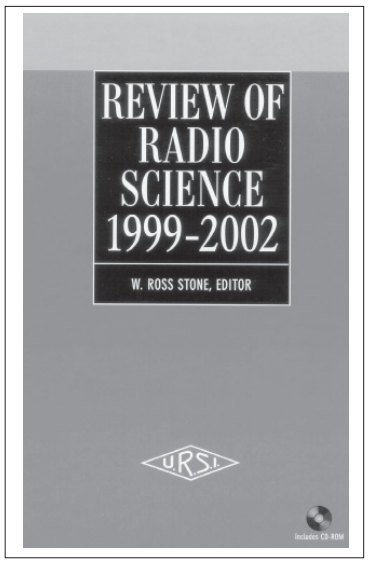

Review of Radio Science 1999-2002

Editor: W. Ross Stone
July 2002/Hardcover/977 pp
ISBN 0-471-26866-6
List Price : USD 125.00 Member Price : USD 106.25
IEEE Product No. #18493

Published by Wiley-Interscience
in cooperation with URSI and IEEE Press
Order can be sent to John Wiley & Sons, Inc.
from 8.30 a.m. to 5.30 p.m. :
1-732-469-4400 (Worldwide)
1-800-225-5945 (USA & Canada)
Fax 1-732 302-2370
E-mail : customer@wiley.com

Handbook on Radiopropagation Related to Satellite Communications in Tropical and Subtropical Countries

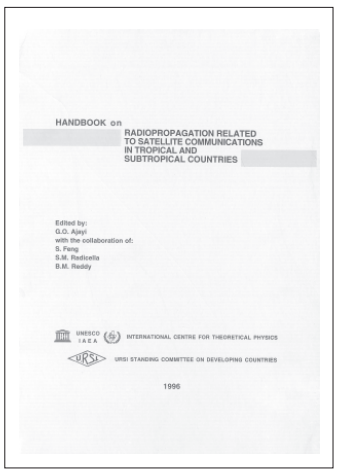

Editor: G.O. Ajayi
with the collaboration of :
S. Feng, S.M. Radicella, B.M. Reddy

Available from the URSI Secretariat
c/o Ghent University (INTEC)
Sint-Pietersnieuwstraat 41
B-9000 Gent, Belgium
tel. +32 9-264-33-20
fax +32 9-264-42-88
e-mail : info@ursi.org

Wireless Networks

The journal of mobile communication, computation and information

Editor-in-Chief:
Imrich Chlamtac
Distinguished Chair in Telecommunications
Professor of Electrical Engineering
The University of Texas at Dallas
P.O. Box 830688, MS EC33
Richardson, TX 75083-0688
email: chlamtac@acm.org

Aims & Scope:
The wireless communication revolution is bringing fundamental changes to data networking, telecommunication, and is making integrated networks a reality. By freeing the user from the cord, personal communications networks, wireless LAN's, mobile radio networks and cellular systems, harbor the promise of fully distributed mobile computing and communications, any time, anywhere. Numerous wireless services are also maturing and are poised to change the way and scope of communication. WINET focuses on the networking and user aspects of this field. It provides a single common and global forum for archival value contributions documenting these fast growing areas of interest. The journal publishes refereed articles dealing with research, experience and management issues of wireless networks. Its aim is to allow the reader to benefit from experience, problems and solutions described. Regularly addressed issues include: Network architectures for Personal Communications Systems, wireless LAN's, radio , tactical and other wireless networks, design and analysis of protocols, network management and network performance, network services and service integration, nomadic computing, internetworking with cable and other wireless networks, standardization and regulatory issues, specific system descriptions, applications and user interface, and enabling technologies for wireless networks.

Wireless Networks is a joint publication of the ACM and Baltzer Science Publishers. Officially sponsored by URSI

For a complete overview on what has been and will be published in Telecommunication Systems please consult our homepage:

BALTZER SCIENCE PUBLISHERSHOMEPAGE
http://www.baltzer.nl/winet

Special Discount for URSI Radioscientists

Euro 62 / US$ 65
(including mailing and handling)

Wireless Networks ISSN 1022-0038
Contact: Mrs. Inge Heleu
Fax +32 9 264 42 88 E-mail ursi@intec.rug.ac.be
Non members/Institutions: contact Baltzer Science Publishers

BALTZER SCIENCE PUBLISHERS
P.O.Box 221, 1400 AE Bussum, The Netherlands
Tel: +31 35 6954250 Fax: +31 35 6954 258 E-mail: publish@baltzer.nl

The Journal of Atmospheric and Solar-Terrestrial Physics

SPECIAL OFFER TO URSI CORRESPONDENTS

AIMS AND SCOPE

The *Journal of Atmospheric and Terrestrial Physics* (JASTP) first appeared in print in 1951, at the very start of what is termed the "Space Age". The first papers grappled with such novel subjects as the Earth's ionosphere and photographic studies of the aurora. Since that early, seminal work, the Journal has continuously evolved and expanded its scope in concert with - and in support of - the exciting evolution of a dynamic, rapidly growing field of scientific endeavour: the Earth and Space Sciences. At its Golden Anniversary, the now re-named *Journal of Atmospheric and Solar-Terrestrial Physics* (JASTP) continues its development as the premier international journal dedicated to the physics of the Earth's atmospheric and space environment, especially the highly varied and highly variable physical phenomena that occur in this natural laboratory and the processes that couple them. The *Journal of Atmospheric and Solar-Terrestrial Physics* is an international journal concerned with the inter-disciplinary science of the Sun-Earth connection, defined very broadly. The journal referees and publishes original research papers, using rigorous standards of review, and focusing on the following: The results of experiments and their interpretations, and results of theoretical or modelling studies; Papers dealing with remote sensing carried out from the ground or space and with in situ studies made from rockets or from satellites orbiting the Earth; and, Plans for future research, often carried out within programs of international scope. The Journal also encourages papers involving: large scale collaborations, especially those with an international perspective; rapid communications; papers dealing with novel techniques or methodologies; commissioned review papers on topical subjects; and, special issues arising from chosen scientific symposia or workshops. The journal covers the physical processes operating in the troposphere, stratosphere, mesosphere, thermosphere, ionosphere, magnetosphere, the Sun, interplanetary medium, and heliosphere. Phenomena occurring in other "spheres", solar influences on climate, and supporting laboratory measurements are also considered. The journal deals especially with the coupling between the different regions. Solar flares, coronal mass ejections, and other energetic events on the Sun create interesting and important perturbations in the near-Earth space environment. The physics of this subject, now termed "space weather", is central to the Journal of Atmospheric and Solar-Terrestrial Physics and the journal welcomes papers that lead in the direction of a predictive understanding of the coupled system. Regarding the upper atmosphere, the subjects of aeronomy, geomagnetism and geoelectricity, auroral phenomena, radio wave propagation, and plasma instabilities, are examples within the broad field of solar-terrestrial physics which emphasise the energy exchange between the solar wind, the magnetospheric and ionosphericplasmas, and the neutral gas. In the lower atmosphere, topics covered range from mesoscale to global scale dynamics, to atmospheric electricity, lightning and its effects, and to anthropogenic changes. Helpful, novel schematic diagrams are encouraged. Short animations and ancillary data sets can also be accommodated. Prospective authors should review the *Instructions to Authors* at the back of each issue.

Complimentary Information about this journal:
http://www.elsevier.com/locate/JASTP?
http://earth.elsevier.com/geophysics

Audience:
Atmospheric physicists, geophysicists and astrophysicists.

Abstracted/indexed in:
CAM SCI Abstr
Curr Cont SCISEARCH Data
Curr Cont Sci Cit Ind
Curr Cont/Phys Chem & Sci
INSPEC Data
Meteoro & Geoastrophys Abstr
Res Alert

Editor-in-Chief:
T.L. Killeen, National Centre for Atmospheric Research, Boulder, Colorado, 80307 USA

Editorial Office:
P.O. Box 1930, 1000 BX Amsterdam, The Netherlands

Special Rate for URSI Radioscientists 2003:
Euro 149.00 (US$ 149.00)
Subscription Information
2002: Volume 65 (18 issues)
Subscription price: Euro 2659 (US$ 2975)
ISSN: 1364-6826

CONTENTS DIRECT:
The table of contents for this journal is now available pre-publication, via e-mail, as part of the free ContentsDirect service from Elsevier Science. Please send an e-mail message to cdhelp@elsevier.co.uk for further information about this service.

For ordering information please contact Elsevier Regional Sales Offices:

Asia & Australasia/ e-mail: asiainfo@elsevier.com
Europe, Middle East & Africa: e-mail: nlinfo-f@elsevier.com
Japan: Email: info@elsevier.co.jp
Latin America : e-mail: rsola.info@elsevier.com.br
United States & Canada : e-mail: usinfo-f@elsevier.com

Information for authors

Content

The *Radio Science Bulletin* is published four times per year by the Radio Science Press on behalf of URSI, the International Union of Radio Science. The content of the *Bulletin* falls into three categories: peer-reviewed scientific papers, correspondence items (short technical notes, letters to the editor, reports on meetings, and reviews), and general and administrative information issued by the URSI Secretariat. Scientific papers may be invited (such as papers in the *Reviews of Radio Science* series, from the Commissions of URSI) or contributed. Papers may include original contributions, but should preferably also be of a sufficiently tutorial or review nature to be of interest to a wide range of radio scientists. The *Radio Science Bulletin* is indexed and abstracted by INSPEC.

Scientific papers are subjected to peer review. The content should be original and should not duplicate information or material that has been previously published (if use is made of previously published material, this must be identified to the Editor at the time of submission). Submission of a manuscript constitutes an implicit statement by the author(s) that it has not been submitted, accepted for publication, published, or copyrighted elsewhere, unless stated differently by the author(s) at time of submission. Accepted material will not be returned unless requested by the author(s) at time of submission.

Submissions

Material submitted for publication in the scientific section of the *Bulletin* should be addressed to the Editor, whereas administrative material is handled directly with the Secretariat. Submission in electronic format according to the instructions below is preferred. There are typically no page charges for contributions following the guidelines. No free reprints are provided.

Style and Format

There are no set limits on the length of papers, but they typically range from three to 15 published pages including figures. The official languages of URSI are French and English: contributions in either language are acceptable. No specific style for the manuscript is required as the final layout of the material is done by the URSI Secretariat. Manuscripts should generally be prepared in one column for printing on one side of the paper, with as little use of automatic formatting features of word processors as possible. A complete style guide for the *Reviews of Radio Science* can be downloaded from http://www.ips.gov.au/IPSHosted/NCRS/reviews/. The style instructions in this can be followed for all other *Bulletin* contributions, as well. The name, affiliation, address, telephone and fax numbers, and e-mail address for all authors must be included with all submissions. All papers accepted for publication are subject to editing to provide uniformity of style and clarity of language. The publication schedule does not usually permit providing galleys to the author.

Figure captions should be on a separate page in proper style; see the above guide or any issue for examples. All lettering on figures must be of sufficient size to be at least 9 pt in size after reduction to column width. Each illustration should be identified on the back or at the bottom of the sheet with the figure number and name of author(s). If possible, the figures should also be provided in electronic format. TIF is preferred, although other formats are possible as well: please contact the Editor. Electronic versions of figures *must* be of sufficient resolution to permit good quality in print. As a rough guideline, when sized to column width, line art should have a minimum resolution of 300 dpi; color photographs should have a minimum resolution of 150 dpi with a color depth of 24 bits. 72 dpi images intended for the Web are generally *not* acceptable. Contact the Editor for further information.

Electronic Submission

A version of Microsoft *Word* is the preferred format for submissions. Submissions in versions of T_EX can be accepted in some circumstances: please contact the Editor before submitting. *A paper copy of all electronic submissions must be mailed to the Editor, including originals of all figures.* Please do *not* include figures in the same file as the text of a contribution. Electronic files can be send to the Editor in three ways: (1) By sending a floppy diskette or CD-R; (2) By attachment to an e-mail message to the Editor (the maximum size for attachments *after* MIME encoding is about 7 MB); (3) By e-mailing the Editor instructions for downloading the material from an ftp site.

Review Process

The review process usually requires about three months. Authors may be asked to modify the manuscript if it is not accepted in its original form. The elapsed time between receipt of a manuscript and publication is usually less than twelve months.

Copyright

Submission of a contribution to the *Radio Science Bulletin* will be interpreted as assignment and release of copyright and any and all other rights to the Radio Science Press, acting as agent and trustee for URSI. Submission for publication implicitly indicates the author(s) agreement with such assignment, and certification that publication will not violate any other copyrights or other rights associated with the submitted material.

APPLICATION FOR AN URSI RADIOSCIENTIST

I have not attended the last URSI General Assembly, and I wish to remain/become an URSI Radioscientist in the 2003-2005 triennium. Subscription to *The Radio Science Bulletin* is included in the fee.
(please type or print in BLOCK LETTERS)

Name: Prof./Dr./Mr./Mrs./Ms. _____
Family Name *First Name* *Middle Initials*

Present job title: _____

Years of professional experience: _____

Professional affiliation: _____

I request that all information, including the bulletin, be sent to my ☐ home ☐ business address, i.e.:

Company name: _____

Department: _____

Street address: _____

City and postal / zip code: _____

Province / State: _____ Country: _____

Phone: _____ ext: _____ Fax: _____

E-mail: _____

Areas of interest (please tick)

☐ A Electromagnetic Metrology
☐ B Fields and Waves
☐ C Signals and Systems
☐ D Electronics and Photonics
☐ E Electromagnetic Noise & Interference
☐ F Wave Propagation & Remote Sensing
☐ G Ionospheric Radio and Propagation
☐ H Waves in Plasmas
☐ J Radio Astronomy
☐ K Electromagnetics in Biology & Medicine

The fee is 40 Euro.
(The URSI Board of Officers will consider waiving of the fee if the case is made to them in writing)

Method of payment: VISA / MASTERCARD (we do not accept cheques)

Credit Card No ☐☐☐☐ ☐☐☐☐ ☐☐☐☐ ☐☐☐☐ Exp. date: _____

Date: _____ Signed _____

Please return this signed form to:

The URSI Secretariat
c /o Ghent University / INTEC
Sint-Pietersnieuwstraat 41
B-9000 GENT, BELGIUM
fax (32) 9-264.42.88